PENINSULA TECHNIKON

Department of Electrical Engineering

Faculty of Engineering

AN INVESTIGATION AND DESIGN OF AN INFRARED RADIATION HEAT PROFILE CONTROLLER

by

Marco Leroy Adonis

Submitted in fulfillment of the requirement for

Masters degree of Technology (MTech): Electrical engineering

Under the supervision of

Mohammed Tariq Ekeramodien Khan

DECEMBER 2002

DECLARATION

I, Marco Leroy Adonis, hereby declare that the dissertation presented here is my own work and the opinions contained herein are my own and do not necessarily reflect those of the Technikon. All references used have been accurately reported.

Name: Marco Leroy Adonis

Signature:

Date: December 2002

Acknowledgements

A work of this nature requires the help and support of many people. Though many had a part in helping me in several ways, some do deserve special mention.

I would like to thank my supervisor, Mr. Mohammed Tariq Ekeramodien Khan, for his guidance and assistance throughout the time of my research and whose leadership and direction steered the course of this research to its completion. Mr. P. Mostert also deserves my thanks and gratitude, he offered the impetus at the conception of this work and continued throughout to provide meaningful insight. Special mention must be made of Prof. R. Tzoneva whose expert knowledge of control theory and willingness to help is greatly appreciated. To the Electrical Department of Peninsula Technikon, thank you for availing me the facilities in which to continue my research. My gratitude also extends to my sponsors, the National Research Foundation (NRF), whose financial assistance provided me a platform to conduct this research, which proved both interesting and rewarding.

Then to my family whose support and understanding during this research helped me focus my efforts and bring it to conclusion. To my fellow research colleagues and friends, thank you for your motivation and inspiration it proved invaluable.

AN INVESTIGATION AND DESIGN OF AN INFRARED RADIATION HEAT PROFILE CONTROLLER

by

Marco Leroy Adonis

Abstract

This research outlines the development and design of an infrared radiation heating profile controller. The study includes both the theoretical aspects of the design process as well as giving an overview of the practical facets involved. The controller was subjected to comparative testing with a proportional control model, in order to observe its performance and validate its effectiveness.

A need exists for these types of controllers and proved to be the motivation to embark on this investigation. Controllers of this nature that are commercially available either lacks the functionality of this unit or are too expensive to implement for research purposes. This unit was designed with cost effectiveness in mind but still meet the standards required of an industrial style controller. To this end the construction was completed using low cost and affordable electronic components. Heating profiles are necessary and useful tools for the proper processing of a host of materials. The controller developed in this research is able to within a fair degree of accuracy track a heating profile. The results confirm that this programmable control model to be a benefit and a valuable tool in temperature regulation. This means that intensive studies into the effects of infrared radiation on materials are now feasible. Research of this nature could possibly expand the application of infrared as a heating mechanism.

Although tests were conducted on this controller, they are not meant to serve as an exhaustive analysis. The conclusions of these examinations do reveal the benefit of such a controller. More rigorous investigation is suggested as a subject for further study.

TABLE OF CONTENTS

List of Figures

List of Tables

Nomenclature

q	heat flux	W/m^2
k_c	thermal conductivity	$W/(mK)$
T	*temperature*	K
h_c	convective heat transfer coefficient	$W/(m^2K)$
ν	frequency	Hz
c	speed of light, $2.998 \cdot 10^8$	m/s
λ	wavelength	m
h	Planck's constant, $6.626 \cdot 10^{-34}$	Js
e	photon energy	J
ε	emissivity	-
ρ	resistivity	$\Omega \cdot cm$
α	absorbtivity	-
τ	transmissivity	-
r	reflectivity	-
G_λ	spectral irradiation	$W/m^2 \cdot \mu m$
G	total irradiation	W/m^2
I_λ	spectral intensity	W/m^2
E_λ	spectral emissive power	W/m^2
σ	Stefan-Boltzman constant, $5.67 \cdot 10^{-8}$	$W/(m^2K)$
C_1	first Planck's law constant, $3.74 \cdot 10^{-16}$	W/m^2
C_2	second Plank's law constant, $1.44 \cdot 10^{-2}$	mK
q	radiative heat flux	W
A	area	m²

J	*radiosity*	W/m^2
F	*view factor*	-

$G(s)$	feedforward path transfer function
$H(s)$	feedback path transfer function
$c(t)$	controlled output
$r(t)$	reference input
K_p	proportional gain
T_i	integral time
T_d	derivative time
$u(t)$	controller output
$e(t)$	actuating error signal

Subscripts

b	blackbody value
x	in x-direction

1. INTRODUCTION

Since the dawn of time, the transfer of heat from a warm to a cool place has formed an integral part of our way of life. By harnessing the power of fire we could carve out a very comfortable existence. The advent of the industrial revolution demanded controlled forms of heat to increase production and improve product quality. Infrared in the form of light bulbs fitted with external reflectors has been used in the commercial sector since the late 1930's. This technique proved very successful for curing synthetic enamels on car bodies. During the Second World War infrared heating became more widely recognised as a method to speed up metal finishing for military equipment. Although these applications featured light bulbs with very low power densities compared to today's standards, they offered much faster drying and curing than the convection ovens of the time. Today infrared is available in a variety of configurations and power densities.

1.1 Modes of heat transfer

Heat transfer occurs through three different methods: conduction, convection and radiation. In the case of conduction in a solid, energy is transferred through the atomic lattice by free electrons or by vibrational energy in the interatomic bonds. In gases and liquids, energy transfer is by molecular interactions, when the more energetic molecules collide with less energetic molecules. Similarly, convection involves the movement of large numbers of molecules in the presence of a temperature gradient in a fluid motion. Thermal radiation is energy emitted by matter that is at a temperature above absolute zero. The heat transfer is through electromagnetic waves (or photons). Unlike the energy transfer in conduction and convection that require the presence of a material medium, radiation does not. In addition, radiation transfer occurs most efficiently in a vacuum. Thermal radiation includes infrared (IR) radiation, visible light and a portion of the ultraviolet (UV) radiation. The region of thermal radiation of interest to this research is the infrared (IR) radiation spectrum, which extends from 076μm to 100μm. Conduction and convection are effective over short distances, whereas radiation can be effective over long distances. For example, the transfer of heat from the surface of the sun to the earth through the vacuum of space occurs exclusively by radiation.

Concerns in industry revolve around questions of efficiency, as this has a direct bearing on financial decisions and planning. This also directly affects the financial viability of implementing changes to existing systems. Industrial processes incorporating heating and energy exchange traditionally rely on convection and conduction methods. When IR is compared to these traditional methods however, particularly for applications involving surface heating, certain applications using IR are far more effective and efficient and the quality of the finished product is much improved (Howard, 1996). There is no significant heating of the surrounding air as is the case in convection heating and the heating process is not completely dependent on the thermal conductivity of the material being heated, as is the case in conduction heating. Consequently the IR heating process is of a higher efficiency because the energy losses are minimum.

Although much information exists on the applications of IR not much technical information is available on the effects of IR on various materials. Information on the spectral and average absorptivities of materials is still limited and methods for predicting the performance of IR emitters for heating, curing and drying is needed. Not much is known of IR radiation, in terms of its effects on materials. This could explain why many industries suited to IR are not employing it to good effect. Nevertheless, in recent years the benefits of IR have gained wide acceptance and implementation.

Furthermore, the mathematical equations that describe these three mechanisms of heat transfer are given. Fourier's law, equation (1.1) describes conduction as the following:

$$q_x = -k_c \frac{\partial T}{\partial x} \tag{1.1}$$

Newton's law of cooling, equation (1.2) describes convective heat transfer as the following:

$$q = h_c (T_b - T_\infty) \tag{1.2}$$

The constants k and h above depend in some degree on temperature, but not heavily. However, radiation heat transfer rates are generally proportional to differences in temperature to the fourth power as expressed in equation (1.3):

$$q \propto \left(T^4 - T_\infty^{\ 4}\right) \qquad (1.3)$$

As the temperature of a body increases, infrared (IR) radiation becomes the dominant form of heat transfer. At high temperatures, a body appears to glow and becomes red hot, as some of the radiation emitted is the wavelengths of visible red light. The body appears yellow to white as the temperature is increased even further. Today commercially available infrared heaters are finding success in many industrial processes.

1.2 Purpose of this research

In addition to the applications of IR technology, other important issues are presented in sections 1.3 and 1.4. In many industrial processes what is currently lacking is an effective and robust control of the infrared heating process. This research has successfully developed a controller to achieve this. A programmable controller based on a closed loop control structure has been developed. Using the controller, the necessary referenced heating profile for various materials used in IR applications could be followed. A referenced heating (temperature) profile is a range of temperatures with a definite period that are necessary for the proper processing of a material. By automating the following of these profiles, industrial processes are more effective and efficient.

The programmable controller developed fills a gap in the market. The IR controllers commercially available are generally of two types. The first is a dedicated system suited only to a specific application, an example of this is the Infradry Reflow System, manufactured by Heraeus (Heraeus, 1992). This unit used exclusively for reflow soldering. Another type of controller on the market is a solid-state power controller, this type of unit controls the power input to IR heaters but is not programmable. The heating control is achieved through manual means or by a thermostat and an example is the

ControlIR model 930/935 manufactured by Research Inc. (ControlIR-930/935-D-01-B). Solid-state power control units manufactured by Gefran are useful for various industrial applications (Gefran, 1999). With the above issues in mind, this research has developed a programmable controller that completely automates the IR heating process. It is predicted that this controller will be better than some of the other controllers currently available today. Many of these controllers are based on the principle of an open loop control structure, which is not very effective and useful in industry as the output temperature of the material is not known or controlled. Only the output temperature of the IR emitter is monitored in some way.

In essence the completion of this research is a universal adaptable device. Meaning that the unit is able to function and can be used in many different industrial situations. It is this capability to be adaptable and robust that makes this unit stand apart from others on the market. The controller developed in this research uses low cost digital components and power electronics techniques to improve the usefulness of an industrial IR emitter in infrared heating profile applications. The ability to control the input power to the IR emitter is through the mechanism of the pulse-width modulation (PWM) technique. This technique varies the output temperature of an infrared emitter connected to the power controller.

1.3 Typical applications of infrared heating

What makes IR technology attractive to industry is that is clean, fast, has a high power output yield and probably most important is the efficiency that this kind of heating imparts on the many industrial applications where it is employed (Lavitt, 1996), (Van Denend, 1998), (Anon, 1997).

A distinction is made between electric IR emitters and gas-fired types, however the former is the type to be used in this research. The industries currently exploiting the benefits of IR technology are mainly found in those processes involving surface heating and drying. Furthermore, they fall into three categories namely; process heating, curing and drying (Howard, 1996). Heating applications include printed circuit infrared soldering (Dow, 1984), thermoforming of plastics (Knights, 1997a), (Knights, 1997b), (Myers, 1984), the heat-treating of metals, (Cox& McGee, 1989), (Foster, 1996). Curing applications include the curing of adhesives and sealants (Anon, 1996a), baking powder coatings (Anon, 1993) and curing resin composites (Howard, 1996). Drying applications are found in the textile industry (Broadbent, 1998),(Dhib,1999), the drying and setting of fabric dyes(Van Denend,1998), drying colour film laminates(Anon,1996b) and the drying of water-based coatings(Anon,1994). A specific application suited only to the use of IR is that of vacuum and thin-film conditions. It is here that the advantage of IR is unquestionable and beyond any doubt, because IR means that there is no contact between the heat source and material, which suits vacuum room conditions (Heraeus, 1992).

1.3.1 Drying applications

A closer look at the reason why applications employing drying are so prevalent in IR systems is presented here. The applications employed in water-based and moisture rich products and materials that require drying are readily solved with the use of IR technology. Water has a particularly broad absorption spectrum in the medium to long-wave range. In figure 1.1 various materials are shown with their characteristic absorption spectra (IR2000, 1998). The generally good absorption ranges in the medium and long-wave ranges can clearly be seen. In comparison aluminium is an excellent reflector material.

1.4 Concerns addressed by infrared technology

The research undertaken combines the power of infrared heat with a programmable controller, which is able to vary the output power of an infrared emitter, connected to it. It is this ability to control the output characteristics of an infrared (IR) radiator, which makes this project particularly suited to meet the needs of various industrial processes. These output characteristics are the emitter temperature and the infrared wavelength. The use of temperature profiles, which can be duplicated by this controller offer real benefits for industry and consequently have definite application to many industrial processes (Blanc,1999). These temperature profiles are useful in the industrial

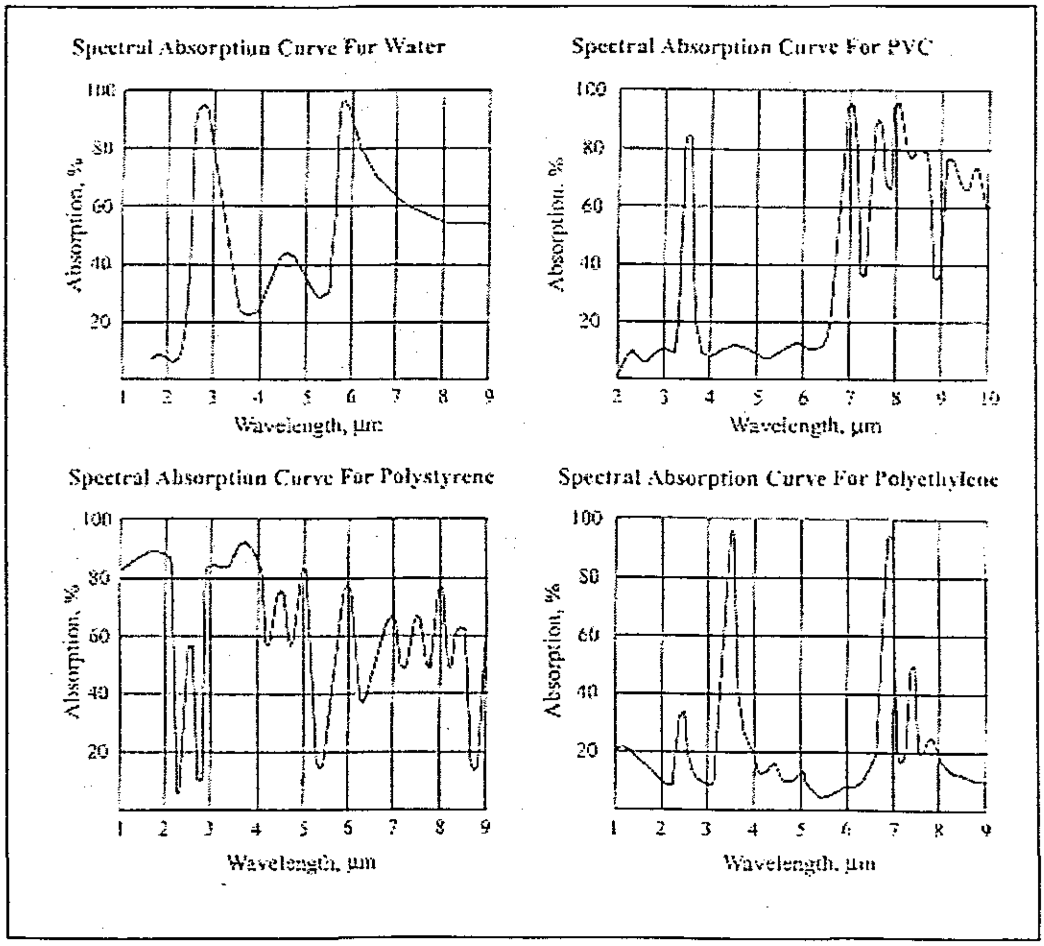

Figure 1.1 Absorption spectra of different materials

processing of various materials. The problems that this research and indeed IR in general aims to address and solve are presented below. These are compared to those problems which are associated with the traditional methods namely conduction and convection. The benefits of IR technology has been widely published and researched and consequently has found many industrial applications.

That IR radiation can offer real solutions to many industries is undisputed and acknowledged by a variety of industries gaining benefit from this technology (Knights, 1997a), (Van Denend, 1998). Increased competitiveness in the market place is persuading companies to explore many new and experimental methods in order to produce better products. Combinations of market forces are also pushing many companies suitable for IR to explore this possibility.

1.4.1 Material damage

The temperature profiles to be duplicated by this research project will be those that through prototype testing have proved to be optimum and are useful for industrial applications. In practical systems there exist generally four broad zones of heating profiles that are applied to such systems with good effect, for the purposes of control, namely:

- Preheating or pre-drying zone;
- Stabilization zone;
- Activation zone, and
- Cooling zone.

These profile phases if set-up properly can enhance the desired response from a material. An example is in the reflow soldering process, where these profiles together with hot air reduce the effects of delamination of the circuit boards. (Schumacher, 1996). A practical example of reflow soldering is shown in figure 1.2 below (Altera, 1999). In the pre-heat stage, the solder paste dries while its more volatile ingredients evaporate.

During the flux activation stage, the solder on all areas of the board is roughly at the same temperature. The flux cleans all the bonding surfaces and is a prerequisite for soldering. During the reflow stage the solder melts and flows onto the bonding surfaces. The cool down phase allows the solder to harden and form joints. Decrease in product rejects because of proper setting of the temperature profiles is another problem overcome.

1.4.2 Cost effectiveness

The IR products currently on the market solve the problems associated with efficiency and cost effectiveness of industrial processes. The cost effectiveness of an IR system implies that the resulting savings can be utilised in other areas in order to streamline a company's throughput . The concerns surrounding the financial viability of implementing an IR system are offset by the advantages derived from such a process.

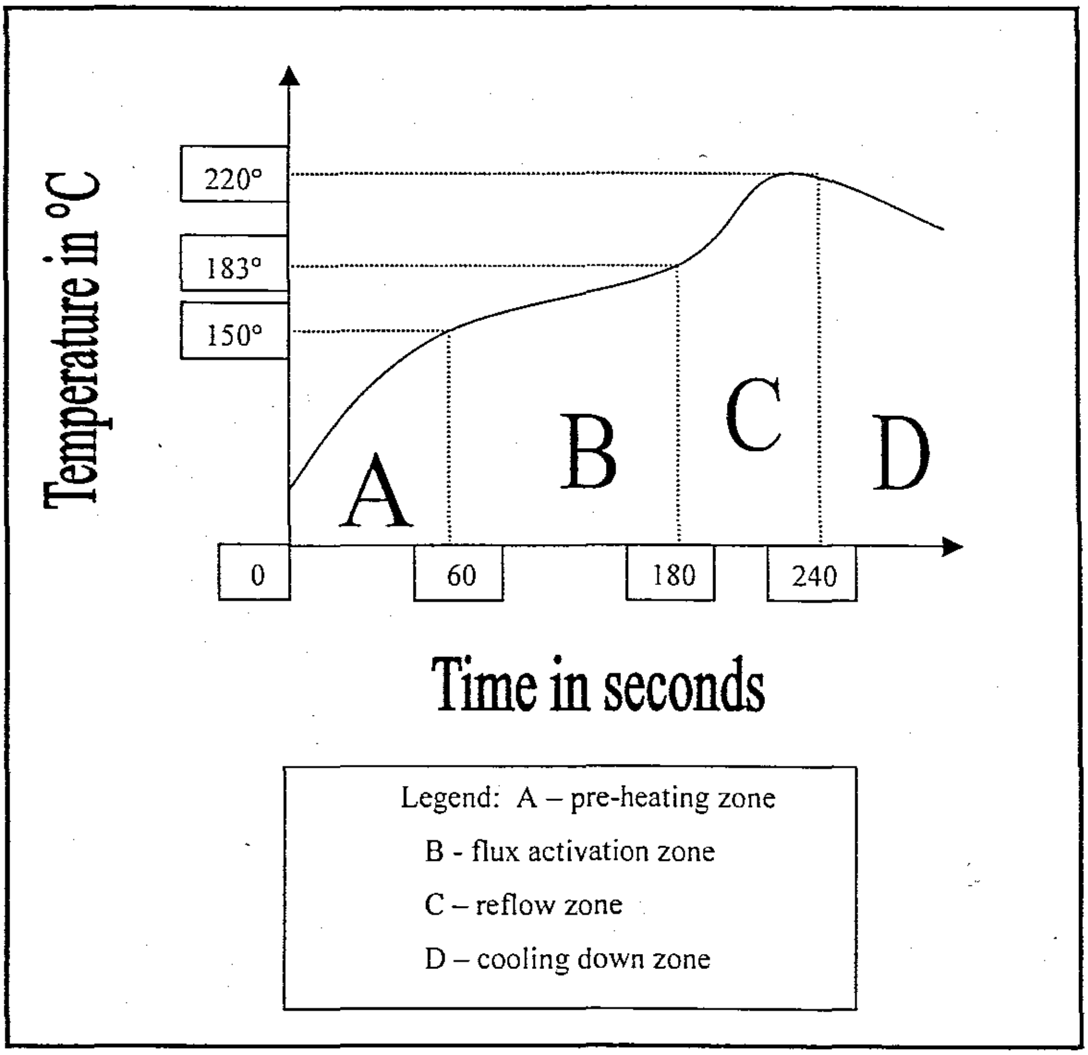

Figure 1.2 Temperature profile for reflow soldering

1.4.3 Quality products

Consumers are continually demanding better and improved results from their processes and in many instances IR solves their problems. Industries in metal coating, wood, paper, glass, plastic and textiles require more lustrous, longer lasting and wear-resistant finishes. Since IR heats the material directly, there is no need to blow hot air through the oven to achieve heat transfer. Translating into a superior surface finish and fewer rejects due to surface blemishes from entering dust (Howard, 1996).

1.4.4 Increased productivity

The speed of an IR system, which is related to the properties of infrared radiation, is a contributing factor to increased productivity. Also associated with the improved quality of the finished product, is the resultant increase in productivity. The process and the system do not experience many stoppages or down time as result of resetting the machines. These factors also contribute to the cost effectiveness of an IR system.

1.4.5 Environmental impact

In addition to this the environmental impact of an IR system is minimal and less intrusive if compared to the traditional methods used in the past (Broadbent, 1998). This factor in many instances compels companies to find alternative and more effective processes for their systems, also because government regulations force them to. Surely any product that does not negatively impact on the environment is in a favourable position to gain wider acceptance into the future.

1.4.6 Energy efficiency

Most of the energy in systems that are properly designed is transferred by radiation to the material. It therefore acts directly on the material resulting in a faster process and lowering energy costs. There is no significant heating of the surrounding air as is the case in convection heating and the heating process is not completely dependent on the thermal conductivity of the material being heated, as is the case in conduction heating. Consequently the IR heating process is of a higher efficiency because the energy losses are minimum. Processing time can be reduced by as much as 50% to 85 % when compared to convection ovens (Howard, 1996).

1.4.7 Time and space savings

Faster heating means shorter ovens. IR equipment therefore occupies less floor space than convection ovens. They can also be added to existing convection ovens and production line with little difficulty. IR ovens are easily adjusted and reconfigured as the product requirements change (Howard, 1996).

1.4.8 On-going research

Research in infrared is by no means only limited to the above, but has expanded to include such diverse topics as the investigations in IR radiation effects on the functional characteristics of wheat flour (Botero, 1997). Studies were conducted on IR heating and welding of thermoplastics and composites (Chen, 1995) and the possible inclusion of an IR emitter in microwave ovens (Anon, 1998).

1.5 Aim and outline of dissertation

The aim of this dissertation is to present the developmental stages undertaken in the design of an infrared radiation heating profile controller.

Several chapters that provide a background of information and put the work in perspective will introduce the dissertation. Chapter 2 offers an overview and brief theory of infrared radiation, presenting some of the scientific laws and definitions that govern this phenomenon. Chapter 3 covers the relevant theoretical aspects in the development of the infrared controller outlining the mathematical model. Chapter 4 provides the practical aspects in the development of the infrared controller, highlighting the various power control methods tried and tested. Chapter 5 summarises some of the results obtained through experiments conducted on the controller. Finally, chapter 6 presents a number of conclusions and suggestions for future work.

2. BRIEF THEORY OF INFRARED RADIATION

The many types of electromagnetic radiation are produced through diverse methods. Gamma rays are produced by nuclear reactions, the bombardment of metals with high-energy electrons results in X-rays, microwaves are produced by special types of electron tubes for example klystrons and magnetrons and radio waves by the agitation of certain types crystals or through the flow of alternating current in electric conductors. Of interest in heat transfer is thermal radiation, which is emitted as a result of the vibrational and rotational motions of molecules, atoms and electrons of a substance. Temperature is a measure of the strength of these events at the microscopic level.

2.1 The nature of thermal radiation

Radio waves, ultraviolet, visible light and thermal radiation are some examples of electromagnetic radiation. Electromagnetic radiation (EM) can be viewed as being composed of waves or massless energy particles (photons). It is accepted that neither approach adequately describes all radiation phenomena and the literature widely speaks of the wave-particle nature of EM radiation.

The method of emission relates to the energy released resulting from the oscillations and translations of the numerous electrons that constitute matter. The internal energy as a measure of its temperature sustains these oscillations within matter. All forms of matter emit radiation. In the case of gases as well as some semitransparent solids for example salt crystals and glass at high temperatures, the type of emission is known as a volumetric phenomena. However for opaque solids such as metals, rocks and wood as well as liquids, the radiation emitted by interior regions are strongly absorbed by adjoining molecules. In this case the type of emission is known as a surface phenomena. Only molecules within 1μm of the surface emit any significant amounts of radiation. Additionally, applying thin layers of radiation sensitive coatings to them can alter their surface characteristics (Çengel, 1997).

All EM waves propagate at the speed of light, *c*, and the waves or photons can be described by the following quantities: frequency, ν, and wavelength, λ, by the equation (2.1),

$$\nu = \frac{c}{\lambda} \tag{2.1}$$

Associated with every wave or photon is a particular amount of energy, e, derived from quantum mechanics to be:

$$e = h\nu \tag{2.2}$$

Typically wavelengths between 0.1μm and 100μm are the most relevant for heat transfer since they correspond to the internal energy levels we call heat. This part of the

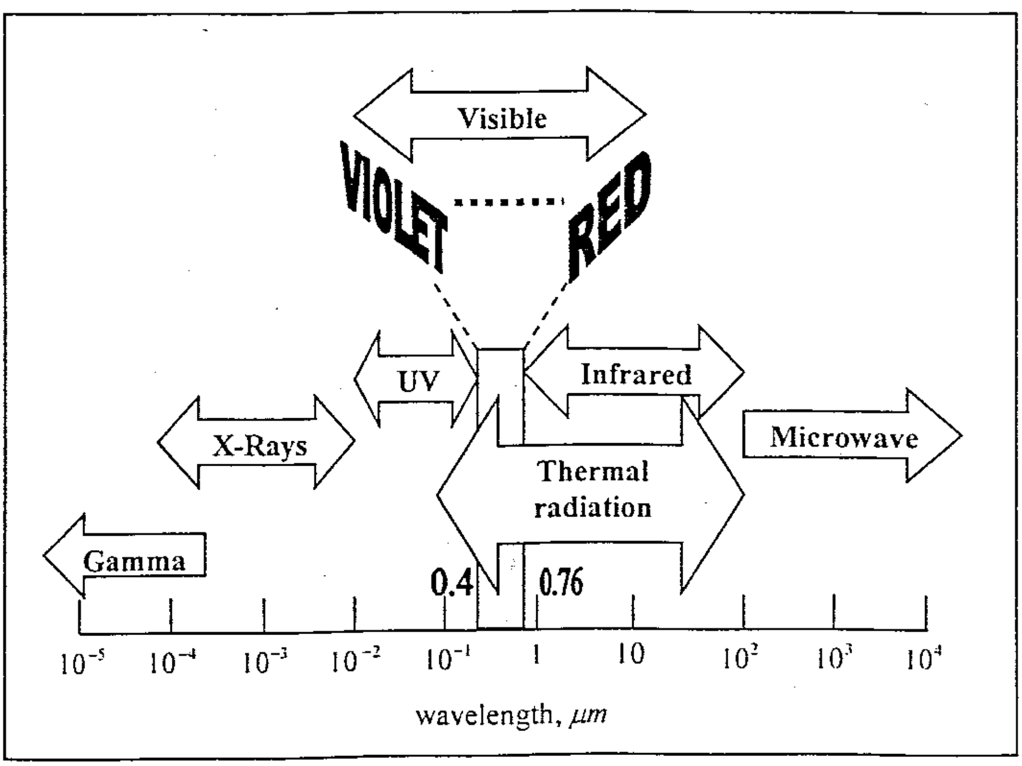

Figure 2.1 Electromagnetic wave spectrum

EM spectrum is often referred to as thermal radiation since these wavelengths have a heating effect when absorbed. A significant amount of this energy lies in the infrared region, between 0.76μm and 100μm. The infrared region is still further subdivided into three ranges: the short-wave or near infrared range, 0.76μm to 2 μm; the medium infrared range, 2μm to 4 μm and the long-wave or far infrared range, 4μm to 100μm.

2.2 Basic laws and definitions

When the surface of a body is irradiated by electromagnetic radiation, the waves may be reflected, absorbed or transmitted. A characteristic of an opaque surface is that the radiation impinging on it is reflected and absorbed but none is transmitted. However, a transparent surface prevents any radiation from being absorbed, whereas a semi-transparent surface only partially absorbs and partially transmits radiation. The type of material and its thickness determines whether a surface is termed opaque, transparent or semitransparent.

An idealized body termed a blackbody serves as a standard against which radiative properties of real surfaces are compared. The characteristic properties of a blackbody are that:

- No surface can emit more energy at any specified temperature and wavelength.
- It absorbs all incident radiation on its surface, regardless of wavelength and direction, i.e. it is a perfect absorber.
- Is a diffuse emitter. The radiation emitted although being characterized by wavelength and temperature, is independent of direction, i.e. is a perfect emitter.

The energy emitted from a real surface to that of a blackbody is known as the emissivity, ε, which is defined by relation (2.3) as,

$$\varepsilon = \frac{\text{energy emitted from a real surface}}{\text{energy emitted from a blackbody at same temperature}} \qquad (2.3)$$

The emissivity of a surface varies between zero and one, $0 \le \varepsilon \le 1$, with $\varepsilon = 1$ for a blackbody. For a real surface the emissivity is not a constant, rather it varies with temperature, wavelength and the direction of the emitted radiation. Subscripts λ, θ and n may be assigned to differentiate monochromatic, directional, and surface-normal values, respectively, from the total hemispherical value.

With respect to emissivity some generalizations are possible. Metals generally have low emissivities, as low as 0.02 for polished surfaces, whereas nonmetals such as ceramics and organic materials have higher ones. Generally, the emissivity of metals increases with temperature. Additionally oxidation causes a considerable increase in the emissivity of metals. The data presented in the literature should be interpreted with caution, since emissivity is strongly affected by surface conditions such as oxidation, roughness, the type of finish and cleanliness (Çengel, 1997). Specifically, polished metals have low emissivities in infrared. For $\lambda \ge 8\mu m$, ε_λ can be approximated by $0.00365\sqrt{\rho/\lambda}$ where ρ is the resistivity in $ohm \cdot cm$ and λ in μm. At shorter wavelengths the emissivity increases and for many metals has values of 0.4 to 0.8 in the visible range of the spectrum. The emissivity is approximately proportional to the square root of the absolute temperature $\left(\varepsilon_\lambda \propto \sqrt{\rho} \text{ and } \rho \propto T\right)$ in the far infrared range and temperature insensitive in the near infrared range (Hottel and Sarofim, 1996).

For refractory materials, grain size and concentration of trace impurities are important. Most refractory materials have emissivities between 0.8 and 1.0 at wavelengths between 2 and 4 μm (medium infrared range). Small concentrations of FeO and Cr_2O_3 or other coloured oxides can cause a marked increase in emissivity of materials that are normally white. The emissivity increases as grain-size increases in the range of 1 to 200 μm (Hottel and Sarofim, 1996).

In general, when a surface is irradiated as shown in figure 2.2, three fundamental properties can be defined: the reflectivity, r; the absorptivity, α; and the transmissivity, τ. These radiative properties are defined by the relations in (2.4) below

$$r = \frac{\text{refected part of irradiation}}{\text{total irradiation}}$$

$$\alpha = \frac{\text{absorbed part of irradiation}}{\text{total irradiation}} \quad (2.4)$$

$$\tau = \frac{\text{transmitted part of irradiation}}{\text{total irradiation}}$$

Therefore it follows that for a semitransparent surface that the following relation should hold true:

$$r + \alpha + \tau = 1 \quad (2.5)$$

If the surface is opaque, then there is no transmission and equation (2.6) reduces to the following:

$$r + \alpha = 1 \quad (2.6)$$

Spectral irradiation, G_λ, is defined as the rate at which radiation of wavelength λ is incident on a surface per unit area of the surface and per unit wavelength interval $d\lambda$ about λ.

$$G_\lambda(\lambda) = \int_0^{2\pi} \int_0^{\frac{\pi}{2}} I_{\lambda,i}(\lambda, \theta, \phi) \cos\theta \sin\theta \, d\theta \, d\phi \quad (2.7)$$

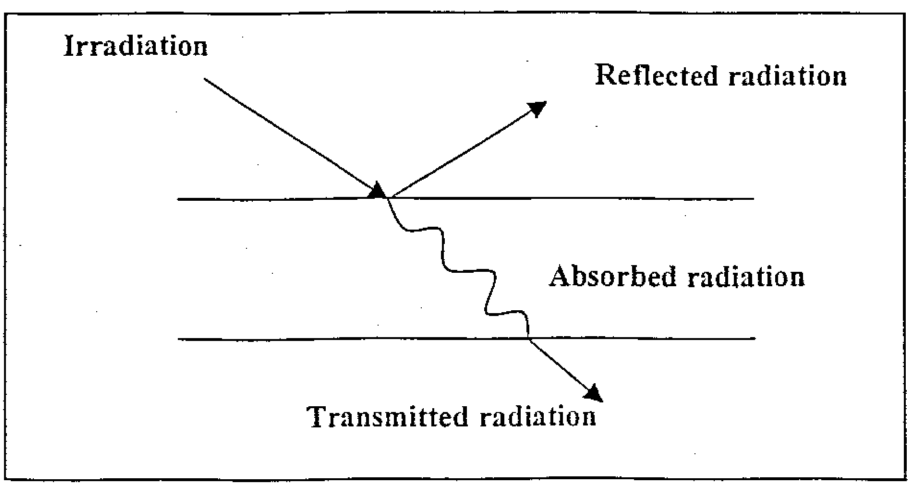

Figure 2.2 Absorption, reflection and transmission by a finite medium

Where the spectral intensity, $I_{\lambda,i}(\lambda,\theta,\phi)$, is defined as the rate at which radiant energy of wavelength λ is incident from the (θ,ϕ) direction, per unit area of the intercepting surface normal to this direction, per unit solid angle about this direction, and per unit wavelength interval $d\lambda$ about λ.

The total irradiation, G, represents the rate at which radiation is incident per unit area from all directions and at all wavelengths.

$$G = \int_0^\infty G_\lambda(\lambda)d\lambda \tag{2.8}$$

Further expanding the relations of (2.4) in terms of irradiation G, the total hemispherical absorptivity, α, is defined as:

$$\alpha \equiv \frac{G_{abs}}{G},\ 0 \le \alpha \le 1 \tag{2.9a}$$

The total hemispherical reflectivity, r, is defined as the following,

$$r \equiv \frac{G_{ref}}{G},\ 0 \le r \le 1 \tag{2.9b}$$

The total hemispherical transmissivity, τ, is defined as the following,

$$\tau \equiv \frac{G_{tr}}{G},\ 0 \le \tau \le 1 \tag{2.9c}$$

Planck first determined the spectral emission of a blackbody (Incropera, F and DeWitt, P, 1996). The Planck distribution, equation (2.10), describes the spectral emissive power of a blackbody as follows:

$$E_{\lambda,b}(\lambda,T) = \frac{C_1}{\lambda^5[\exp(C_2/\lambda T)-1]} \tag{2.10}$$

The graphical representation of this distribution is given in figure 2.3 and some important deductions can be made from this figure:

- The emitted radiation varies continuously with wavelength. At any specified temperature, there is an increase in wavelength, reaching a peak and then decreases with increasing wavelength.
- At any wavelength, the amount of emitted radiation increases with increasing temperature.
- The temperature determines the spectral region in which radiation is concentrated. Noting that as the temperature increases more radiation appears at shorter wavelengths.
- A significant fraction of solar radiation, which is considered a blackbody at 5800 K, is in the visible region of the spectrum. However surfaces at ≤ 800 K emit almost entirely in the infrared region.

From figure 2.3 it is evident that the blackbody spectral distribution has a maximum and in addition that the corresponding wavelength λ_{MAX} depends solely on temperature. Differentiating equation (2.10) with respect to λ and setting the result equal to zero, Wien's displacement law is obtained, equation (2.11).

$$\lambda_{MAX}T = 2897.8\mu m \cdot K \tag{2.11}$$

Since the sun emits as a blackbody at approximately 5800 K, from equation (2.11), $\lambda_{MAX} \approx 0.5\mu m$. Another example is a tungsten filament lamp operating at 2900 K ($\lambda_{MAX} \approx 1\mu m$), which emits white light, but most of the emission is in the IR region. Making this type of lamp not a very efficient light source.

The Stefan-Boltzmann law, equation (2.12), enables the calculation of the amount of radiation emitted in all directions (diffuse) and over all wavelengths, from knowledge of the temperature of a blackbody. The total blackbody emissive power, E_b, is given by (2.12),

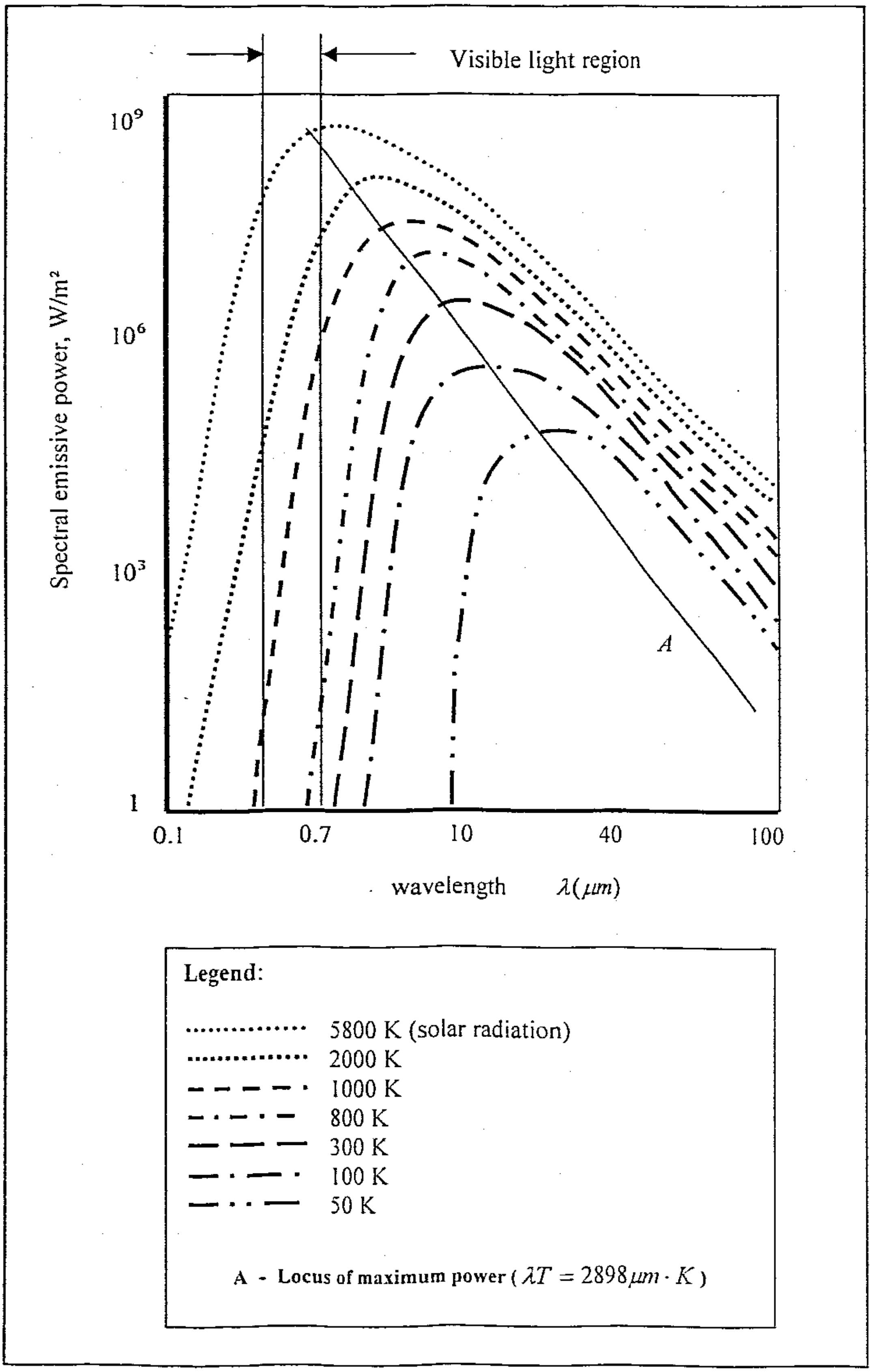

Figure 2.3 Spectral blackbody emissive power, $E_{\lambda b}$

$$E_b = \sigma T^4 \tag{2.12}$$

A corresponding form of equation (2.12) that relates to real surfaces is given below. Equation (2.13) gives $E(T)$, the total emissive power of a real surface as:

$$E(T) = \varepsilon(T)\sigma T^4 \tag{2.13}$$

The radiation emitted by a unit area of a real surface at temperature T is obtained by the product of the radiation emitted by a blackbody at temperature T and the emissivity of a real surface. It follows from equation (2.13) that the total hemispherical emissivity, $\varepsilon(T)$, can be defined as follows:

$$\varepsilon(T) \equiv \frac{E(T)}{E_b(T)} \tag{2.14}$$

This represents the average over all possible directions and wavelengths.

When two bodies are at thermal equilibrium, i.e. $T_1 = T_2$, under steady-state conditions, the net rate of energy exchange between the bodies must be zero. Applying an energy balance to one of these surfaces it follows that the total hemispherical emissivity equals the total hemispherical absorptivity.

$$\varepsilon = \alpha \tag{2.15}$$

Equation (2.15) is known as Kirchoff's law, the restriction being that it is applicable to blackbody conditions only. However real surfaces are better approximated by gray surfaces. The emissivity of a gray surface is independent of wavelength. Accepting the fact that under certain conditions the spectral, directional emissivity and absorptivity are equal, equation 2.16 is obtained.

$$\varepsilon_{\lambda,\theta} = \alpha_{\lambda,\theta} \tag{2.16}$$

For this equation to hold true, either one of the following conditions is to be satisfied:

- The irradiation is diffuse, i.e. if the spectral intensity is independent of direction.
- The surface is diffuse, i.e. if the emissivity and absorptivity are independent of direction.

In addition to these conditions being satisfied, for $\alpha_\lambda = \varepsilon_\lambda$, either of the following conditions is satisfied:

- The irradiation corresponds to emission from a blackbody at the surface temperature, T, such that $G_\lambda(\lambda) = E_{\lambda,b}(\lambda,T)$ and $G = E_b(T)$.
- The surface is gray, i.e. α_λ and ε_λ is independent of λ.

To assume gray surface behaviour, α_λ and ε_λ need only be independent of λ over the spectral regions of the irradiation and the surface. As an example consider figure 2.4, the emissivity function can be approximated reasonably well by a step function of the form,

$$\varepsilon_\lambda = \begin{cases} \varepsilon_1 = \text{constant}, \ldots 0 \le \lambda \le \lambda_1 \\ \varepsilon_2 = \text{constant}, \ldots \lambda_1 \le \lambda \le \lambda_2 \\ \varepsilon_3 = \text{constant}, \ldots \lambda_2 \le \lambda \le \infty \end{cases}$$

The significance of gray surface approximation lies in the fact that a gray surface should emit as much radiation as the real surface it represents at a similar temperature. Consequently the areas under the mission curves of the real and gray surfaces ought to be equal. This means that $\varepsilon(T)\sigma T^4 = \int_0^\infty \varepsilon_\lambda(T) E_{b\lambda}(T) d\lambda$. This integration is simplified by

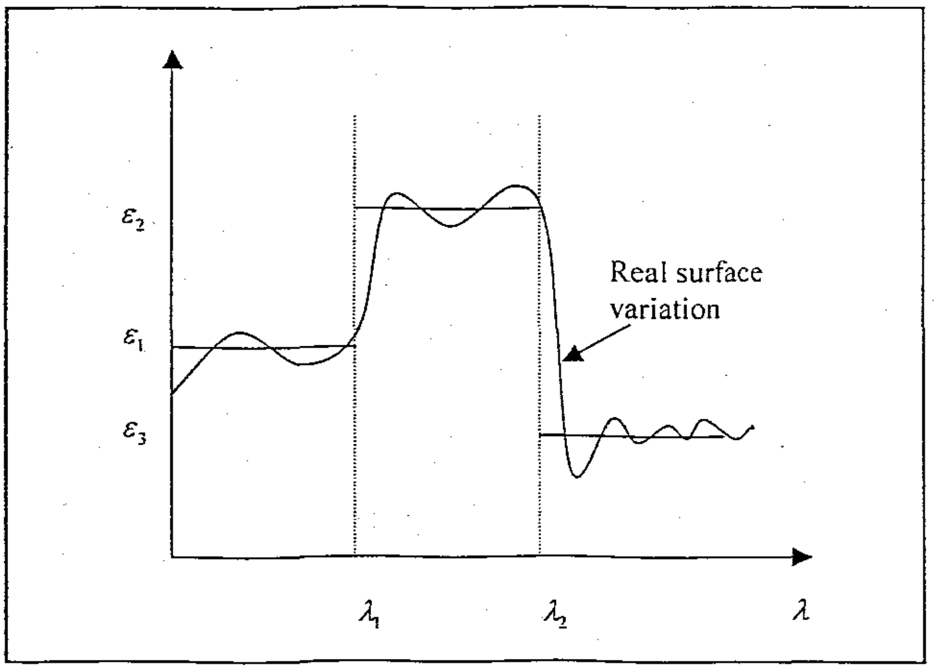

Figure 2.4 Approximating a real surface emissivity variation with wavelength by a step function.

separating the spectrum into a number of *wavelength bands* and assuming the emissivity remains continuous over each band. The average emissivity can be determined from the definition of blackbody radiation.

$$\varepsilon(T) = \frac{\varepsilon_1 \int_0^{\lambda_1} E_{b\lambda}(T)d\lambda}{\sigma T^4} + \frac{\varepsilon_2 \int_{\lambda_1}^{\lambda_2} E_{b\lambda}(T)d\lambda}{\sigma T^4} + \frac{\varepsilon_3 \int_{\lambda_2}^{\infty} E_{b\lambda}(T)d\lambda}{\sigma T^4} \tag{2.17}$$

$$= \varepsilon_1 f_{0-\lambda_1}(T) + \varepsilon_2 f_{\lambda_1-\lambda_2}(T) + \varepsilon_3 f_{\lambda_2-\infty}(T)$$

2.3 Geometric considerations

In many industrial applications the exchange of radiation heat transfer between different solid surfaces is unaffected by the medium separating them. This is a common occurrence since air and most gases are termed as nonparticipating media. Since such media neither emits, absorbs nor scatters, it does not affect the transfer of radiation between surfaces. Radiative heat transfer between two or more surfaces depends to some degree on their orientation relative to each other, size, separation distance and temperature.

Calculations in radiative heat transfer are simplified by only considering the geometric features of the surfaces involved. Thus neglecting the effects of surface temperature and surface properties. Performing a radiation analysis on surfaces based on the effects of orientation alone is termed as the *view factor*. View factors considered here are based on the assumption that the surfaces are diffuse emitters and diffuse reflectors, hence *diffuse view factors*. Specular view factors are not considered in this study. Performing a radiation analysis for one surface requires that all surfaces that can exchange radiative energy with one another be considered simultaneously.

Consider the two surfaces in figure 2.5. The view factor, F_{ij}, is defined as the fraction of the radiation leaving surface *i* that is intercepted by surface *j* directly. Mathematically the view factor is described by the double integral of equation (2.18).

$$F_{ij} = \frac{1}{A_i} \int_{A_i} \int_{A_j} \frac{\cos\theta_i \cos\theta_j}{\pi R^2} dA_i dA_j \qquad (2.18)$$

The values for the view factor are a numerical constant between zero and one. Some special conditions are be presented here (Çengel, 1997):

- The view factor from a surface to itself will be zero for a plane or convex surface, i.e. $F_{ii} = 0$. However for concave surfaces, $F_{ii} \neq 0$.

- If surface *j* completely surrounds surface *i*, so that all the radiation leaving surface *i* is intercepted by surface *j*, then $F_{ij} = 1$.

- When two surfaces do not have a direct view of each other, such that radiation leaving surface *i* is unable to strike surface *j*, $F_{ij} = 0$.

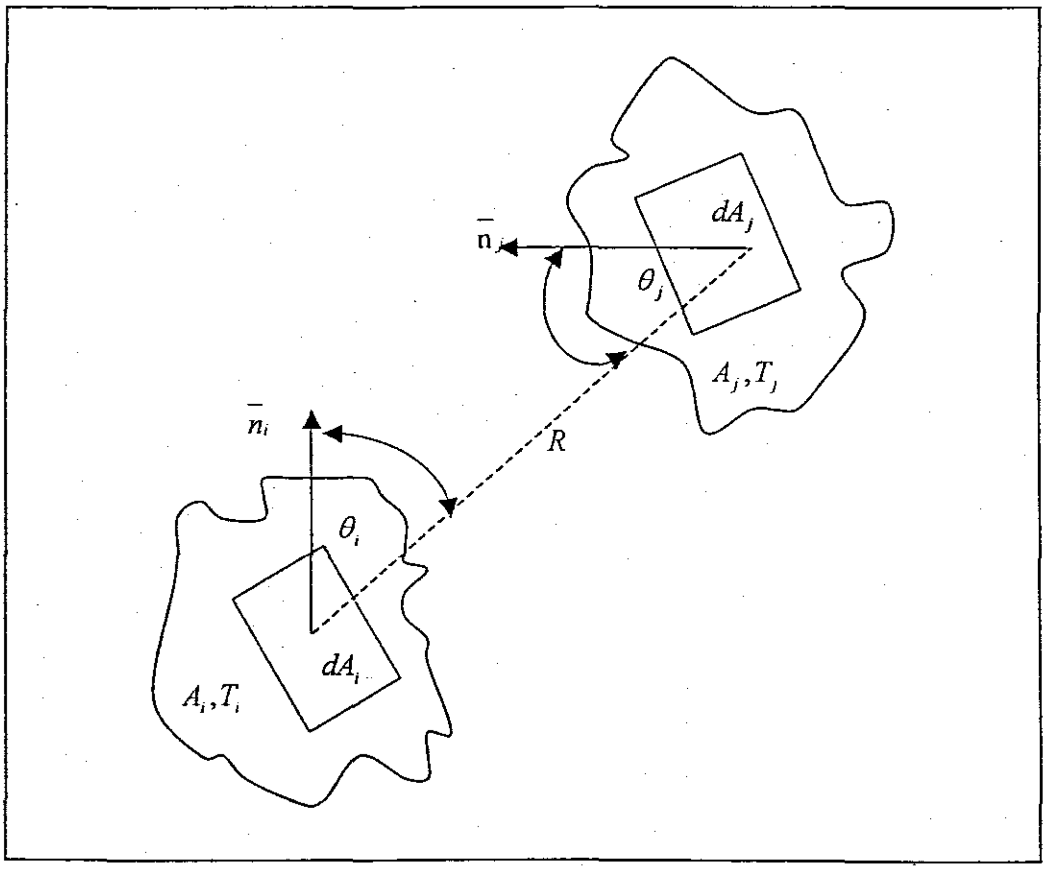

Figure 2.5 Radiative exchange between two elemental surfaces.

2.3.1 View factor algebra

When studying the view factors for various surfaces and orientations, it useful to consider these as relating to an enclosure. The analysis however would require the evaluation of N^2 for an enclosure consisting of N surfaces, which is neither practical nor necessary. This approach however is computationally intensive, but by utalising some fundamental relations for view factors, simple geometries are solved for.

2.3.1.1 The reciprocity rule

$$A_i F_{ij} = A_j F_{ji} \qquad (2.19)$$

This enables the determination of the counterpart of a view factor by knowing the view factor itself and the areas of the two surfaces.

2.3.1.2 The summation rule

$$\sum_{j=1}^{N} F_{ij} \qquad (2.20)$$

In an enclosure the conservation of energy principle stipulates that the entire radiation leaving any surface i within, be intercepted by the surfaces of the enclosure. The definition given in equation (2.20) is expressed as *the sum of the view factors from surface i of an enclosure to all surfaces of the enclosure, including itself, must equal unity.*

2.3.1.3 The superposition rule

If a view factor to be determined for a certain geometry is not available in the standard tables and charts, the superposition principle is useful. The view factors of known geometries are added or subtracted so as to closely approximate the required geometry. Consider the geometry of figure 2.8, the rule can be expressed as follows: *the view factor from surface i to a surface j equals the sum of the view factors from surface i to parts of surface j.*

A mathematical relationship is given in equation (2.21).

$$F_{i(j,k)} = F_{ij} + F_{ik} \qquad (2.21)$$

This rule is however not reversible such that the view factor from a surface j to a surface i is *not* equal to the sum of the view factors from surface j to parts of surface i.

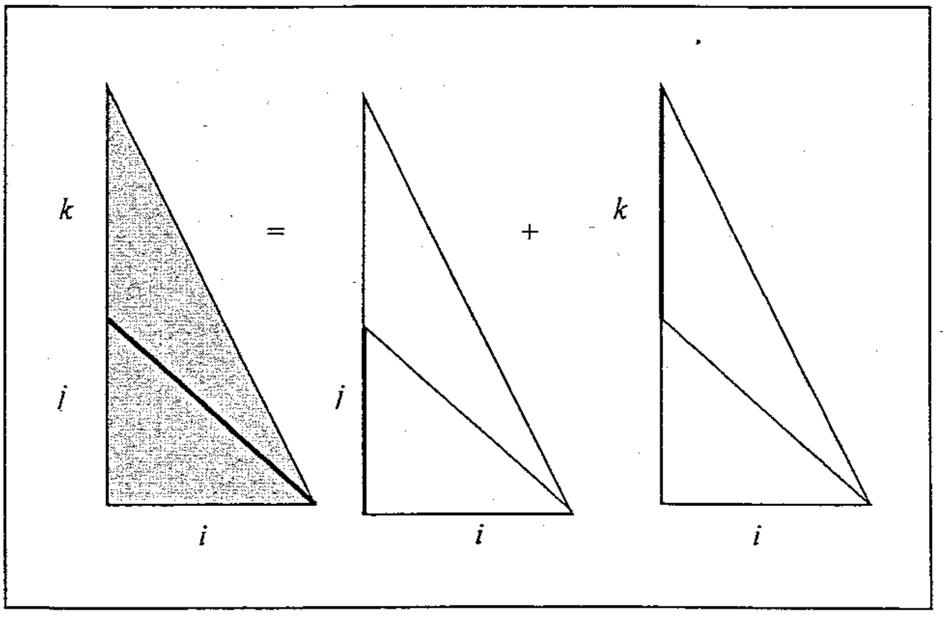

Figure 2.6 The view factor from a surface to a composite surface

2.3.1.4 The symmetry rule

Further simplification in the determination of a view factor is possible if the geometry involved possesses a degree of symmetry. Expressed as follows: *two or more surfaces that possess symmetry about a third surface will have identical view factors from that surface.* If surfaces j and k are symmetric about surface i the following holds true:

$$F_{ij} = F_{ik} \tag{2.22}$$

This relation is also true for the rule of reciprocity.

View factors for many conventional geometries are analysed and evaluated in several publications. These derivations include results for two and three-dimensional geometries.

2.4 Radiation heat transfer between black surfaces

Radiation may leave a surface due to both emission and reflection. The investigation of radiation exchange between surfaces, in general, is complicated because of reflection: a radiation beam leaving a surface may be reflected many times, with partial absorption occurring at each surface, before it is finally absorbed. The analysis is greatly simplified if the surfaces involved can be approximated as blackbodies, because of the absence of reflection.

The net rate of radiation heat transfer between two black surfaces of arbitrary shape and maintained at uniform temperatures T_i and T_j is given by the relation (2.23).

$$q_{ij} = A_i E_{bi} F_{ij} - A_j E_{bj} F_{ji} \tag{2.23}$$

Applying the reciprocity rule to (2.21) it yields,

$$q_{ij} = A_i F_{ij} \sigma \left(T_i^4 - T_j^4\right) \tag{2.24}$$

The net radiation heat transfer can also be defined as, $q_{ij} = q_{ij} - q_{ji}$, if q_{ij} is negative then the net radiation heat transfer is to the surface, i.e. surface *i* gains energy instead of losing. For an enclosure consisting of *N black* surfaces maintained at specified temperatures, the net radiation heat transfer from any surface *i* to each of the surfaces in the enclosure can be expressed as,

$$q_i = \sum_{j=1}^{N} q_{ij} = \sum_{j=1}^{N} A_i F_{ij} \sigma \left(T_i^4 - T_j^4\right) \tag{2.25}$$

2.5 Radiation heat transfer between diffuse, gray surfaces in an enclosure.

Radiation exchange formulae are available for blackbodies, because these results can differ considerably from the practical realisation; its usefulness is generally limited to analytical analysis. A blackbody is an idealisation that can be closely approximated by some surfaces, but is never accurately achieved. Calculations involving real non-blackbody surfaces do present increased mathematical complications; therefore these calculations invariably assume certain conditions. The calculations involved in analyzing radiation exchange can be simplified by making certain assumptions. These conditions include:

- The surfaces of the enclosure are isothermal, which is indicated by a uniform radiosity and irradiation.
- Surface behaviour is opaque, diffuse and gray.
- The medium within the enclosure is nonparticipating.

The aim of many calculations is to determine the net radiative heat flux q_i, knowing the temperature T_i associated with each surface of an enclosure. The radiosity J is defined as the total diffuse energy leaving a surface through emission and reflection. Where the radiosity of a blackbody is given by: $J = E_b = \sigma T^4$. Such that its radiosity equals its emissive power since it does not reflect any radiation.

For a surface i that is opaque, diffuse and gray ($\varepsilon_i = \alpha_i$ and $\alpha_i + r_i = 1$), the radiosity is expressed as:

$$
\begin{aligned}
J_i &= (\text{radiation emitted by surface } i) + (\text{radiation reflected by surface } i) \\
&= \varepsilon_i E_{bi} + r_i G_i \\
&= \varepsilon_i E_{bi} + (1 - \varepsilon_i) G_i \qquad (2.26)
\end{aligned}
$$

2.5.1 Net radiation heat transfer at a surface

The effect of radiative interactions at a surface determine whether a surface losses energy or whether it gains energy. A surface loses energy by emitting radiation and gains energy by absorbing radiation emitted by other surfaces. Depending on which quantity is greater a surface will experience an overall gain or loss of energy.

The net rate at which radiation heat transfers from a surface i of surface area A_i given as q_i, is expressed as:

$$
\begin{aligned}
q_i &= \text{(radiation leaving entire surface } i\text{)} - \text{(radiation incident on entire surface } i\text{)} \\
&= A_i(J_i - G_i) \\
&= \frac{(E_{bi} - J_i)}{(1-\varepsilon_i)/\varepsilon_i A_i}
\end{aligned}
\tag{2.27}
$$

Depending on the relative magnitudes of the radiosity (J_i) and the emissive power of a blackbody at the temperature of the surface (E_{bi}), the direction of the net rate of heat transfer is determined. If $E_{bi} > J_i$, the direction is from the surface and if $E_{bi} < J_i$, the direction is to the surface. If q_i is negative, it indicates that the heat transfer is to the surface.

2.5.2 Net radiation heat transfer between surfaces

The net rate of radiation heat transfer from surface i to the sum of the surfaces involved in the radiative exchange can be expressed as the following:

$$
q_{ij} = \begin{pmatrix} \text{radiation leaving entire} \\ \text{surface } i \text{ that} \\ \text{strikes surface } j \end{pmatrix} - \begin{pmatrix} \text{radiation leaving entire} \\ \text{surface } j \text{ that} \\ \text{strikes surface } i \end{pmatrix}
$$

$$= A_i J_i F_{ij} - A_j J_j F_{ji}$$

$$= \sum_{j=1}^{N} A_i F_{ij} \left(J_i - J_j\right) \tag{2.28}$$

2.6 Methods of solving radiation problems

When an analysis of the radiation of an enclosure is performed, either the surface temperature, T_i, or the net rate of heat transfer, q_i, must be known for each surface. This is necessary to obtain a unique solution for the unknown surface temperatures and heat transfer rates.

The conservation of energy principle requires that in an N-surface enclosure, the net heat transfer from surface i be equal to the sum of the net heat transfers from surface i to each of the N surfaces of the enclosure. The relation that describes this principle is given in equation (2.29).

$$q_i = \sum_{j=1}^{N} q_{ij} = \sum_{j=1}^{N} \frac{\left(J_i - J_j\right)}{\left(A_i F_{ij}\right)^{-1}} \tag{2.29}$$

This relation is especially useful when the net radiation heat transfer rate, q_i is known. However this may not always be the case. Typically the situation exists that the surface temperature, T_i (hence E_{bi}) is known and equation (2.30) proves more useful. This equation is a combination of equations (2.27) and (2.29), which is given as,

$$\frac{\left(E_{bi} - J_i\right)}{\left(1-\varepsilon_i\right)/\varepsilon_i A_i} = \sum_{j=1}^{N} \frac{\left(J_i - J_j\right)}{\left(A_i F_{ij}\right)^{-1}} \tag{2.30}$$

The equations (2.29) and (2.30) give rise to N linear algebraic equations when determining the N unknown radiosities for an N-surface enclosure. After determining the radiosities $J_1, J_2, \ldots, J_N$ the unknown surface temperatures and heat transfer rates are derived from equations (2.29) and (2.30) respectively.

The *matrix method* is a direct means of solving radiation heat transfer problems. These problems typically involve the use matrices especially when many surfaces are engaged. The use of iteration or matrix inversion to solve a problem involving any N number of surfaces may be obtained by rearranging equation (2.29) or (2.30) to get the following system of N equations:

$$\begin{bmatrix} a_{11}J_1 + \ldots + a_{1i}J_i + \ldots + a_{1N}J_N = C_1 \\ \ldots\ldots\ldots\ldots\ldots\ldots \\ \ldots\ldots\ldots\ldots\ldots\ldots \\ a_{i1}J_1 + \ldots + a_{ii}Ji + \ldots + a_{iN}J_N = C_i \\ \ldots\ldots\ldots\ldots\ldots\ldots \\ \ldots\ldots\ldots\ldots\ldots\ldots \\ a_{N1}J_1 + \ldots + a_{Ni}J_i + \ldots + a_{NN}J_N = C_N \end{bmatrix}$$

$$[A][J] = [C]$$

where: $$[A] = \begin{bmatrix} a_{11}\ldots a_{1i}\ldots a_{1N} \\ \ldots\ldots\ldots \\ \ldots\ldots\ldots \\ a_{11}\ldots a_{1i}\ldots a_{1N} \\ \ldots\ldots\ldots \\ \ldots\ldots\ldots \\ a_{11}\ldots a_{1i}\ldots a_{1N} \end{bmatrix} \qquad [J] = \begin{bmatrix} J_I \\ . \\ . \\ J_i \\ . \\ . \\ J_N \end{bmatrix} \qquad [C] = \begin{bmatrix} C_I \\ . \\ . \\ C_i \\ . \\ . \\ C_N \end{bmatrix}$$

$$\begin{bmatrix} J_1 = b_{11}C_1 + \ldots + b_{1i}C_i + \ldots + b_{1N}C_N \\ \ldots\ldots\ldots\ldots\ldots\ldots \\ \ldots\ldots\ldots\ldots\ldots\ldots \\ J_i = b_{i1}C_1 + \ldots + b_{ii}C_i + \ldots + b_{iN}C_N \\ \ldots\ldots\ldots\ldots\ldots\ldots \\ \ldots\ldots\ldots\ldots\ldots\ldots \\ J_N = b_{N1}C_1 + \ldots + b_{Ni}C_i + \ldots + b_{NN}C_N \end{bmatrix}$$

$$[J]=[A]^{-1}[C]$$

where:

$$[A]^{-1}=\begin{bmatrix} b_{11}..b_{1i}..b_{1N} \\ .... \\ .... \\ b_{i1}..b_{ij}..b_{iN} \\ .... \\ .... \\ b_{N1}..b_{Ni}..b_{NN} \end{bmatrix}$$

An alternative method called the *network method* is based on the electrical network analogy (Ohm's law). Oppenheim first suggested this method in the 1950's and because of its simplicity and emphasis on the physics of the problem found widespread acceptance. This method involves representing a *surface resistance* related to each surface of an enclosure and joining this with space resistances.

From equation 2.27, the surface resistance to radiation is obtained as follows,

$$R_i=\left(\frac{1-\varepsilon_i}{\varepsilon_i A_i}\right) \tag{2.31}$$

Equation 2.21 then becomes,

$$q_i=\frac{(E_{bi}-J_i)}{R_i} \tag{2.32}$$

Applying Ohm's law to equation (2.32), the electrical analogy relates the quantity $(E_{bi}-J_i)$ to a potential difference and the net rate of heat transfer corresponds to current as illustrated in fig 2.7 below.

The surface resistance to radiation for a blackbody is *zero*, since $\varepsilon_i=1$ and $E_{bi}=J_i$.

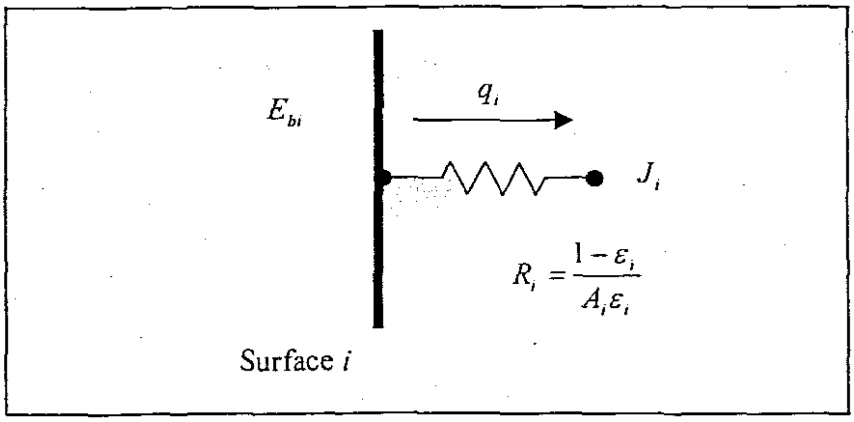

Figure 2.7 Electrical analogy of surface resistance to radiation

A real surface can be modelled as being *adiabatic*, if one of its sides is well insulated and the effect of convection on the other side is negligible and steady-state conditions are achieved, the net rate of heat transfer though the surface is zero. This means that the surface looses as much energy as it gains. Such a surface is known as a *reradiating surface* and from equation (2.32) setting $q_i = 0$ yields the following:

$$J_i = E_{bi} = \sigma T_i^4 \qquad (2.33)$$

The temperature of a reradiating surface is *independent of its emissivity.* The surface resistance of a reradiating surface is neglected because there is no net heat transfer across it. (Similar to the electrical analogy if there is no current through a resistor it can be neglected.)

The *space resistance* is obtained from equation (2.28) and expressed as,

$$R_{ij} = \left(A_i F_{ij}\right)^{-1} \qquad (2.34)$$

Equation 2.28 then becomes,

$$q_{ij} = \sum_{j=1}^{N} \frac{(J_i - J_j)}{R_{ij}} \tag{2.35}$$

Repeating the Ohm's law analogy in equation (2.28), $(J_i - J_j)$ relates to a potential difference and the net rate of heat transfer between two surfaces correlates to current as shown in figure 2.8.

When applying the network method it is generally limited to simple enclosures i.e. enclosures consisting of three or four surfaces, due to the increased complexity of the network.

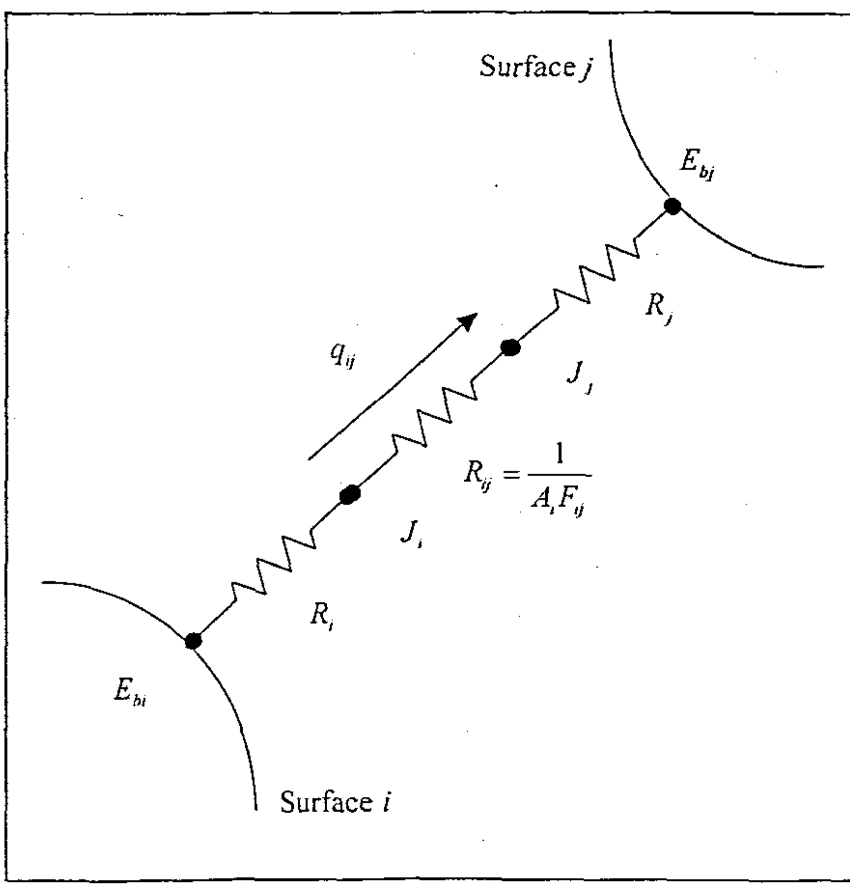

Figure 2.8 Electrical analogy of space resistance to radiation

2.7 Radiation heat transfer in two-surface enclosures

The simplest example of an enclosure is one consisting of two opaque surfaces at individual temperatures T_1 and T_2, that exchange radiation only with each other as illustrated in fig 2.9. The net rate of radiation heat transfer *from* surface 1, q_1, should equal the net rate of radiation heat transfer *to* surface 2, $-q_2$, and furthermore the sum of these quantities should equal the rate at which radiation heat is transferred between 1 and 2, expressed as, $q_1 = -q_2 = q_{12}$.

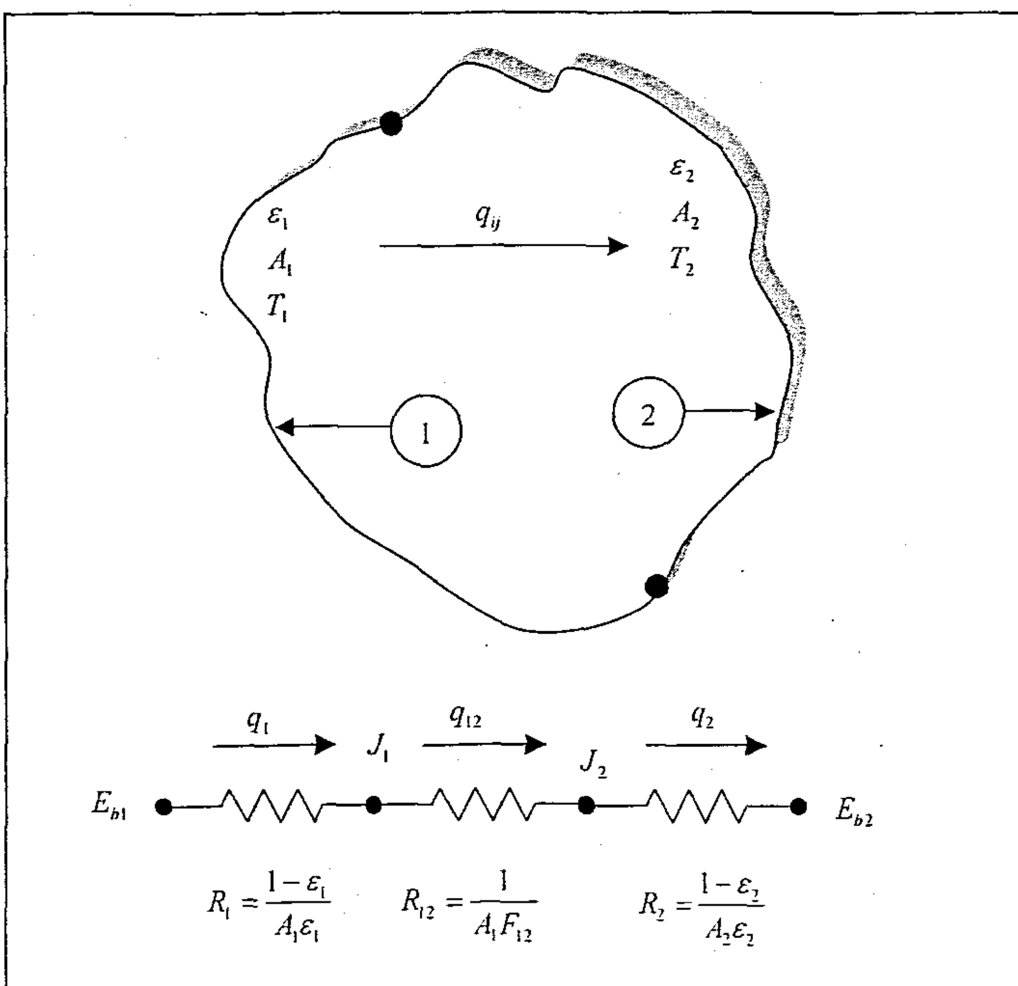

Figure 2.9 Schematic of a two-surface enclosure and the radiation network associated with it.

The network representation of this enclosure consists of two surface resistances and one space resistance, as shown in fig. 2.9. When determining the electrical current through a series of resistances in an electrical network, the potential difference across the total resistance is divided by the sum of these resistances. The net rate of radiation heat transfer is obtained in a similar manner, and may be expressed as

$$q_{12} = \frac{\sigma\left(T_1^4 - T_2^4\right)}{\frac{1-\varepsilon_1}{\varepsilon_1 A_1} + \frac{1}{A_1 F_{12}} + \frac{1-\varepsilon_2}{\varepsilon_2 A_2}} \tag{2.36}$$

This significant result may be used for any two diffuse, gray, opaque surfaces that form an enclosure. The geometry of the enclosure determines the view factor F_{12}. Table 2.1 below summarises some special cases where $F_{12} = 1$.

2.8 Radiation heat transfer in three-surface enclosures

For an enclosure constituting three opaque, diffuse, gray surfaces, as depicted in fig. 2.10, with the surfaces having respective emissivities, surface areas and uniform temperatures, the network of this geometry is evaluated by representing surface resistances for each of the surfaces and joining these with space resistances, as illustrated in fig. 2.11. If the surface temperatures are known, the end-point potentials E_{b1}, E_{b2} and E_{b3} are then simply derived. The radiosities J_1, J_2 and J_3 are solved from the condition that the *algebraic sum of the currents (net radiation heat transfer) at each node must equal zero.* The set of equations obtained from this requirement that need to be solved for are given below.

$$\begin{aligned}
&\frac{E_{b1} - J_1}{R_1} + \frac{J_2 - J_1}{R_{12}} + \frac{J_3 - J_1}{R_{13}} = 0 \\
&\frac{J_1 - J_2}{R_{12}} + \frac{E_{b2} - J_2}{R_2} + \frac{J_3 - J_2}{R_{23}} = 0 \\
&\frac{J_1 - J_3}{R_{13}} + \frac{J_2 - J_3}{R_{23}} + \frac{E_{b3} - J_3}{R_3} = 0
\end{aligned} \tag{2.37}$$

Table 2.1 Special Diffuse, Gray, Two-Surface Enclosures

Large (infinite) Parallel Planes

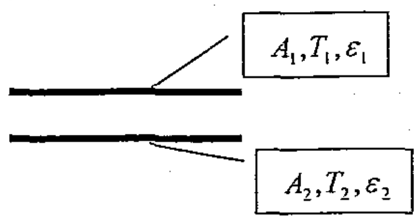

$A_1 = A_2 = A$ and $F_{12} = 1$

$$q_{12} = \frac{A\sigma\left(T_1^4 - T_2^4\right)}{\frac{1}{\varepsilon_1} + \frac{1}{\varepsilon_2} - 1} \qquad (2.37a)$$

Long (infinite) Concentric Cylinders

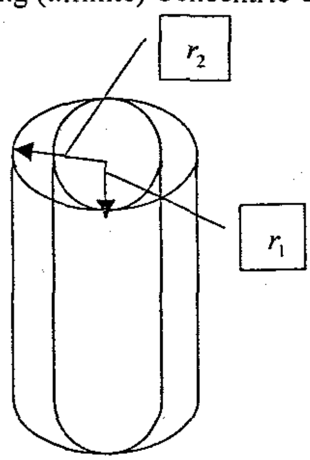

$\frac{A_1}{A_2} = \frac{r_1}{r_2}$ and $F_{12} = 1$

$$q_{12} = \frac{\sigma A_1\left(T_1^4 - T_2^4\right)}{\frac{1}{\varepsilon_1} + \frac{1-\varepsilon_2}{\varepsilon_2}\left(\frac{r_1}{r_2}\right)} \qquad (2.37b)$$

Concentric Spheres

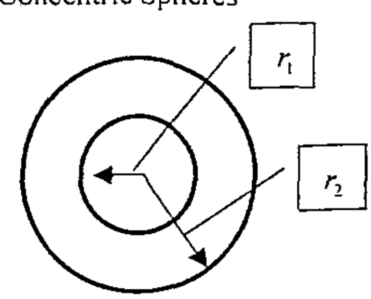

$\frac{A_1}{A_2} = \frac{r_1^2}{r_2^2}$ and $F_{12} = 1$

$$q_{12} = \frac{\sigma A_1\left(T_1^4 - T_2^4\right)}{\frac{1}{\varepsilon_1} + \frac{1-\varepsilon_2}{\varepsilon_2}\left(\frac{r_1}{r_2}\right)^2} \qquad (2.37c)$$

Small Convex Object in a Large Cavity

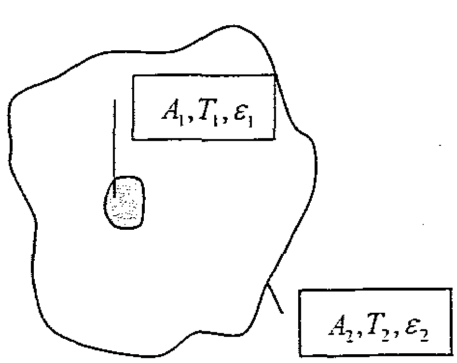

$\frac{A_1}{A_2} \approx 0$ and $F_{12} = 1$

$$q_{12} = \sigma A_1 \varepsilon_1\left(T_1^4 - T_2^4\right) \qquad (2.37d)$$

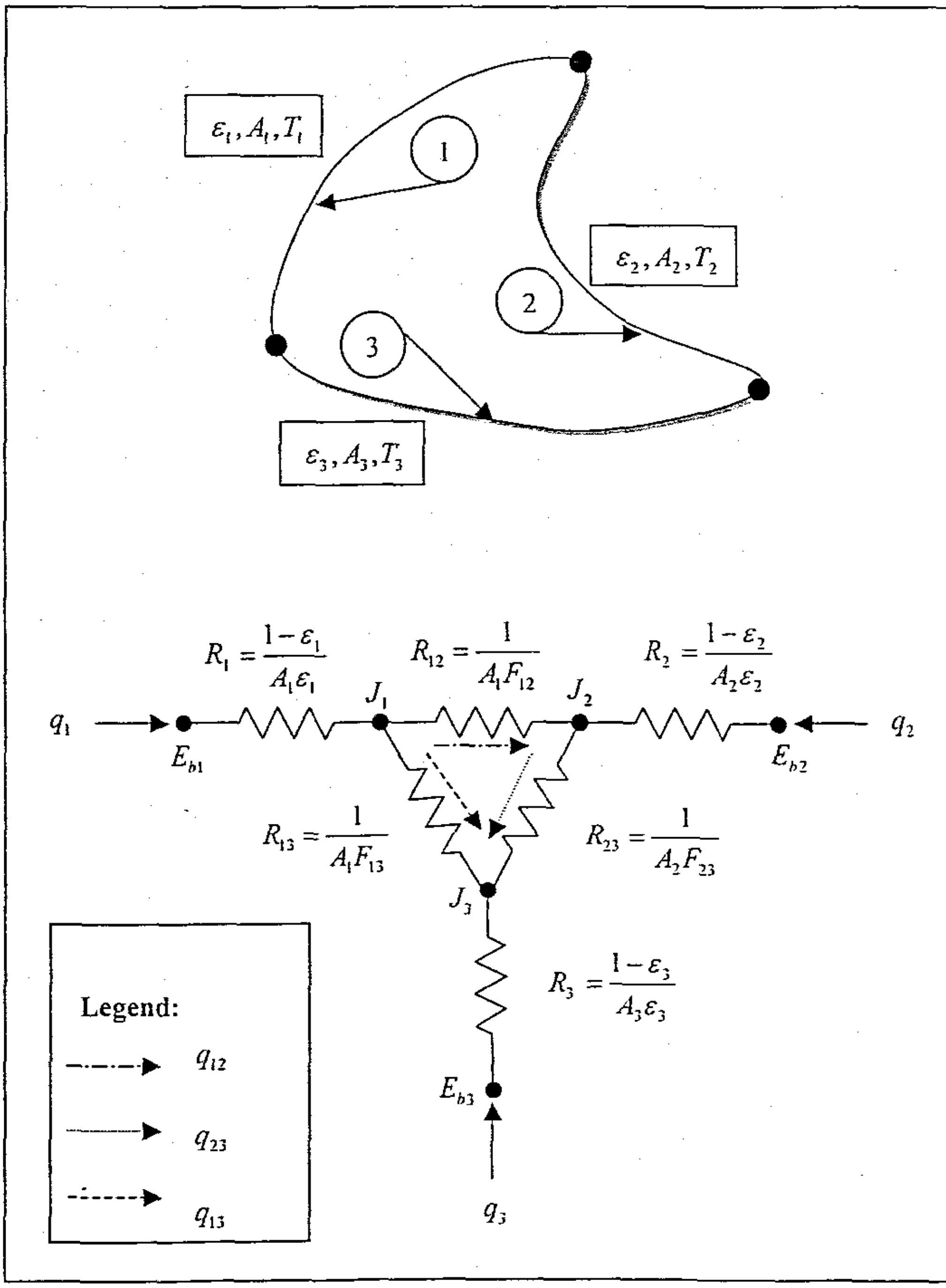

Figure 2.10 Schematic of a three-surface enclosure and the radiation network associated with it.

After finding the radiosities J_1, J_2 and J_3, using equation (2.35) the net rate of radiation heat transfer at each surface is determined. Further simplification of the set of equalities in equation 2.37 is possible if one or more surfaces exhibit blackbody behaviour such that $J_i = E_{bi} = \sigma T_i$ or if one surface is reradiating then $q_i = 0$.

2.9 Radiation shields

Sometimes it may be necessary to reduce the net radiation heat transfer between two surfaces using a *radiation shield* that is constructed of material with a low emissivity (high reflectivity). This material inserted between the two surfaces diminishes the rate of radiation heat transfer by introducing additional resistances in the path of radiation heat flow. A shield with a low emissivity represents a high resistance.

Equation (2.37a) represents the radiation heat transfer (with no shield) between two large parallel plates with emissivities ε_1 and ε_2 sustained at uniform temperatures T_1 and T_2. If a radiation shield were inserted between these two plates as depicted in fig. 2.11, the resultant net rate of radiation heat transfer is given by equation 2.38.

The emissivity associated with one side of the shield ($\varepsilon_{3,1}$) may differ from that associated with the opposite side ($\varepsilon_{3,2}$) and consequently the radiosities will differ. Applying the network method to this geometry and recognizing that $F_{13} = F_{32} = 1$, also that $A_1 = A_2 = A_3 = A$ for parallel plates an expression for the net rate of radiation heat transfer is simplified as shown below.

$$q_{12} = \frac{A\sigma(T_1^4 - T_2^4)}{\left(\frac{1}{\varepsilon_1} + \frac{1}{\varepsilon_2} - 1\right) + \left(\frac{1}{\varepsilon_{3,1}} + \frac{1}{\varepsilon_{3,2}} - 1\right)} \qquad (2.38)$$

The equilibrium temperature of the shield, T_3, is determined from the fact that at steady-state conditions $q_{12} = q_{13} = q_{32}$ and expressing equation (2.37a) for q_{13} or q_{32}. For a configuration consisting of N radiation shields the net rate of radiation heat transfer is expressed as:

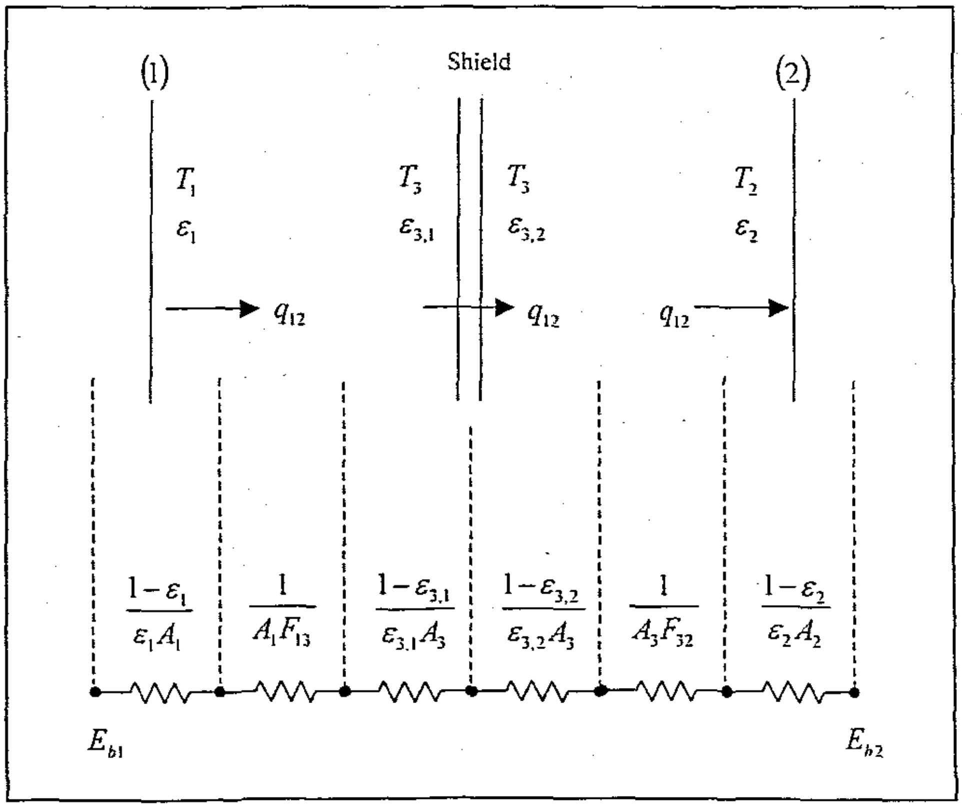

Figure 2.11 The radiation network associated with a radiation shield placed between two parallel plates.

$$q_{12,N\text{ shields}} = \frac{A\sigma(T_1^4 - T_2^4)}{\left(\frac{1}{\varepsilon_1} + \frac{1}{\varepsilon_2} - 1\right) + \left(\frac{1}{\varepsilon_{3,1}} + \frac{1}{\varepsilon_{3,2}} - 1\right) + \ldots + \left(\frac{1}{\varepsilon_{N,1}} + \frac{1}{\varepsilon_{N,2}} - 1\right)} \tag{2.39}$$

For the special case when the emissivities of all the surfaces are equal, equation 2.39 becomes,

$$q_{12,N\text{ shields}} = \left(\frac{1}{N+1}\right)\left(q_{12,\text{no shields}}\right) \tag{2.40}$$

2.10 Participating Media

The means developed thus far for predicting radiation exchange between surfaces has inherent restrictions. We have considered isothermal, opaque, gray surfaces that emit and reflect diffusely and additionally also characterized by uniform surface radiosity and irradiation. For enclosures, the medium separating them was considered nonparticipating or transparent, which means it neither absorbs nor scatters the surface radiation and emits no radiation of its own, it does not participate in the heat transfer process.

The equations based on the preceding assumptions in most instances provide highly accurate results for radiation heat transfer in an enclosure. This is the case when the space separating the radiating surfaces is occupied by vacuum or by a gas with monatomic or symmetrical diatomic molecules (nonpolar). The gases that satisfy this criteria include the following; the main components of air (N_2, O_2), H_2, Ne, Ar and Xe. There are times however when the preceding assumptions are inappropriate because the separating medium scatters or absorbs radiation passing through it and emits radiation of its own. Examples of these types of media are strongly polar gases such as CO_2, H_2O (vapour), NH_3, SO_2, hydrocarbons and alcohols.

Gaseous radiation as opposed to radiation from a solid or liquid is not a surface phenomenon but characterized by a volumetric absorption, transmission and emission of radiation. Gaseous radiation is concentrated in specific wavelength intervals or bands. Radiation with a wavelength outside these bands will pass unattenuated through the medium and with respect only to this radiation the medium is nonparticipating.

Spectral radiation absorption in a gas (or in a semitransparent liquid or solid) is a function of the thickness L of the medium and the absorption coefficient κ_λ, which has units m^{-1}. If a monochromatic beam of intensity $I_{\lambda,0}$ is incident on the medium, the intensity is reduced due to absorption. Beer's law, equation 2.41, is a useful tool in approximate radiation analysis and may be used to infer the overall spectral absorptivity of the medium.

$$I_{\lambda,L} = I_{\lambda,0} e^{-\kappa_\lambda L} \tag{2.41}$$

The transmissivity of the medium is defined as,

$$\tau_\lambda = \frac{I_{\lambda,L}}{I_{\lambda,0}} = e^{-\kappa_\lambda L} \tag{2.42}$$

and the absorptivity of the medium is given as,

$$\alpha_\lambda = 1 - \tau_\lambda = 1 - e^{-\kappa_\lambda L} \tag{2.43}$$

In addition if the temperature of the gas T_g is uniform and does not differ noticeably from the temperature T_s of the surface that produced the beam of intensity $I_{\lambda,0}$, we may assume Kirchoff's law as valid such that,

$$\varepsilon_\lambda = \alpha_\lambda = 1 - e^{-\kappa_\lambda L} \tag{2.44}$$

2.10.1 Gaseous Emission and Absorption

A method to determine the radiant heat flux from a gas to an adjoining surface was developed by Hottel (1954). This is a simplified procedure that involves determining radiation emission from a hemispherical gas mass of temperature T_g, to a small area A_s, which is located at the center of the hemisphere's base. The radiation heat rate that is emitted by the gas and arrives at A_s is,

$$q_{g \to s} = \varepsilon_g A_s \sigma T_g^4 \tag{2.45}$$

The gas emissivity ε_g is obtained by correlating data in terms the temperature T_g, the total pressure p of the gas, the partial pressure p_g of the radiating species and the radius L of the hemisphere. This result is sufficient when the gas mixture consists of one radiating gas for instance water vapour or carbon dioxide and other nonradiating species. However when two radiating gases appear together in a mixture with other nonradiating gases, the total gas emissivity may be expressed as,

$$\varepsilon_g = \varepsilon_w + \varepsilon_c - \Delta\varepsilon \tag{2.46}$$

The correction factor $\Delta\varepsilon$ given in available literature for different values of the gas temperature, accounts for the reduction in emission associated with the mutual absorption of radiation between the two gases. If the surface surrounding the gas is black, it will naturally absorb all the radiation that is emitted by the gas. The net rate at which radiation is exchanged between the surface at T_s and the gas at T_g is given as,

$$q_{g\to s} = A_s\sigma\left(\varepsilon_g T_g^4 - \alpha_g T_s^4\right) \tag{2.47}$$

The total gas absorptivity when both water vapour and carbon dioxide are present may be expressed as, $\alpha_g = \alpha_w + \alpha_c - \Delta\alpha$, where $\Delta\alpha = \Delta\varepsilon$.

In order to calculate the required gas absorptivity α_g of either water vapour or carbon dioxide the following expressions are given by Hottel (1954).

Water: $$\alpha_w = C_w\left(\frac{T_g}{T_s}\right)^{0.45} \times \varepsilon_w\left(T_s, p_w L_e \frac{T_s}{T_g}\right) \tag{2.48}$$

Carbon Dioxide: $$\alpha_c = C_c\left(\frac{T_g}{T_s}\right)^{0.65} \times \varepsilon_c\left(T_s, p_c L_e \frac{T_s}{T_g}\right) \tag{2.49}$$

3. CONTROLLER DESIGN

3.1 Mathematical modeling and experiments

The aspects of modeling in an IR system usually concern either the IR lamp or the industrial application. Infrared dryers are an integral part of many commercial enterprises and infrared drying an essential process for many businesses in manufacturing. Studies of infrared drying kinetics and drying phenomena are limited, but there are several publications concerning heat and energy transfer in infrared dryers and some are presented below.

3.1.1 Overview of infrared drying studies

The studies available are limited to applications involving paint, foodstuffs and continuous sheets of paper and textiles. An experimental study performed by Parouffe *et al* (1992) on the combined effect of infrared and convective drying of glass beads investigated the drying characteristics and the influence of thermal radiation on convective heat and mass transfer. Drying experiments performed by Navarri *et al* (1992) on a wet sand layer subjected to intensive infrared radiation were analysed and a simple model was developed, able to predict drying rates and surface temperatures. A further model resulted from experiments by Navarri and Andrieu (1993), delivered a model that is able to predict drying rates and temperature profiles down to zero moisture content. Studies on infrared drying characteristics of wet porous materials in comparison with convective drying results conducted by Hashimoto and Kameoka (1998) used three kinds of membrane filters with differing mean pore diameters.

A method for the calculation of the drying time and surface temperature of water based paints during both convective and infrared drying was presented by Silventoinen and Palosaari (1982). The model integrated mass and energy balances with an experimental characteristic-drying curve. Rösler *et al* (1995) performed drying experiments with water-based paints and organic coatings using infrared heaters with various emission spectra. In the experimental work of Blanc *et al* (1997a) they presented some models relating convective and infrared drying of reactive automotive paints. These paints are sensitive to the vaporization process and are coupled with a polymerization reaction in the paint film. Experimental and modeled drying curves were presented and techniques for monitoring the reaction and drying kinetics were discussed. Methods for studying the reaction kinetics during the infrared curing of epoxy-based automotive paints were developed by Blanc *et al* (1997b) along with related changes in structure and in rheological behaviour.

An investigation by Le Person *et al* (1998) on the drying of a thin multicomponent film produced for pharmaceutical purposes. Measurements of the internal concentration gradients and the results were combined with drying rate data in order to obtain a better understanding of the drying process and of the multicomponent transport phenomena involved. With this information they were able to explain and prevent the occurrences of mechanisms detrimental to product quality.

An analysis of an application of infrared drying in food manufacturing by Sandu (1986) discussed transport phenomena and process applications. Yamasaki *et al* (1992) investigated the infrared drying of food through the use of gelatinous materials as model substances. Numerous factors that influenced drying rate and shrinkage as well as the radiative properties of the product and heater were examined experimentally and were compared to with a simple drying model. A set of heat and mass transfer equations were proposed by Fasina *et al* (1998) to simulate the infrared drying of agricultural crops. A comparison was made with the model and experimental data on the surface temperature and average moisture content of barley kernels found on a vibrating conveyor exposed to infrared radiation. More drying experiments performed by Afzal and Abe (1999) used an infrared heater to investigate the drying characteristics of potato slices. They investigated the effects of several parameters on drying rate and product temperature history.

An investigation by Broadbent *et al* (1994) on the many parameters that influence drying rates when a number of different textile fabrics were pre-dried in a pilot scale infrared dryer. In another study Dhib *et al* (1994) proposed a transient model, a set of partial differential equations, for the infrared drying of continuous thin sheets and calibrated the model by using data from a large number experiments on an infrared textile dryer. Experiments on varying conditions were investigated and the model predictions were found to be in good agreement with the experimental data. In another paper by Dhib *et al* (1998) these equations were analysed for controllability and observability after being reduced to a model adaptable to direct control. The aim of the model reduction contributed to the design of a model based controller for an infrared dryer.

Modeling experiments by Heikkilä (1993) on the drying of coated sheets of paper by infrared dryers proposed separate balance equations for the base sheet and the coating layer. The radiation energy was assumed to be evenly absorbed throughout the thickness of the sheet and was treated as a source term in the energy equations. Drying simulations by several techniques based on the model were used in a pilot machine and model predictions compared well with experimental results.

In reference to infrared drying in general considering the limited literature available this is an area in which there is a need of considerable research efforts. This is especially important in view of the many industrial applications possible with infrared radiation.

3.1.2 Mathematical models of electric IR heaters

Numerous models of gas-fired IR heaters have been presented in a number of studies in available literature. The models available range in complexity from very simple radiation exchange models to advanced models dealing with combustion and transport phenomena in porous media.

With respect to electric IR heaters, very few models are available. Some work regarding radiation exchange modeling in electric heaters has been conducted in studies concerning infrared paper drying (Lampinen *et al.*, 1991;Ojala *et al.*, 1995). The type of IR heater modeled in this case is of the glass enclosed metal filament type. The models they developed include non-gray radiation heat transfer between the filament, the reflector, the protective glass, the paper sheet and the back reflector. The radiative properties of some of the components were measured using an integrating sphere in the range 0.4 - 20μm. A related model was later developed by Pettersson (1998), which also incorporated the lamp glass in order to validate the spectral distribution of an electric IR heater, similar to that of figure 2.3.

An assumption made was that the temperatures of the various components were known and was used as input data for the model. A further assumption was that all the electricity supplied was converted to radiation at the filament (Pettersson, 1999). Because these models assume the temperature of the heater components to be known, they consequently do not characterise heater models completely. In their opinion Ojala and Lampinen caution that their results can only be regarded as quantitative, because the temperatures involved in their assumptions represent a wide margin of ambiguity. In addition Pettersson (1999) further elaborates that since the approach in the models developed utilised assumed temperatures, these results could possibly lead to impractical consequences with regard to the energy balances considered.

3.2 Overview of process control aspects

3.2.1 Mathematical description of a control system

A block diagram of a general control system in the Laplace domain is shown in figure 3.1 below. The feedforward transmission path transfer function is given by $G(s)$; $H(s)$ represents the feedback path transfer function. Typically the feedback element contains the sensor or transducer that measures a physical quantity, such as temperature and converts this measurement into a voltage. $H(s)$ therefore represents the gain of the sensor. The basic idea in many control systems is to make the controlled output, $c(t)$, follow the reference input, $r(t)$, as closely as possible. Therefore the desired transfer function is:

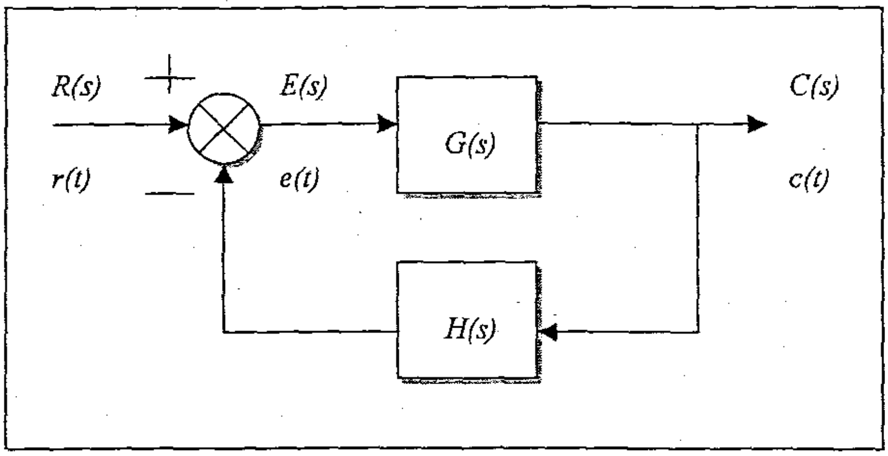

Figure 3.1 General analog control system

$$T(s) = \frac{C(s)}{R(s)} = 1 \tag{3.1}$$

If $r(t)$ varies with time, then the problem is commonly referred to as a tracking problem. However if the input remains constant, it is known as a regulator problem. If the output, $C(s)$, is not measured, $H(s) = 0$ and the system is open loop. Disturbances in the feedforward transmission path usually compound the problem of making $c(t)$ follow $r(t)$. Neglecting any disturbances, figure 3.1 illustrates the closed loop feedback system since the controlled variable is measured and used to control the system.

An expression for the error for the system is given by $E(s) = R(s) - H(s)C(s)$. However $C(s) = G(s)E(s)$. Solving these two equations the closed loop transfer function is:

$$T(s) = \frac{C(s)}{R(s)} = \frac{G(s)}{1 + G(s)H(s)} \tag{3.2}$$

With the addition of a controller to the forward transmission path of the control system, as shown in figure 3.2 the error in the system is diminished. A controller compares the actual value of the plant output, $c(t)$, with the reference input, $r(t)$, which is the desired value, then determines the deviation or error and produces a control signal that will reduces the error to zero or a small value.

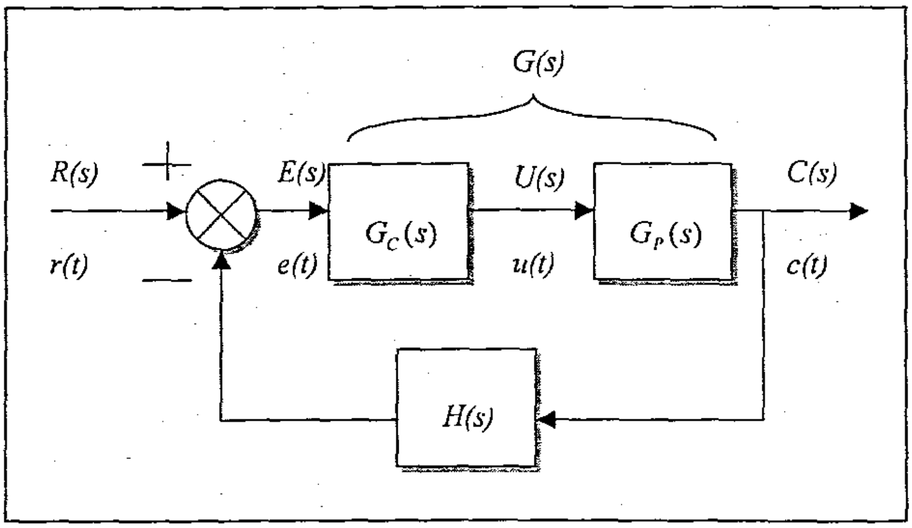

Figure 3.2 General feedback control system with compensation

The transfer function of the control system as depicted in figure 3.2 with unity feedback, *H(s)* = 1, is expressed as:

$$T(s) = \frac{C(s)}{R(s)} = \frac{G_c(s)G_p(s)}{1+G_c(s)G_p(s)} \tag{3.3}$$

The input to controller is the error signal, *E(s)*, and the output of the controller, *U(s)*, is the input to the plant under control, $G_p(s)$. Again the purpose of the controller is to ensure the output follows the input so that the condition in equation 3.1 is satisfied.

3.2.2 PID control of the plant

In practical temperature control applications, the problem or difficulty is the incidence of thermal time lag, which leads to conditions such as overshoot and temperature cycling. These effects are of acute importance when the product being processed or heated is temperature sensitive and in danger of being damaged in this way. While lag is usually unavoidable in a practical process, there are ways of limiting it.

For accurate control of the load temperature an effective controller is required. A closed loop proportional integrated controller (PID) satisfies this need by providing a stable regulated temperature control. It is well known that temperature loop dynamics can be slow because of process heat transfer lags, which is the case in medium and long wave infrared heaters. Short wave infrared heaters, quartz glass enclosed tungsten filament type, usually reach final temperature, typically between 2000°C and 2500°C, within a few seconds. Medium and long wave heaters, ceramic encased electric heating coil type, have heating constants in the order of minutes. Their maximum temperatures typically range from 600°C for long wave and 900°C for medium wave heaters. The slower heating constants for medium and long wave heaters imply the presence of significant dead time. Coupled with the fact that temperature systems are not normally noisy, PID control is usually preferred.

For optimal performance the type of heater chosen for a system should be one that has a low thermal mass (fast reaction time) or the temperature sensor employed should have a fast reaction time. Optical sensors when compared to other forms of sensing, such as thermocouples, provide the quickest temperature measurements and are consequently the type used in this paper. The PID controller required in order to satisfy the above criteria should be capable of reducing the heater power well ahead of the temperature reaching set point. This means that the power has to be minimised in proportion to the distance from the set point. This way the controller is capable of preventing temperature overshoot and cycling. This action describes it as a proportional controller (P). The relationship between the output of the controller and the actuating error signal is,

$$u(t) = K_p e(t) \qquad (3.4)$$

If the gain K_p, is high, the slightest error signal $e(t)$, results in a dramatic change in the output $u(t)$. With an increase in gain the rise time is reduced allowing the output to rapidly follow the input. When the proportional band, the range of error possible, is wide the output can be diminished sooner avoiding overshoot, but a temperature offset is usually the result. To maintain the temperature about the set point as accurately as possible, very often a manual reset of the control parameters is needed.

To automatically and continuously adjust the temperature by adjusting the power input, an integral action is needed. The controller needs to make the power increase in proportional to the deviation from the set point, so that the steady-state error is reduced to zero. The steady-state error is that deviation between system output and input after transient effects have died away. This is type of control is expressed as integral control and defined as,

$$u(t) = K_i \int_0^t e(t)d(t) \tag{3.5}$$

With the addition of this integral action the effect is a proportional + integral controller (PI), defined as,

$$u(t) = K_p e(t) + \frac{K_p}{T_i} \int_0^t e(t)d(t) \tag{3.6}$$

The output, $u(t)$, is controlled by adjusting the proportional gain, K_p and the integral time, T_i.

With the addition of derivative control, the controller anticipates changes in temperature and modifies the input power proportional to the rate of change of temperature. The purpose of this type of action is to minimise and damp unwanted changes and speeds recovery from temperature disturbances, which is effective during transient periods. The ensuing controller known as proportional + integral + derivative (PID) control combines the advantages of the three individual control actions and is defined as,

$$u(t) = K_p e(t) + \frac{K_p}{T_i} \int_0^t e(t)d(t) + K_p T_d \frac{de(t)}{d(t)} \tag{3.7}$$

When a comparison of three types of controllers to a step function is made, the curves obtained in figure 3.3 results. A step function represents a radical change in system input, and the system response is a good indication of the controller's performance

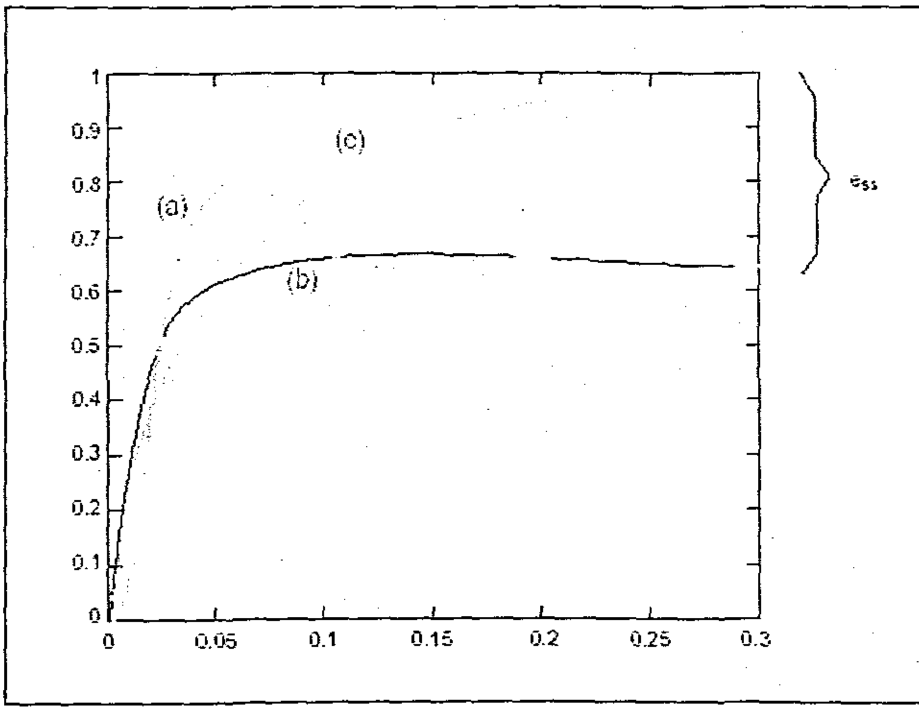

Figure 3.3 Step response of a closed loop feedback system shown for (a) P controller, (b) PI controller and (c) PID controller

when subjected to a disturbance. The PID controller clearly provides the most stable output ensuring that the steady-state error, e_{ss}, is diminished to zero.

If a mathematical model of the plant is not known, then it is possible to apply diverse design techniques for determining parameters of the controller that will satisfy the transient and steady-state specifications of the closed-loop system. The simplest approach in the design of PID controllers is an experimental one.
The process of selecting the controller parameters in order to obtain the required performance conditions is known as controller tuning. Ziegler-Nichols proposed rules for determining values of the proportional gain K_p, integral time T_i and derivative time T_d, based on the transient response characteristics of a given plant (Leigh, 1988). The transfer function $G_c(s)$ of the PID controller is given as:

$$G_c(s) = K_p\left(1+\frac{1}{T_i s}+T_d s\right) \tag{3.8}$$

3.3 Controller Design

3.3.1 Identification of the infrared oven (heater)

In order to obtain a mathematical description of the IR heater, a transfer function, the method outlined below was completed. This method is the Ziegler-Nichols design approach. Known as the process reaction method, it requires the open-loop step response of the process to be recorded and is a practical means of acquiring the transfer function of the IR heater. There are two methods for Ziegler-Nichols tuning, both aimed at obtaining 25% maximum overshoot in step response. The process reaction method was chosen because the curve resulting from a unit-step input resembled an S-shaped curve as depicted in figure 3.4. The type of IR heater used was a medium wave infrared ceramic type. The S-shaped curve is characterised by two constants, delay time L and time constant T. By drawing a tangent line at the inflexion point of the S-shaped curve and determining the intersections of the tangent line with the time axis and the line $c(t) = K$, the values for the delay time and time constant are determined. The transfer

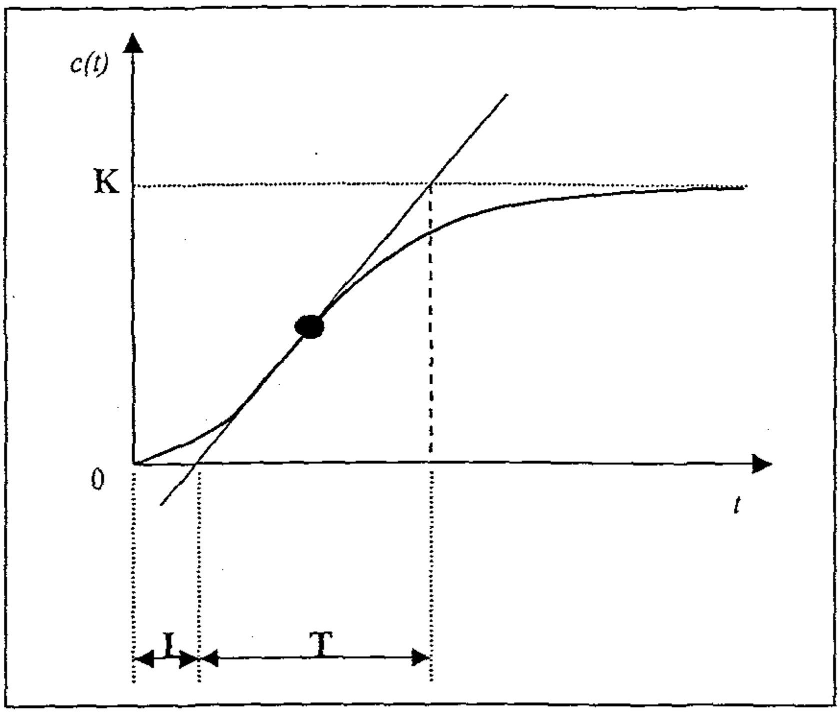

Figure 3.4 S-shaped open loop step response curve

function $G_p(s) = C(s)/U(s)$, equation 3.9, is approximated by a first-order system with a transport lag:

$$G_p(s) = \frac{C(s)}{U(s)} = \frac{Ke^{-Ls}}{Ts+1} \tag{3.9}$$

Table 3.1 indicates the suggested values for the controller parameters as described by Ziegler-Nichols process reaction method.

Table 3.1 Ziegler-Nichols tuning rules based on step response of plant

Type of Controller	K_p	T_i	T_d
P	$\left(T/L\right)$	∞	0
PI	$0.9\left(T/L\right)$	$\left(L/0.3\right)$	0
PID	$1.2\left(T/L\right)$	$2L$	$0.5L$

3.3.2 Experimental Results for step response of the plant

The open loop step response of the IR heater under test resulted in the curves shown in the figures 3.5 to 3.8 below.

The curve in figure 3.8 was chosen as a reasonable compromise for the step response of the plant under test. Using the Ziegler-Nichols process reaction method as described in figure 3.4, the plant (infrared heater) was found to have an approximate transfer function as expressed by equation 3.10.

$$G_p(s) = \frac{3.96e^{-7s}}{140s+1} \tag{3.10}$$

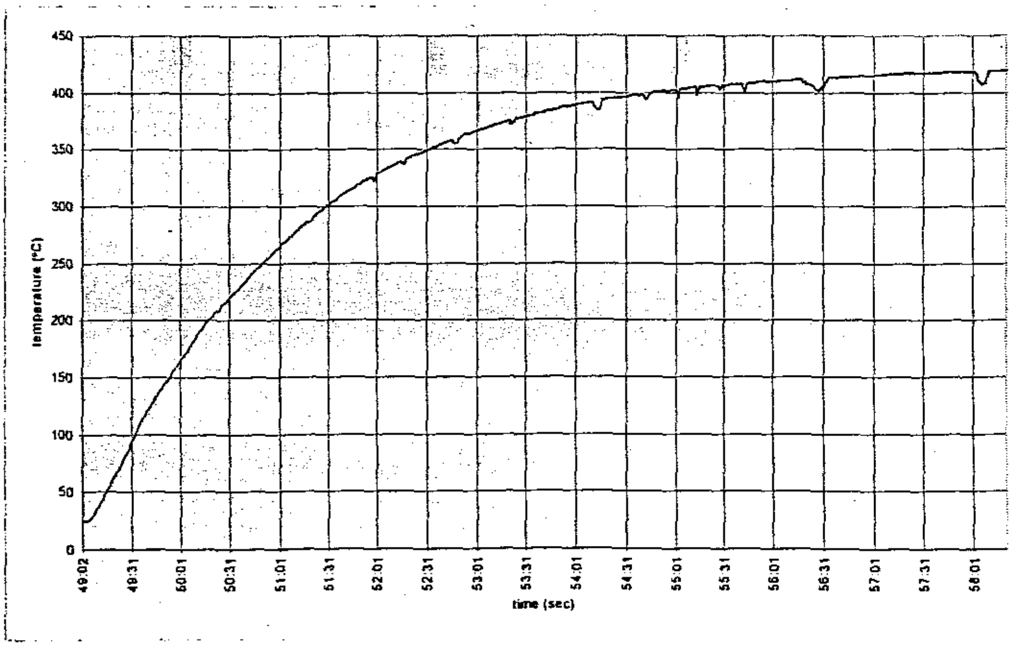

Figure 3.5 Infrared heater warm-up curve (phase 1)

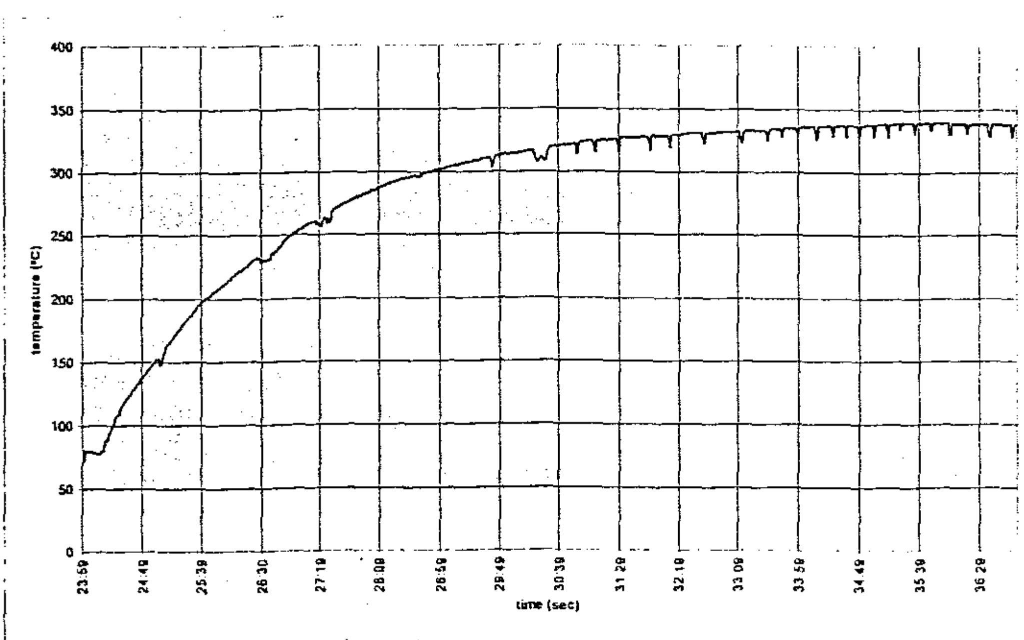

Figure 3.6 Infrared heater warm-up curve (phase 2)

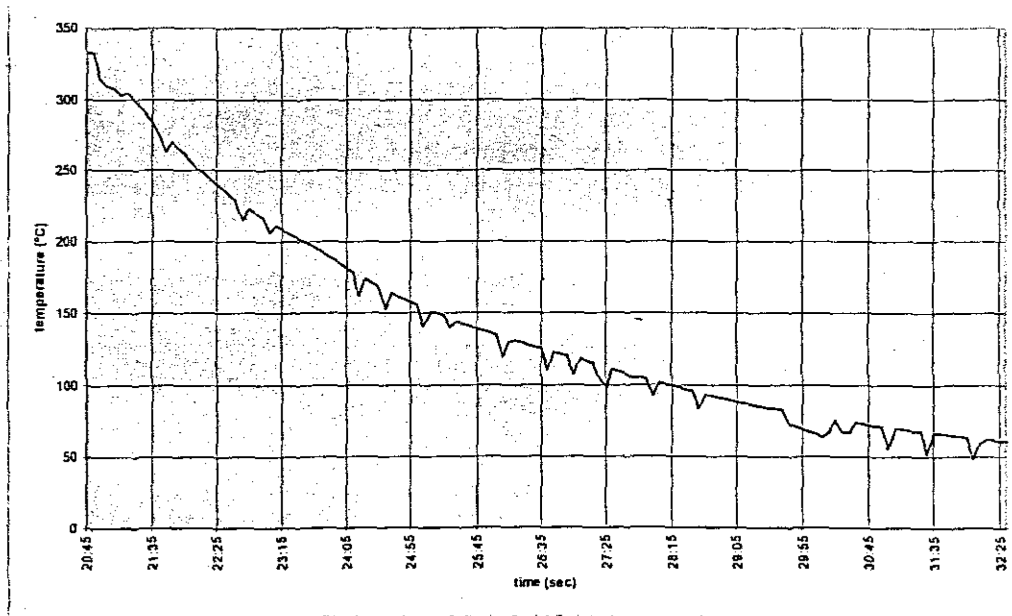

Figure 3.7 Infrared heater cool-down curve (phase 3)

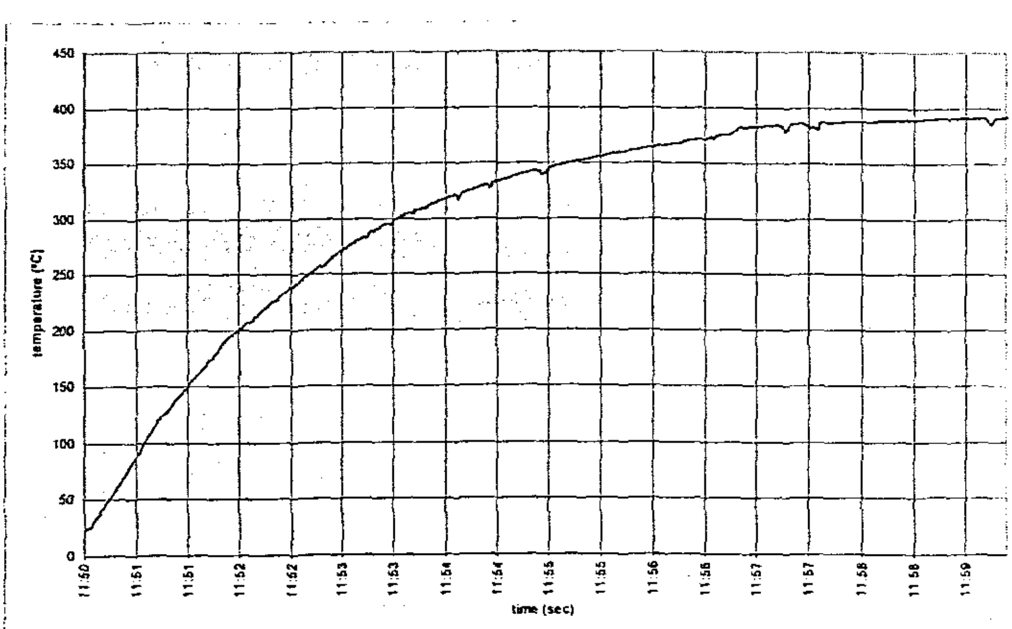

Figure 3.8 Infrared heater warm-up curve (phase 4)

In order to verify the validity of equation 3.10, a simulation of the step response using MATLAB software was performed. The simulation resulted in the curve in figure 3.9. The trajectory in figure 3.9 is fairly accurate, but a slight adjustment of the gain, K_p, from 3.96 to 4.2 provides a better step response for the plant. The curve for the new step response is given in figure 3.10.

3.3.3 Design of a continuous controller followed by discretisation

Using the Ziegler-Nichols rules as described in table 3.1 above, the coefficients of a three-term PID continuous controller calculated resulted in the following values for, K_p, T_i and T_d in equation 3.11. From the general form for a PID controller in equation 3.8, the expression for the continuous PID controller is given.

$$G_c(s) = 6.06\left(1 + \frac{1}{14s} + 3.5s\right) \tag{3.11}$$

In order to implement the controller on a digital platform, as illustrated by figure 3.11, discretisation of the continuous expression is needed. There are various ways to do this, but two methods dominate.

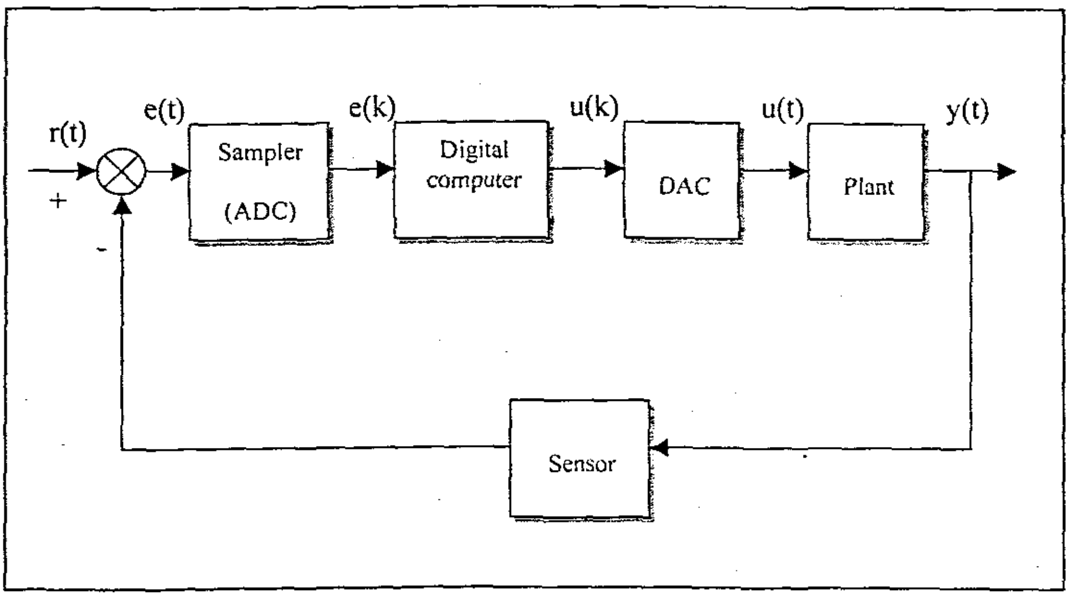

Figure 3.9 Digitally controlled plant

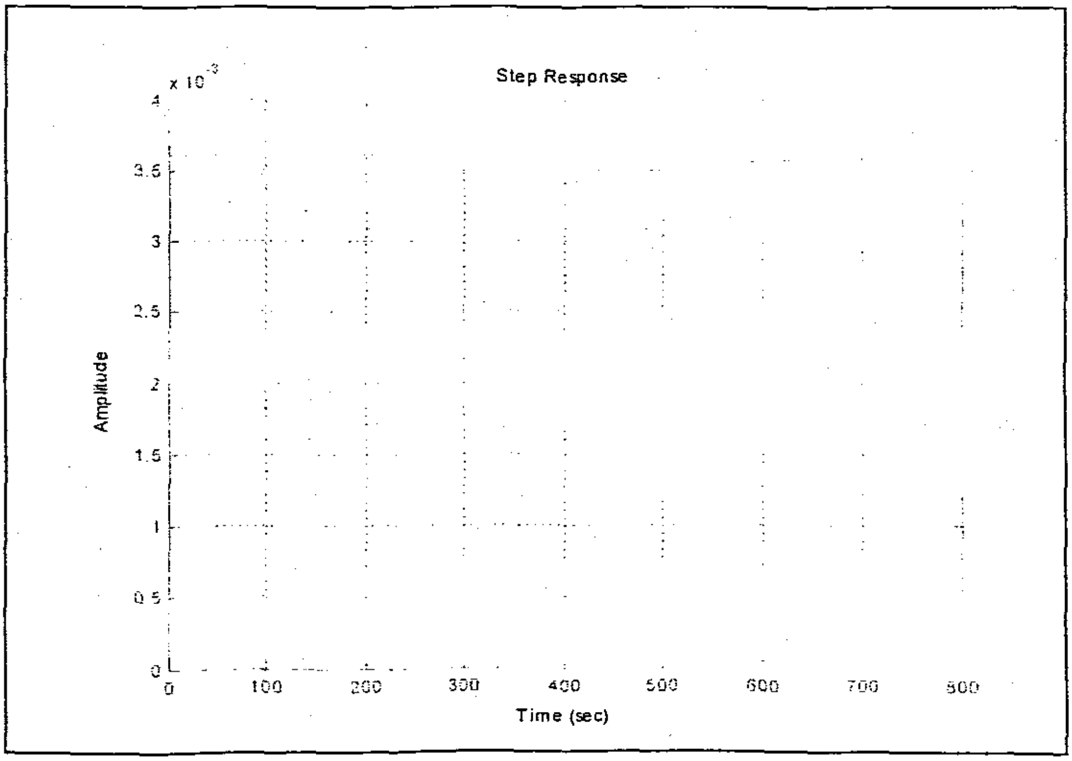

Figure 3.10 Step response of plant with Kp = 3.96

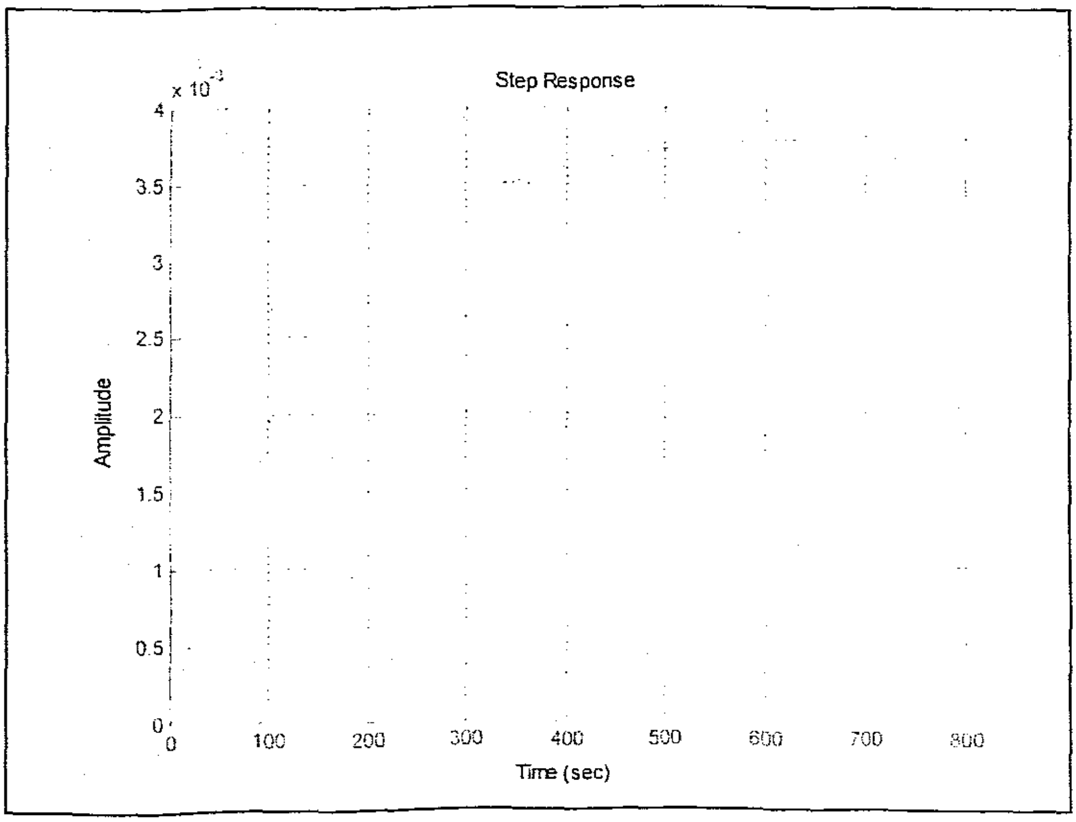

Figure 3.11 Step response of plant with Kp = 4.2

The first method is known as the *position* implementation since it controls the output of the controller, is given in equation 3.12. Using this method the actuator value, u_k, is derived for directly.

$$u_k = u_{k-1} + K_p(e_k) + \frac{K_p T}{T_i}(e_k) + \frac{K_p T_d}{T}(e_k - e_{k-1}) \tag{3.12}$$

Position implementation although simple to implement suffers from some drawbacks. When the controller is switched on for the first time, the values of u_{k-1} and e_{k-1} are not known. The chance that by simply implementing equation 3.12 and obtaining a proper controller output is very remote. As a result the control action of the position implementation suffers from a 'bump'.

In addition another problem with equation 3.12 known as integral windup occurs when the actuator encounters a constraint, which then produces a persistent offset between the plant output and the set point. This then results in the integral term increasing without bound over time.

Reconfiguring equation 3.12 the problems highlighted are overcome. Equation 3.13, known as the *velocity* implementation, computes the increment or change of the actuation rather than the actuation itself.

$$u_k - u_{k-1} = K_p(e_k - e_{k-1}) + \frac{K_p T}{T_i}(e_k) + \frac{K_p T_d}{T}(e_k - 2e_{k-1} + e_{k-2}) \tag{3.13}$$

The equation 3.13 produces a 'bumpless' transfer when it computes the increment of the output of the controller. Using equation 3.11 and table 3.1 the coefficients K_p, T_i, T_d are solved for. The sampling period, T, is set initially to 1 second. The resultant expression for the controller based on these values is given in equation 3.14.

$$u_k = u_{k-1} + 27.7(e_k) - 48.5(e_{k-1}) + 21.2(e_{k-2}) \tag{3.14}$$

Equation 3.14 is a discrete form of a linear difference equation that is sampled at a particular period and provides discrete values for actuator output. In order to directly implement equation 3.14 on a microcontroller, a preliminary understanding of this difference equation is warranted. This expression incorporates values for previous error calculations as well as a previous value for the actuator output. These values need to be stored in on-board memory and be available when the final output is evaluated.

The chosen method for the programming of the algorithm was the high level language, C, because of its powerful ability to compute mathematical intensive calculations and operations involving floating point operations are straightforward. These features are notably absent in the use of an assembly language.

Achieving a 'bumpless' transfer requires that when evaluating equation 3.14, two sampling intervals are passed before entering the control loop. This allows the values for the previous errors, e_{k-1} and e_{k-2} as well as the previous actuator output, u_{k-1}, to be computed. A simplified flowchart depicting the algorithm for the velocity implementation of the PID controller is presented in figure 3.12.

The algorithm functions as follows:

- After variables and functions to be used are initialised, the program waits for the user to enter a value for the set point temperature, via an interrupt service routine (ISR).
- When this is done the program within two sampling periods, measures the heater temperature via the ADC and calculates the two previous error values, e_{k-1} and e_{k-2}, as well as the previous actuator output, u_{k-1}.
- The program then enters the main PID loop and calculates the value of the actuator deviation.
- If the actuator deviation is a positive value (> 0), an appropriate the pulse-width modulation of the firing pulse is determined dependent on the actuator deviation.

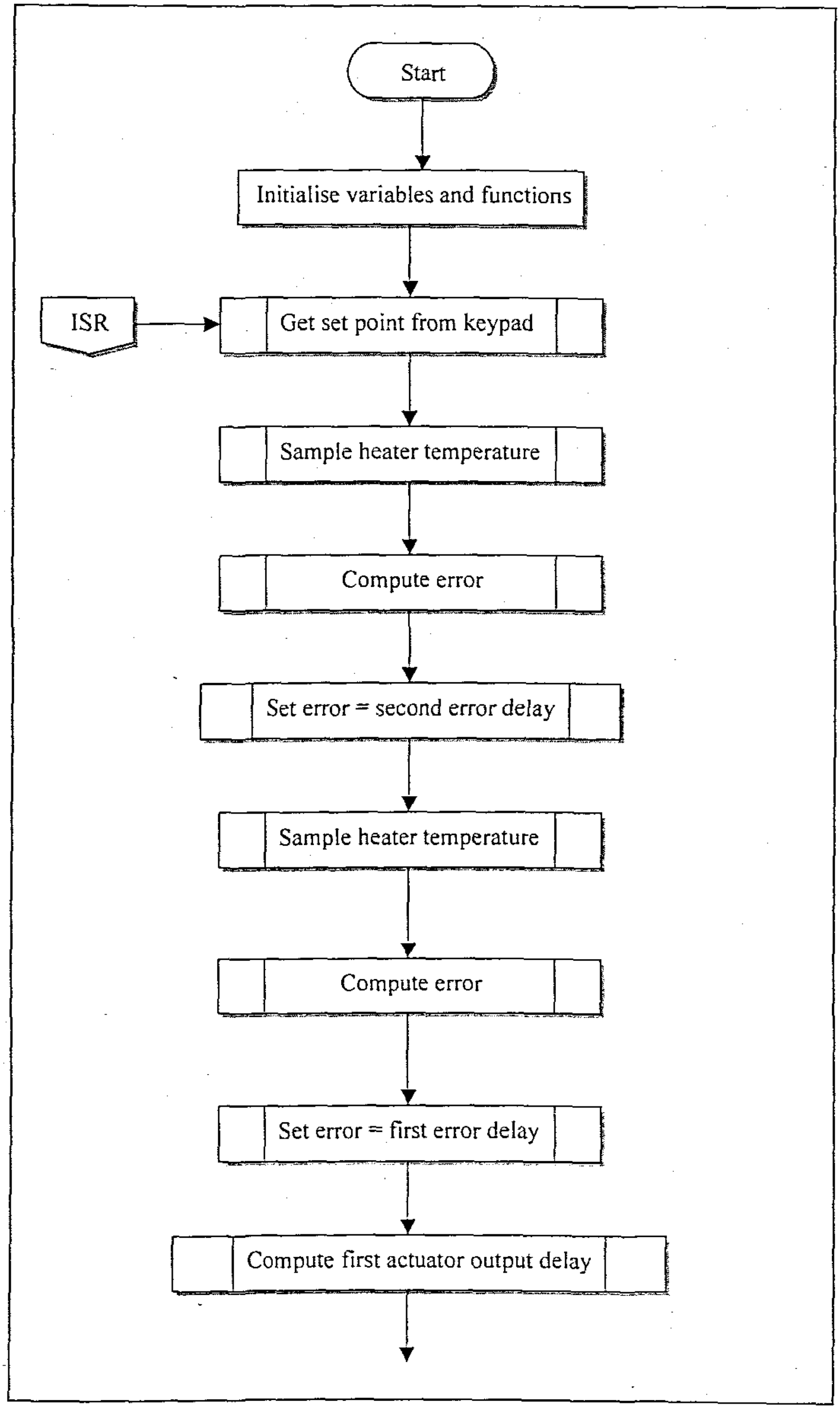
Start
Initialise variables and functions
ISR
Get set point from keypad
Sample heater temperature
Compute error
Set error = second error delay
Sample heater temperature
Compute error
Set error = first error delay
Compute first actuator output delay

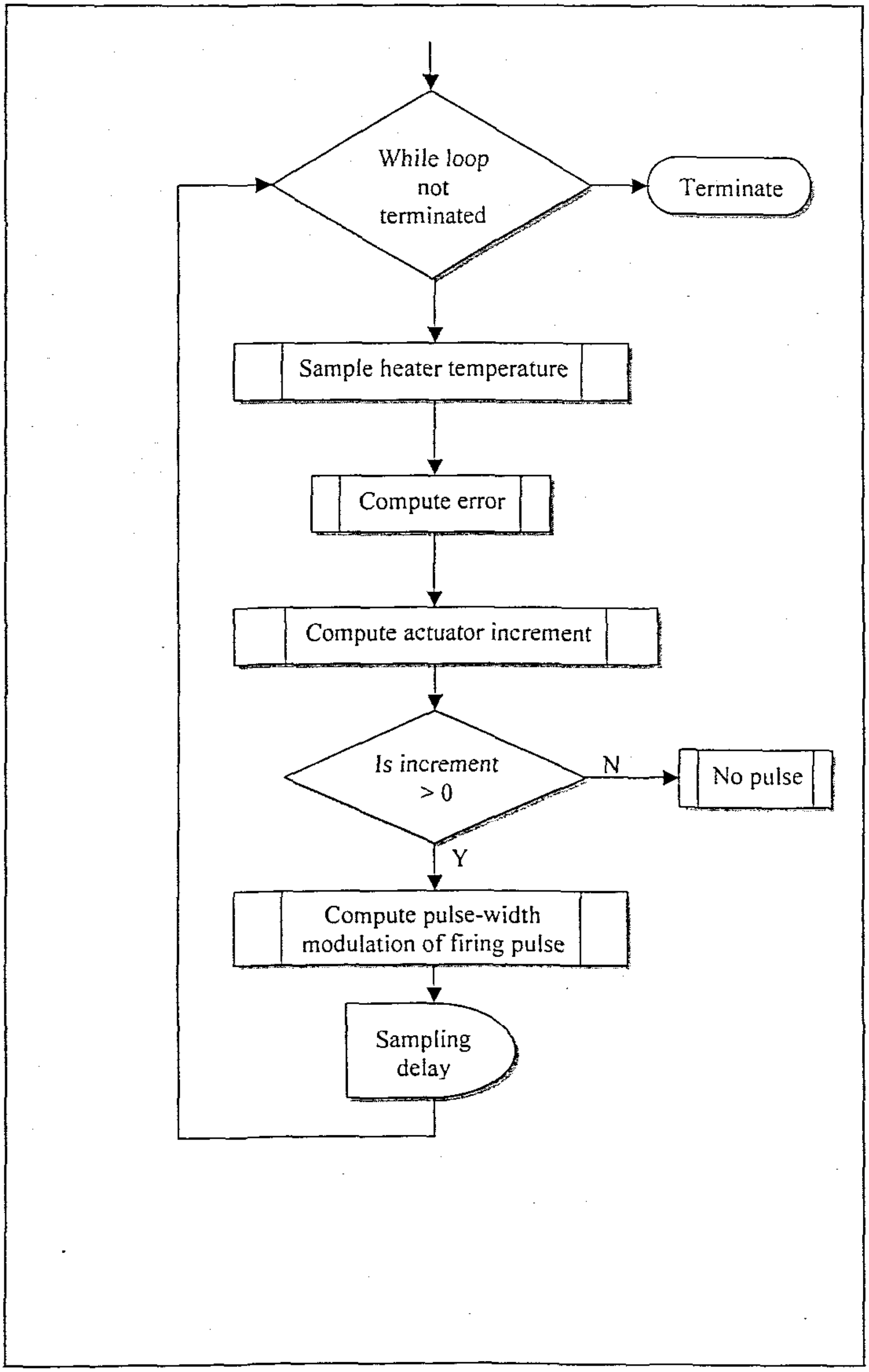

Figure 3.12 Flowchart of the PID algorithm

- If the actuator deviation is negative or equal to zero (<= 0), no firing pulse is initiated.
- The program waits for the sampling period to complete before taking another measurement of the heater temperature and repeats the loop.

A complete listing of the C code for the PID controller designed is provided in the appendix. An excerpt of the source code given below shows how the value for e_{k-2} is evaluated.

```
y_out = ADC();                /*sample output*/

error_0 = r_in - y_out;       /*compute error*/

error_2 = error_0;           /*set error equal to second
                              previous error*/
```

The following excerpt shows how e_{k-1} is computed.

```
y_out = ADC();                /*sample output*/

error_0 = r_in - y_out; /*compute error*/

error_1 = error_0;     /* set error equal to first
                              previous error*/
```

The value for u_{k-1} on start-up is derived using the source code described below.

```
u_old_1 = 28*error_0;

u_old_2 = 49*error_1;

u_old = u_old_1 + u_old_2;      /*compute previous actuator
                                  output*/
```

After the initialisation routine has completed the program proceeds to the main control loop. With every sampling interval the PID model in equation 3.14 is evaluated and an increment of the actuator output computed. An excerpt of the source code used to achieve this is given below.

```
while(!RI){

        y_out = ADC();          /*sample output*/

        error_0 = (r_in - y_out);       /*compute error*/

        u1 = 28*error_0;

        u2 = 49*error_1;

        u3 = 21*error_2;

        u = u1 + u2 + u3 + u_old;       /*compute actuation*/

/* The computation of the incremental actuator output */

        u_delta = (u - u_old);
```

The implementation of the PID controller designed for this paper is based on the Ziegler-Nichols method and represents a significant simplification when compared to some of the other methods available. Especially considering that the system derived for the plant was a first order model plus lag. Other tuning methods available are:

- The trial and error method, whereby the tuning parameters are tweaked and continually adjusted. This method is usually reserved for experienced control engineers.

- Graphical design methods, which include the root-locus, Nyquist and Bode plots. These methods are usually reserved for higher order systems.

The Ziegler-Nichols tuning method was selected because it is the oldest and most established method available. It is also much more simpler to implement than the other methods listed above. Many modifications of the controller developed are possible and probably warranted in some instances. However, for the purposes required of this controller in this study, the design proved adequate as the tests performed in chapter five verify. Chapter four presents an overview and the practical development of the IR controller.

4. PRACTICAL DEVELOPMENT OF THE IR CONTROLLER

The practical procedure for obtaining the mathematical model of the controller in chapter 3 is explained in this section. The description that follows includes various hardware and software aspects that constitute the practical set-up of the experiment.

4.1 Hardware set-up

Figure 4.1 shows the block diagram of the open loop response test. The hardware component for the experiment consists of the microcontroller (80C515); a power

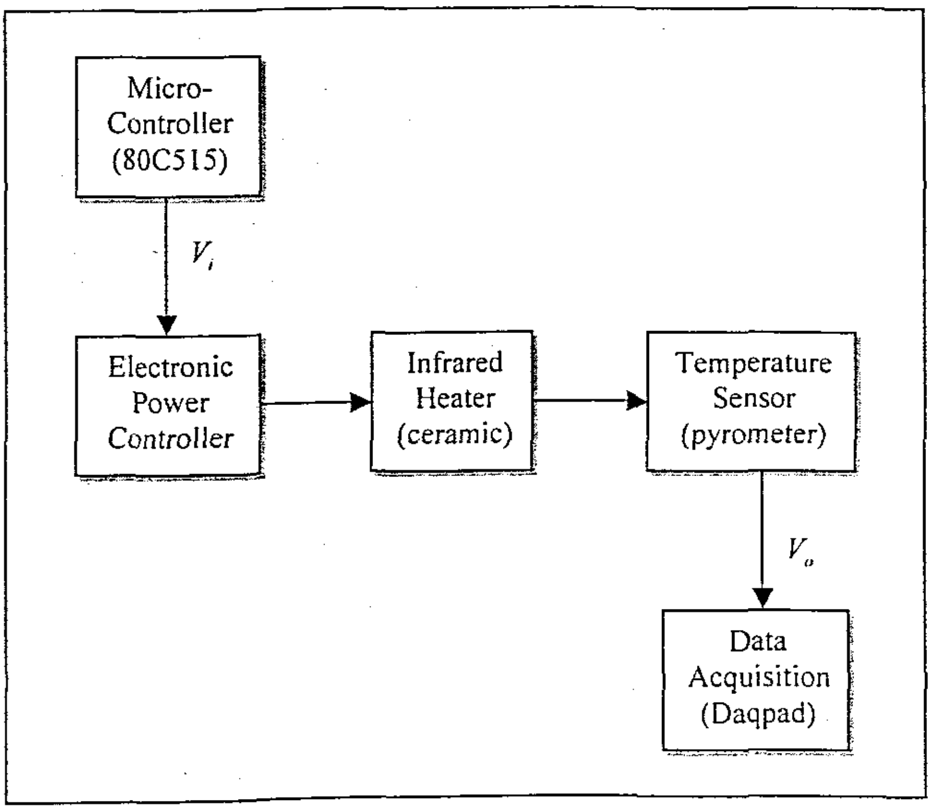

Figure 4.1 Elements of the open-loop step response test

controller, to modify the power input to the IR heater (oven) and a temperature sensor, pyrometer, to measure the output temperatures of the IR heater. The data acquisition successfully accomplished through the use of the National Instruments DAQPad-1200 data acquisition hardware.

4.1.1. The Microcontroller

The 80C515 microcontroller is part of 8051 family and has the following features:

- Is an 8-bit controller with 256 bytes on-board RAM,
- Eight I/O ports, three 16-bit timer/counters,
- On-board analog-to-digital converter, and
- Instruction cycle time of 600ns.

The microcontroller is used to generate a pulse-width-modulated (PWM) waveform, V_t, which is needed in order to drive the power controller, which in turn regulates the output temperature of an infrared radiation heater.

The 80C515 is programmed in C and the details of the software program are given in figures 4.7 and 4.15.

4.1.2 The Power Controller

This unit comprises the power electronic components used to control the voltage input for the infrared heater. The aim in using the power electronic components when designing the power controller incorporated the following features:

- Low cost implementation
- Portable hardware platform
- Readily software programmable
- Provide reliable results with minimum hardware complexity

4.1.2.1 AC Power control aspects

AC power control has undergone somewhat of an evolution when considering the various methods in which this was achieved. The control of voltage and current has always presented the engineer with a challenge but few options. Control circuits today employ the use of some solid-state devices and techniques. Prior to this the most frequent method to control large amounts of voltage involved the use of one or more transformers. The control of large currents meant the use of large variable resistors, rheostats, placed in series with the load being controlled. These methods of control proved expensive, demanded high maintenance and were inefficient.

Three types of power control methods have been investigated for this paper, with the aim being to find the most appropriate type of control for the type of load required. The power controller needs to be able to control and switch large loads, typical currents of up to 10 amps and loads rated for 800 watts. The types of electronic devices used for power control that were studied are as follows:

- The triac
- The insulated gate bipolar transistor (IGBT), and
- The solid-state switch (SSS)

4.1.2.2 The Triac

Today the popular method to control large amounts of voltages and currents is by means of thyristors and has proved very successful. These types of solid-state power devices developed by General Electric Research Laboratories have been around since 1957. Initially the chosen technique of power control intended for work on this paper involved the use of a triac. The triac and silicon controlled rectifier (SCR) have traditionally been used for various types of control including general-purpose power supplies, AC and DC variable-speed motor drives, stepper motor control, servo motor control and light dimming. These semiconductor devices offer advantages that include high reliability, extremely fast response, selectable control parameters and low maintenance. The triac is able to switch both the positive and negative half cycles of an ac input by simply controlling a small amount of current on its gate terminal. One widely used method for controlling the average power to a load is by phase angle control; with this technique the output power is a function of the firing angle. A triac does not conduct until its gate terminal is triggered by a dc pulse or series of pulses. Once triggered into conduction it continues passing current even if the trigger pulse is removed. However the current ceases when the applied ac voltage goes through a zero crossing and requires another trigger pulse before the SCR will conduct. Using this method the rms load current is given by equation 4.1:

$$I_{RMS} = \frac{I_P}{\sqrt{2}} \sqrt{\left(1 - \frac{\Theta_f}{180^\circ}\right) + \left(\frac{\sin 2\Theta_f}{2\pi}\right)} \qquad (4.1)$$

The load under control in this paper is resistive, which presents a simplification of control when compared to an inductive load, where the voltage and current are out of phase. By varying the firing angle of the SCR, the load power is varied accordingly. The firing angle can be adjusted from near 0° to near 180°. Table 4.1 illustrates the approximate relationship between the firing angle and the resultant power output. (With Vac = 220Vrms and R_{LOAD} = 300Ω)

Table 4.1 Percentage power output vs. firing angle

Firing Angle	% Power Output
0°	100%
66°	75%
90°	50%
114°	25%
180°	0%

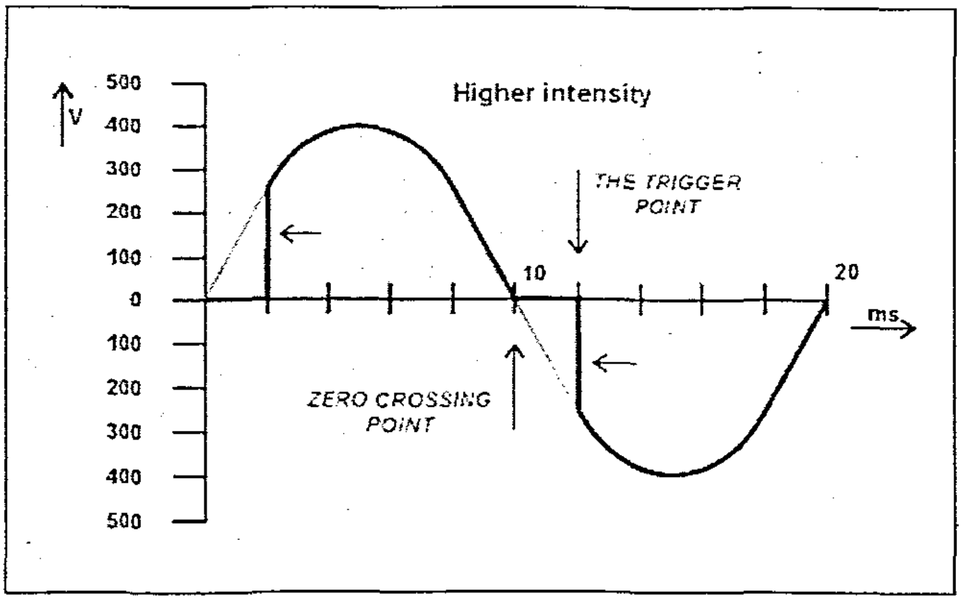

Figure 4.2 Small phase angle yields a high power output

The effect of phase angle delay on the load (assuming a resistive load) is illustrated by the figures below. The figures show the resultant power controller output voltage waveform that is the input for the load. The line frequency is 50Hz and the trigger point or firing angle is indicated in time (milliseconds).

Figure 4.2 indicates the position of the trigger point when high power is delivered to a

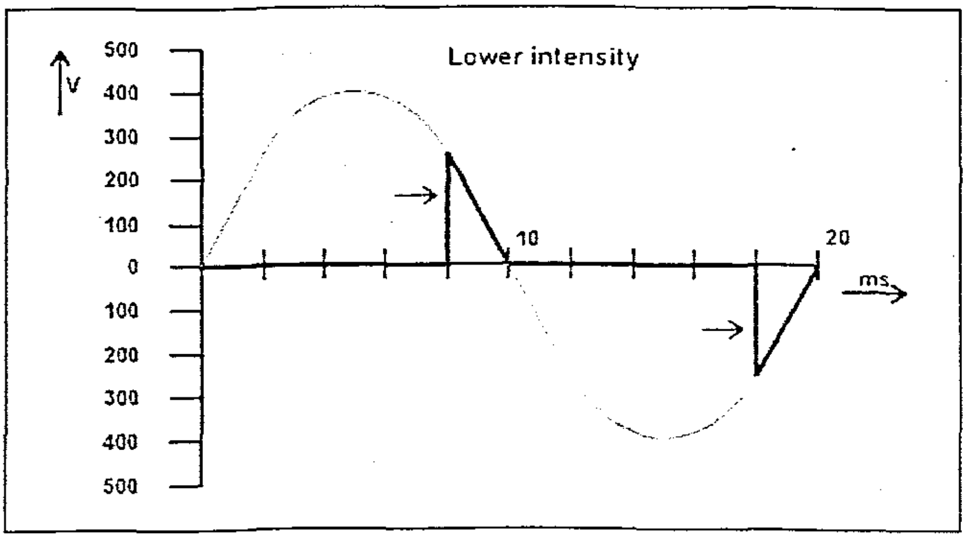

Figure 4.3 Illustration of a larger phase angle and the resultant low power output

load. The trigger point is soon after the zero crossing or the phase angle is small which consequently results in a high power output being delivered to the load. Figure 4.3 illustrates that a larger phase angle or later trigger point yields a lower power output to a load. However there are inherent problems associated with this method of control and numerous ways have been developed to overcome them. One of the problems encountered in triac control is the generation of electromagnetic interference (EMI) and radio frequency interference (RFI) caused by rate of change of current (di/dt). This is normally dealt with by ensuring proper filtering through the use of inductors or chokes, which have the added disadvantage of being less energy efficient. Although alternative control methods such as proportional control or burst firing have been developed there are still certain problems persisting. Some of these include the generation of line transients, caused by ac line disturbances as well as false triac triggering caused by a rapid and large rate of change of voltage (dv/dt). Figure 4.4 illustrates the generation of high instantaneous peak currents at device switch on, which causes mains disturbances and mains frequency noise.

These effects are limited to some degree by the introduction of snubber circuits and many variations are possible for their design and application. The function of a snubber circuit is to reduce the electrical stresses placed on a device during switching by a

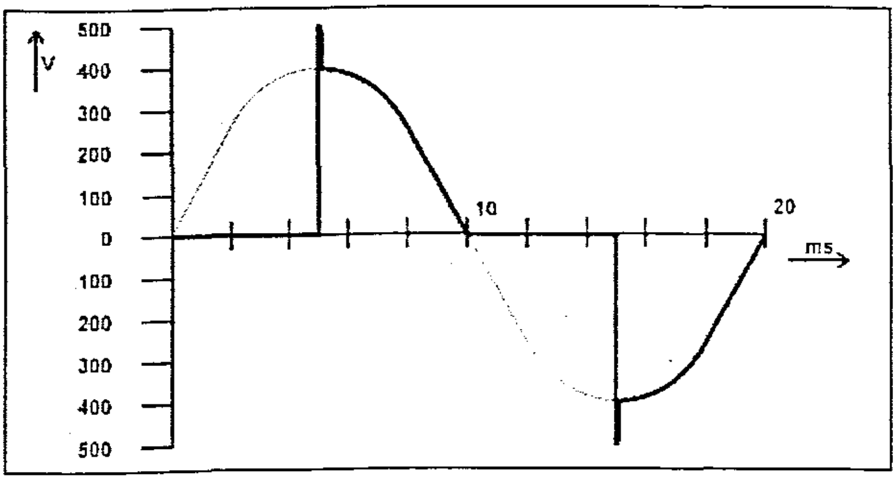

Figure 4.4 Generation of line disturbances with SCR control

power electronics converter to levels that are within the electrical ratings of the device. It accomplishes this by:

- Limiting voltages applied to devices during turn-off transients.
- Limiting device currents during turn-on transients.
- Limiting rate of rise (di/dt) of currents through devices at device turn-on.
- Limiting the rate of rise (dv/dt) of voltages across devices during device turn-off or during reapplied forward blocking voltages (e.g. SCR's during forward blocking state).
- Shaping of the switching trajectory of the device as it turns on and off.

Depending on the circuit topology, there are generally three broad categories of snubber circuits and these include:

- Unpolarised series R-C snubbers used to protect diodes and thyristors by limiting the maximum voltage and dv/dt at reverse recovery.
- Polarized R-C snubbers, used to shape the turn-off portion of the switching trajectory of controllable switches, to clamp voltages applied to the device to safe levels, or limit dv/dt during device turn-off.
- Polarized L-R snubbers, used to shape the turn-on switching trajectory of controllable switches and/or limit di/dt during device turn-on.

As the standards concerning power control for domestic and industrial use become more stringent, triac control type methods stand poised to be subjected to ever more rigorous inspection. The alternative is to develop new methods to overcome these problems or to find an improved method to accomplish power control. New European standards on the generation of mains disturbances will place triac and SCR controlled systems under increasing scrutiny as the amount of electrical disturbances permitted are reduced. The standards on harmonics generated (CENELEC, IEC and VDE), which lead to effects such as EMI and RFI, through the use of power switches, are becoming increasingly restrictive. (Mohan et al, 1995).

4.1.2.3 The Triac Power Controller

Figure 4.5 shows the block diagram of the triac-type controller developed for testing during this research. The triac was chosen because of the ease with which voltage in the load could be controlled in both halves of the ac line voltage.

A detailed circuit diagram of the triac power controller is presented in figure 4.8. The circuit operates from a 220Vac line voltage. Through a step-down transformer (TX) the resistors R9, R10 and R11 form a voltage divider, which provides the input to the zero-crossing circuit. The zero-crossing detector incorporates a differential amplifier (INA132P) and a voltage comparator (LM393). The function of the differential amplifier is to isolate the zero-crossing signal from the zero volt or earth of the line voltage. The square pulse that results is passed through a current buffer (74126), which ensures that the signal strength is the required 5V. This zero crossing signal is interfaced

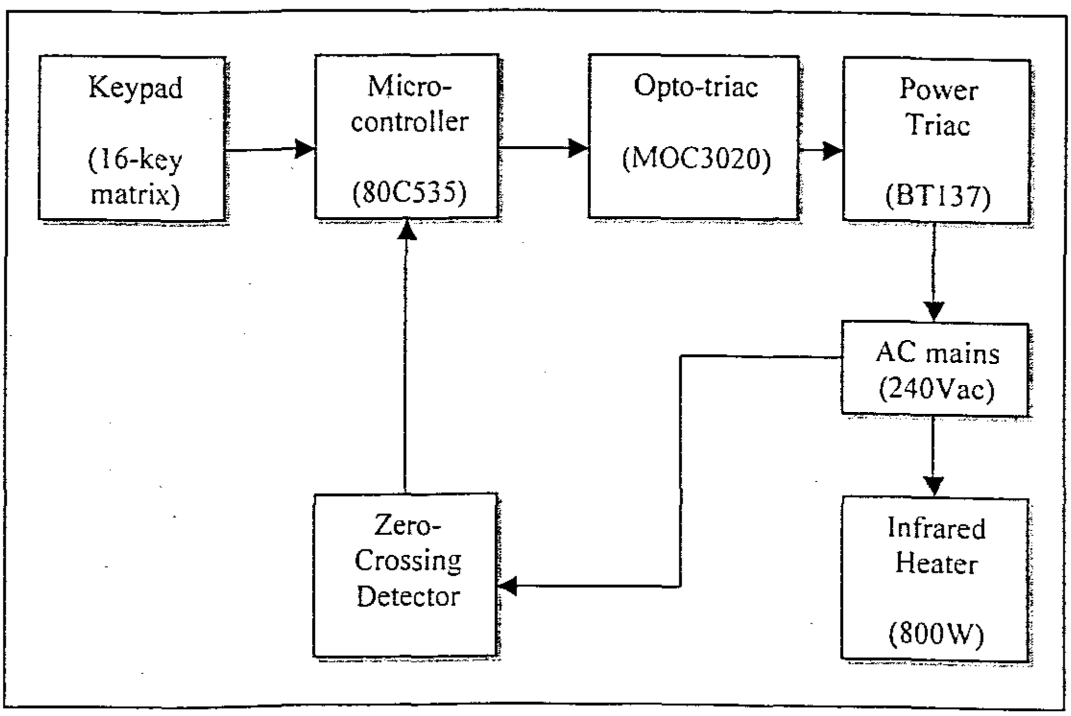

Figure 4.5 Block diagram of power controller using a triac

to a microcontroller external interrupt pin (I/O Port P3.2). The operation of the triac algorithm is presented in figure 4.7 below.

Another current buffer (74126) is used to restore the integrity of the firing pulse before it passes to the opto-coupler (MOC3020). The internal structure is shown in figure 4.6, with an input between pins 1 and 2, a light emitting diode (LED) that activates an opto-triac between pins 6 and 4. The opto-triac is used to generate trigger pulses needed for the power triac (BT137). The opto-coupler also serves to electrically isolate the low power electronic circuitry from the high voltage side. The MOC3020 is rated to isolate peak voltages up to 7200V. The power triac (Q1) is rated to switch loads of up to 8A. Datasheets of all electronic components used in this paper is listed in the appendix.

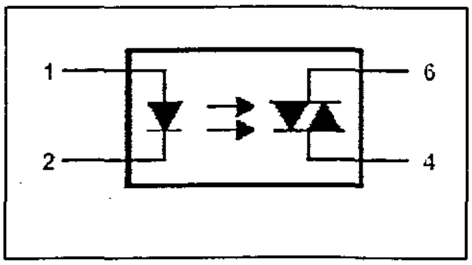

Figure 4.6 MOC3020 opto-coupler

A snubber circuit, represented by R8 (100Ω) and C1 (0.1uF), is used to protect the triac during the switching of load voltages.

4.1.2.4 The software algorithm

The software program written in assembler of which a flowchart is illustrated in figure 4.7 and the program operation is as follows:

- A single key press on the keypad corresponds to a preset firing angle, between 1 and 9 ms.

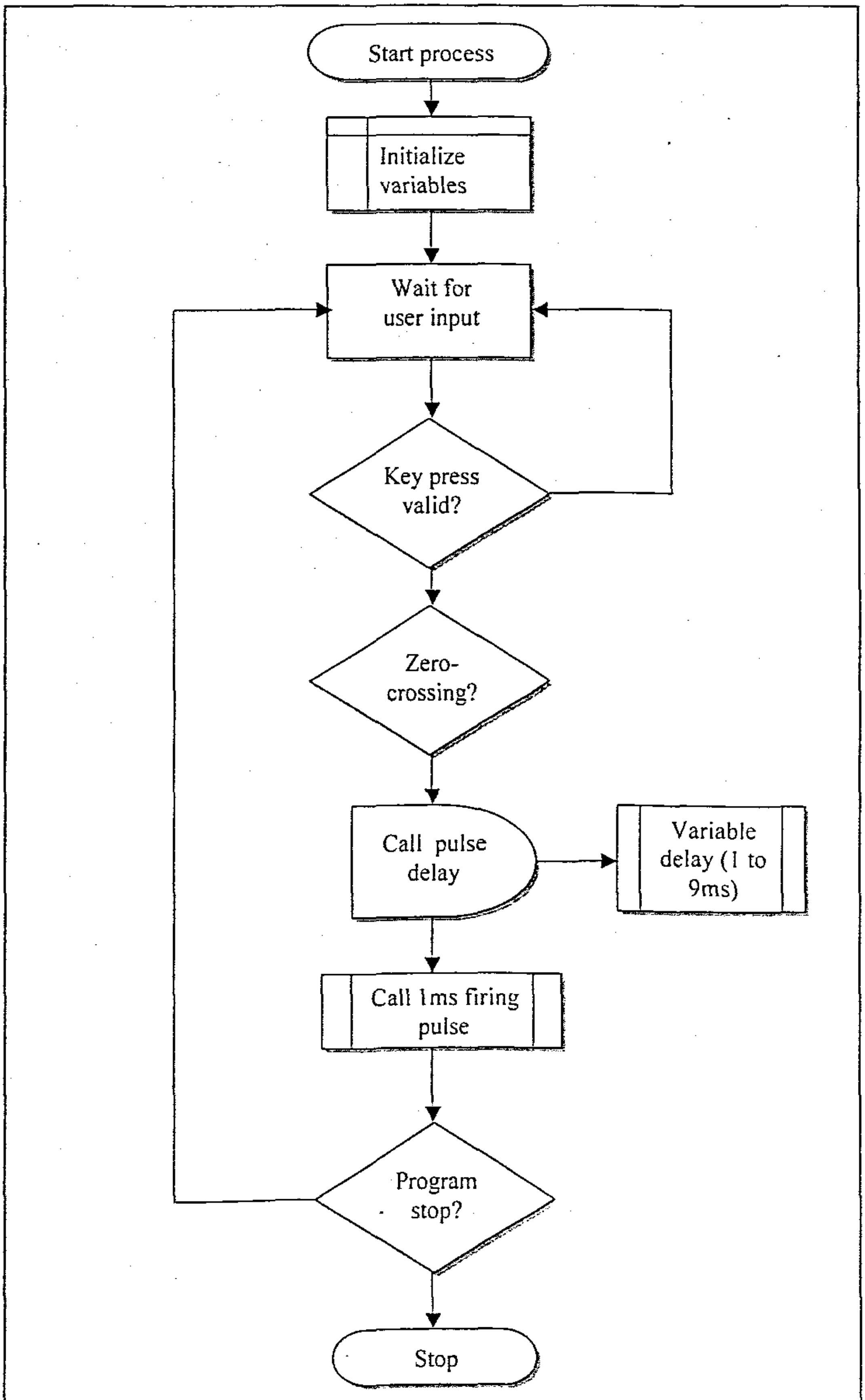

Figure 4.7 Simplified triac control software program

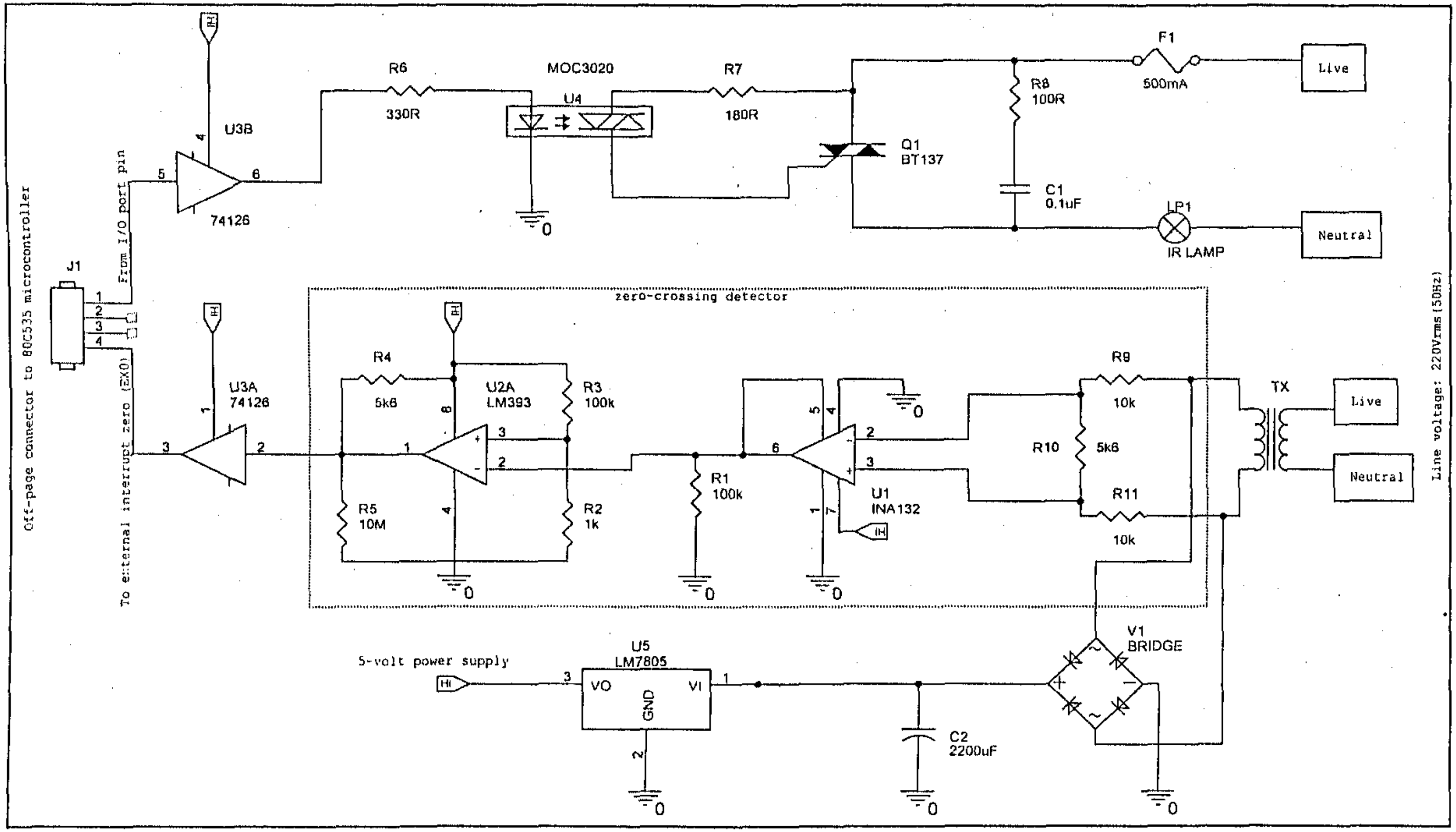

Figure 4.8 Circuit diagram of the triac power controller

- After a key press the program waits for a zero-crossing signal to be detected, this ensures the firing angle is referenced to zero, and also diminishes EMI and RFI affects.
- The interrupt service routine is activated and vectors to the software routine, that in turn selects the firing angle that corresponds to the key press preset value.
- This pulse is delivered through an input/output (I/O) port 4 of the microcontroller.

A 5-volt power supply is generated from the 240V line voltage through V1, a bridge rectifier, a filter capacitor (C2) and a voltage regulator (LM7805). The 5-volts voltage source is used by all the low voltage components including the microcontroller.

4.1.2.5 Evaluation of the triac power control circuit

When the triac power controller is used to drive light loads i.e. less than 1A, it functions remarkably well. An initial test of the circuit functionality had it operating as a light dimmer, driving a 60W incandescent light bulb. The circuit performed well, such that when then the firing angle was varied from a small angle to a larger angle, the light bulb responded by glowing brightly initially to dimming to a dull glow. This load test proved that the circuit elements functioned properly and that the circuit design worked.

After the initial testing the circuit was subjected to its rated load i.e. an infrared radiation heater rated at 800W. The circuit failed to switch this rated load successfully. The circuit element responsible for failure was the power triac. The power triac was upgraded twice with respective higher current ratings of 15A and 20A, but still the circuit failed. The reasons for the failure of the circuit was credited to:

- Although the current ratings of the triac far exceeded the load rating (nominal current of 4A), this value represented an absolute maximum, which in reality was far less. The inrush current on cold start the destroyed the triac. Inrush currents of up to 100A are possible, which would render the triac powerless.

- Subsequently it was realised that the triac is a low power-switching device, this made it unsuitable for the type of loads it needed to control.
- That even when switching the low power incandescent lamp, large voltage spikes were present that degraded the quality of the line voltage by introducing noise disturbances.

Due to these reasons a new method of power control was sought that could successfully handle the rated loads. The effort spent on redesigning and refining the circuit would be better spent on implementing a more rugged power control option. Although the triac is still used in many applications and widely published in literature, for the purposes of this investigation it proved not to meet expectations. (A listing of the software program in C code used for the triac circuit is provided in Appendix 4).

4.1.3 The Insulated Gate Bipolar Transistor Power Controller

The insulated gate bipolar transistor (IGBT) provides a fairly new means of power control and has found a niche in applications that fall in between that of a bipolar transistor (BJT) and the power MOSFET. IGBT's are poised to quickly becoming the preferred means of power control in applications similar to that of the triac and SCR. These applications include automotive, lighting, home appliances and power management uses. The IGBT developed in the early 1980's, combines the simplicity of drive and the excellent fast switching capability of the MOSFET structure with the ability to handle high current values typical of a bipolar device. These devices can be programmed to start on the zero crossing and switch off at some later stage, this technique is known as reverse phase control. Whereas noisy circuits are the product of triac control because of its turn on, switching off controls an IGBT. This eliminates noise, in-rush current and EMI effects. With no instantaneous power change to contend with the controller needs no choke.

The typical voltage output waveforms generated through the use of an IGBT are presented in figure 4.9 An IGBT can be controlled so as to gradually switch the device off, resulting in a smoothed load power waveform. This drastically reduces

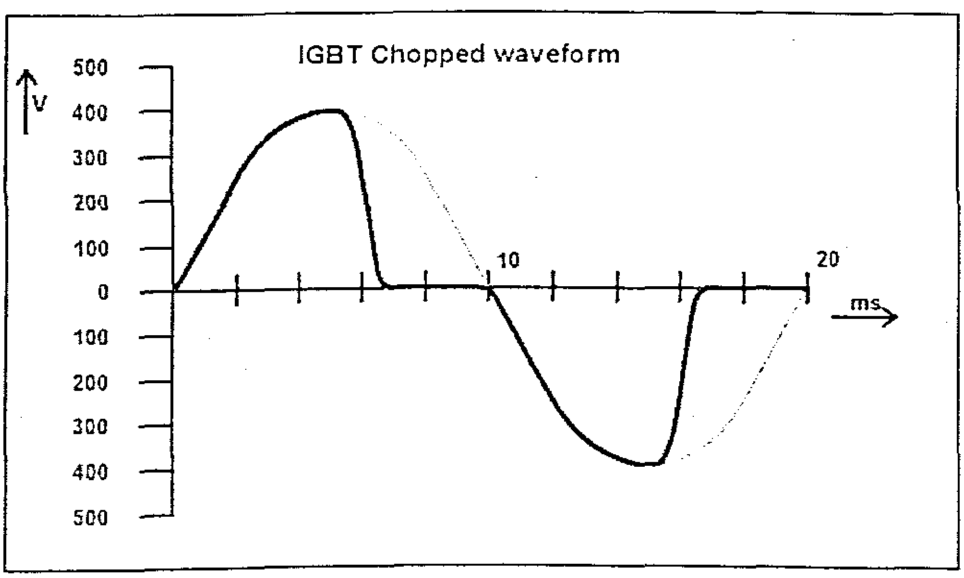

Figure 4.9 IGBT smoothed output voltage waveform

any harmonics produced and noise levels on the mains line are diminished or eliminated ensuring quieter control. The harmonics produced by both the thyristors and IGBT type controllers are given below. Figure 4.10 shows the resultant harmonics produced by triac control. Figure 4.11 clearly indicates the reductions of harmonics produced that are evident with the use of IGBT's. Figure 4.14 shows the circuit diagram of the power controller incorporating an IGBT. This circuit was designed around the IRG4PH30KD IGBT, which is rated at 20 amps maximum collector current. The design uses a three-

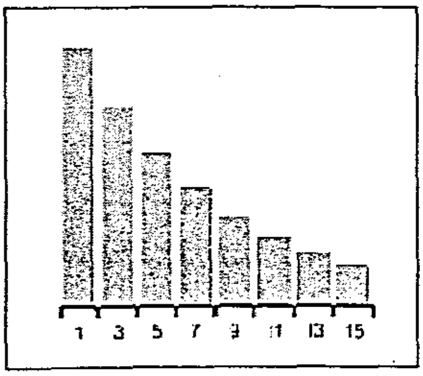

Figure 4.10 Typical harmonic spectrum for a triac controller

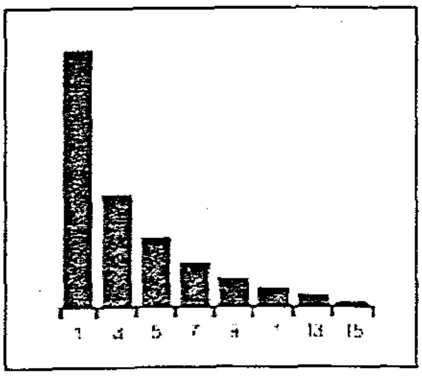

Figure 4.11 Typical harmonic spectrum for a reverse-phase IGBT controller

phase line voltage that is isolated from the rest of the circuit by means of an isolation transformer as shown in figure 4.12. This ac voltage is rectified using stud rectifiers (DN1) and filtered through a 2200uF capacitor (C6) as shown in figure 4.13. The circuit is used as a light dimmer to gauge its performance and its ability to control the power of a load.

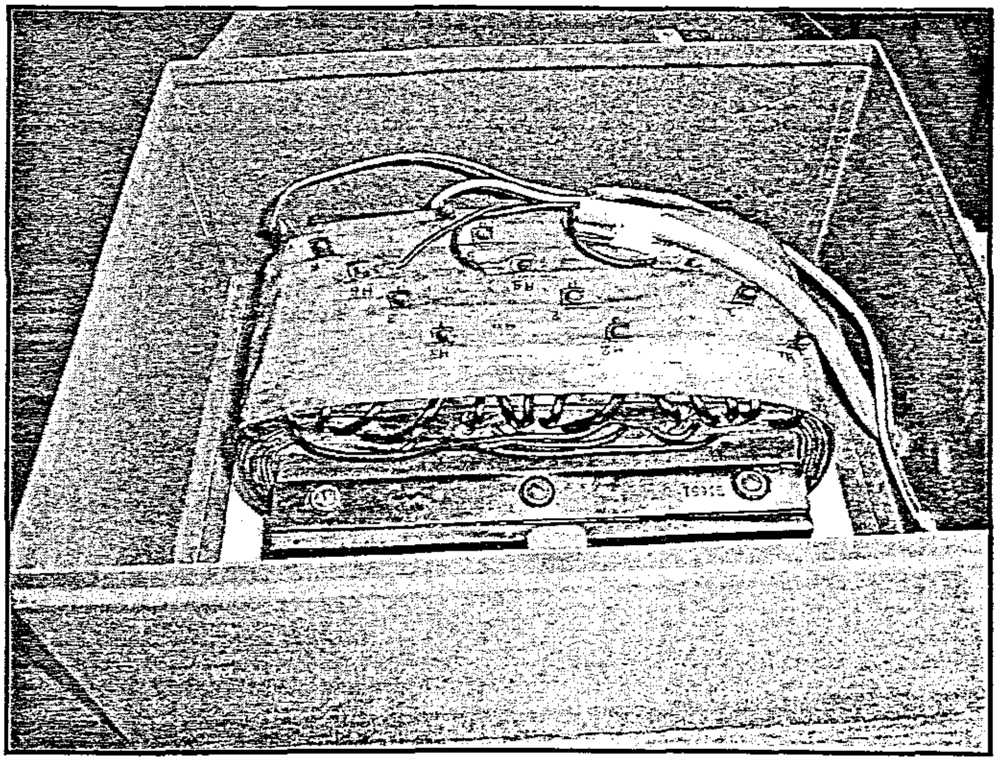

Figure 4.12 Three-phase isolation transformer

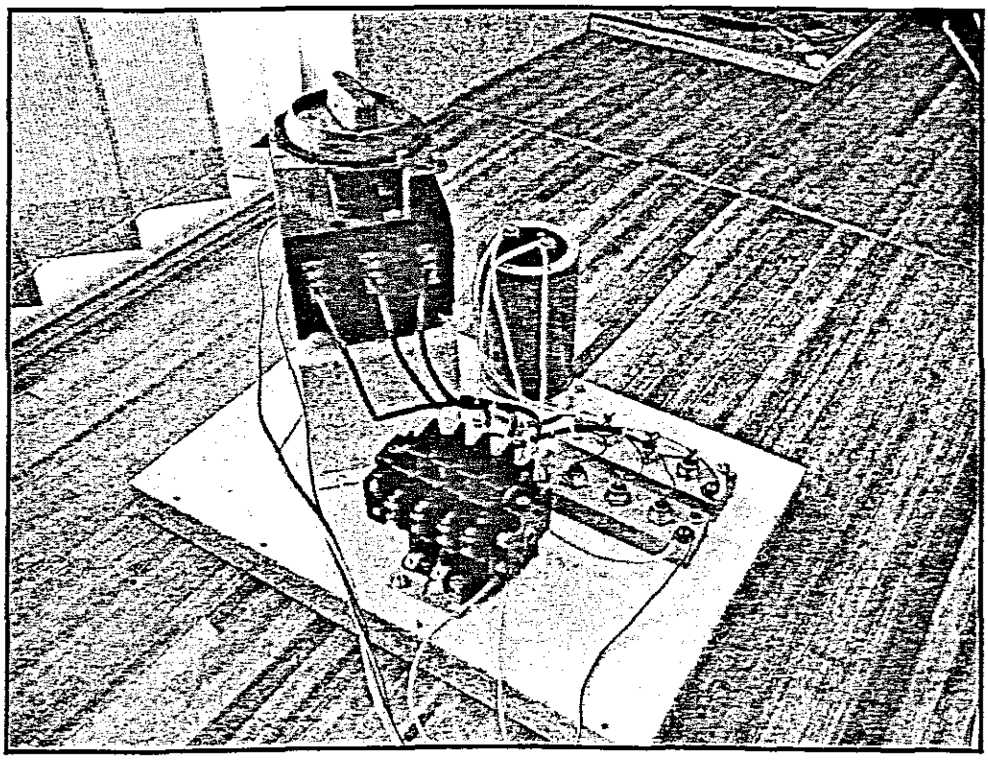

Figure 4.13 Three-phase voltage rectifier and filter capacitor

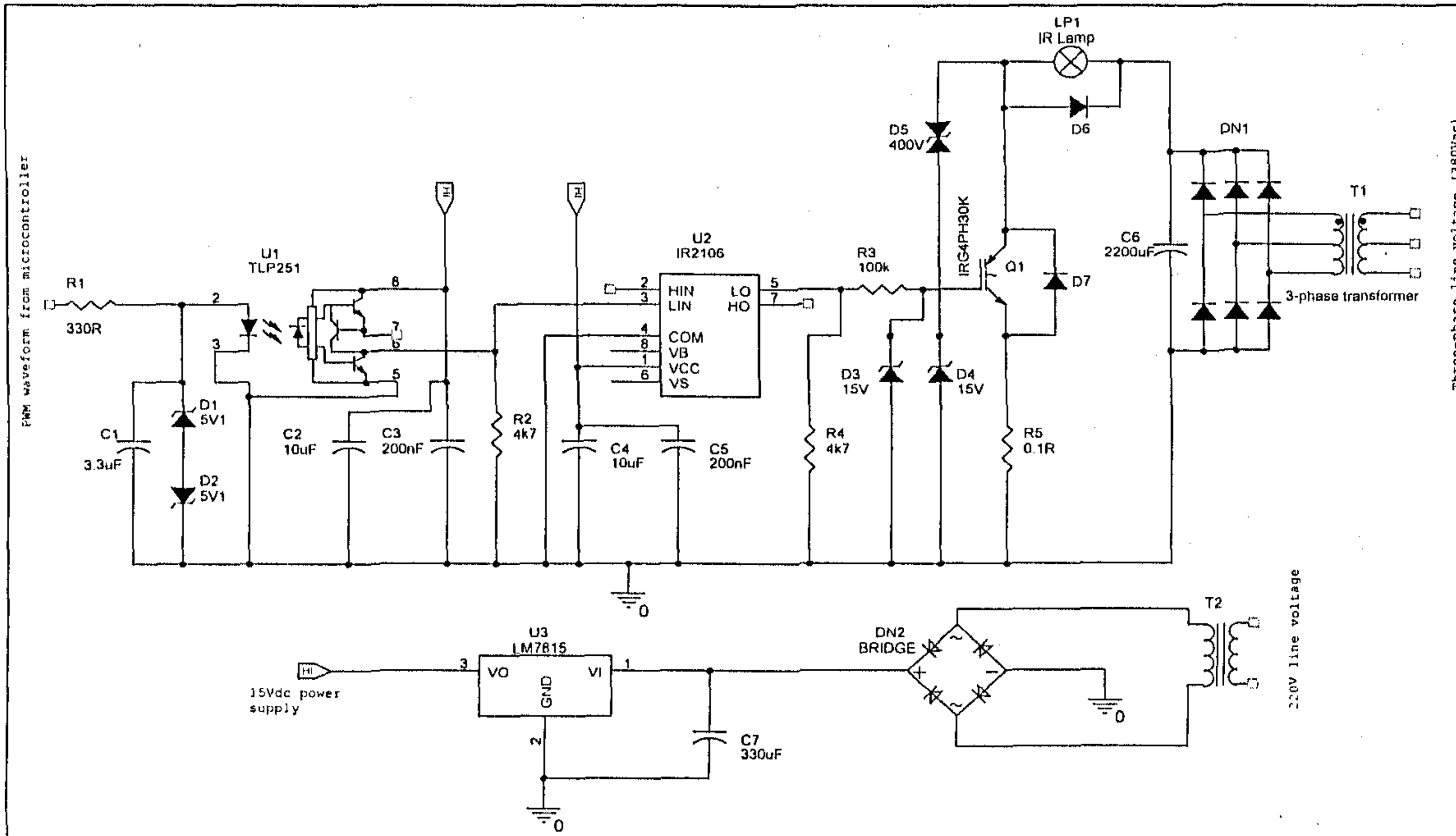

Figure 4.14 Circuit diagram of the IGBT power controller

4.1.3.1 The circuit operation

Using the keypad attached to the 80C515 micro-controller, the user selects the required power level of the load. The software algorithm then deciphers the key press and determines the required pulse-width modulated waveform (PWM) to generate. The program flowchart for the software algorithm is given in figure 4.15 below and its operation is briefly described as follows:

- The user selects the required power output for the load
- The program determines the suitable PWM waveform based on the percentage power output
- The point of the zero crossing of the line voltage is detected
- And the PWM waveform generated is sent from an I/O port to the circuit hardware.

With reference to figure 4.14 the hardware consists of an IGBT opto-isolator, TLP 251 (U1) that isolates the 80C515 microcontroller from the high voltage circuit components. Its isolation voltage is rated to 2500Vrms. The PWM enters at pin 2 of U1, which is the anode of an integrated LED and leaves at pin 6. The PWM then enters pin 3 of the IGBT driver, IR2106 (U2) and on exiting on pin 5 is magnified from a 5V peak PWM waveform to the 15V PWM waveform required by the IGBT. The IGBT (Q1) acts as a dc voltage switch that drives and controls the voltage across the load, LP1.

Short circuit protection is provided by R5 (0.1Ω) this feature eliminates the need for a fuse, which would otherwise be a heat source in the circuit. The dv/dt can be drastically slowed down at IGBT turn-off by using a high value gate resistor, R3 (100kΩ). The typical waveforms for an IGBT at turn-on and at turn-off are depicted in figures 4.16 and 4.17. The IGBT is protected from over-voltage by a transil diode, D5 rated to a voltage of 400V. A series zener diode, D4 (15V) is needed to prevent a dead short circuit occurring across the IGBT in case of the failure of D4. The voltage regulator, LM7815 (U3), provides the 15V supply that is needed by the IC's U1 and U2.

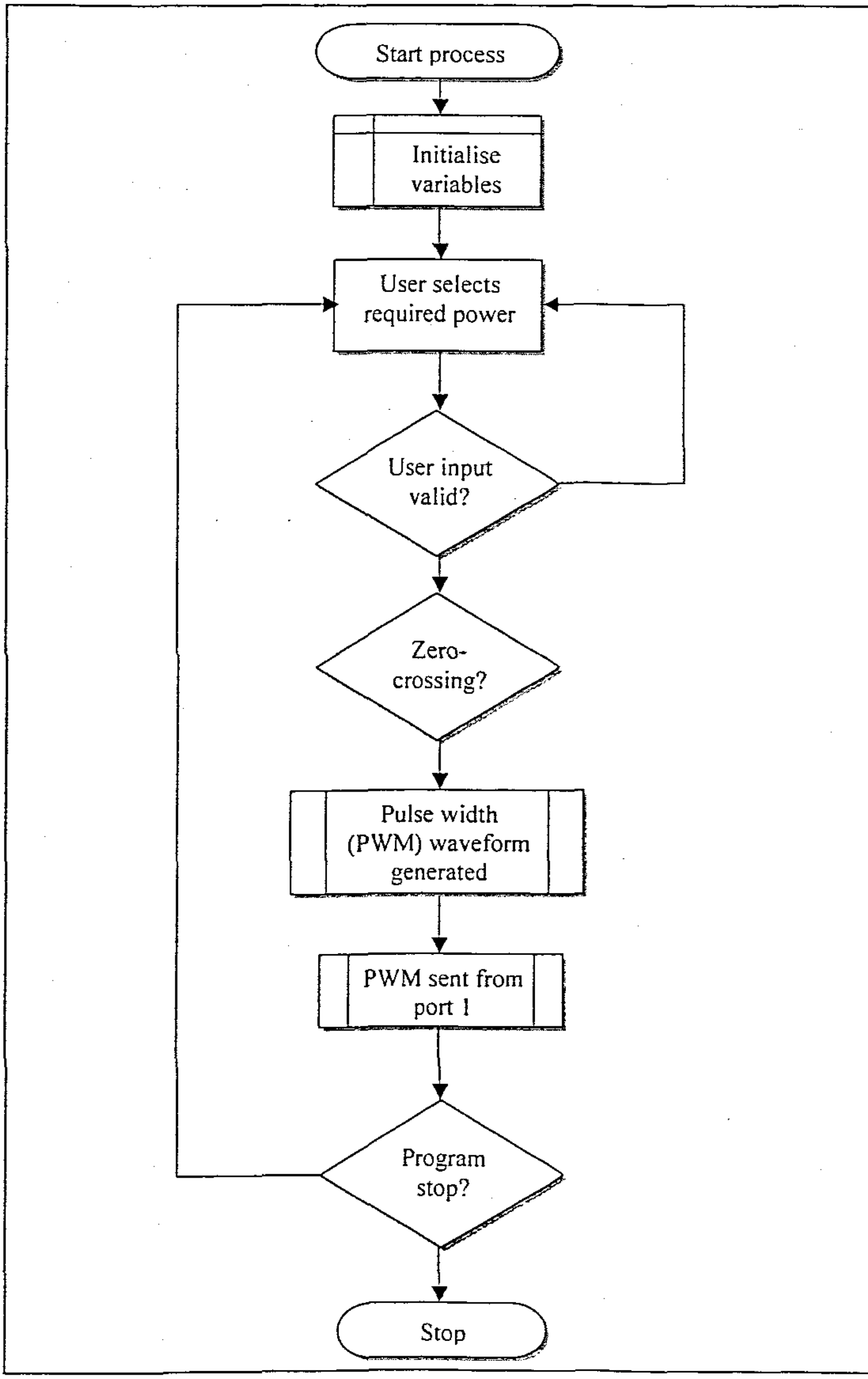

Figure 4.15 Simplified IGBT control software program

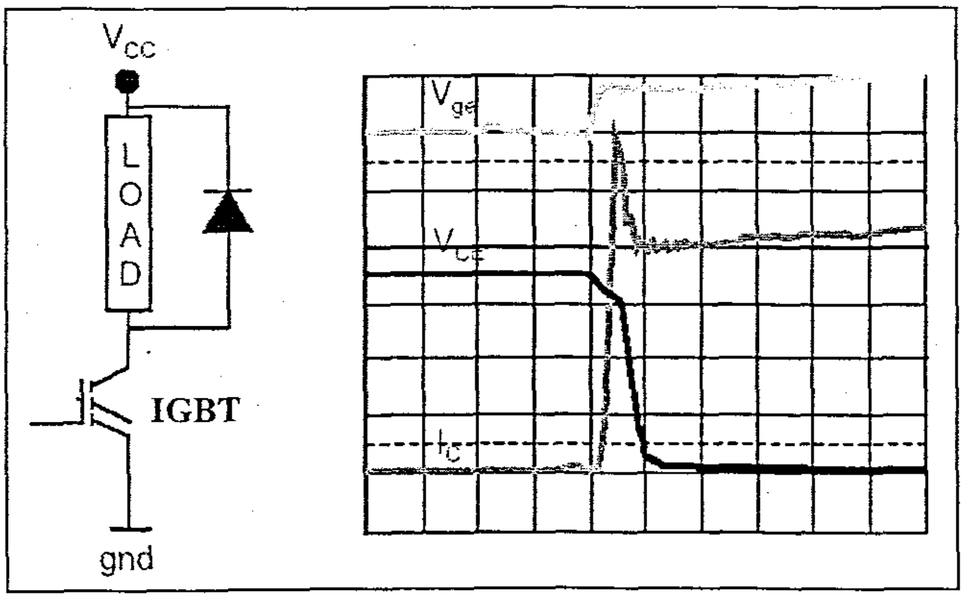

Figure 4.16 Typical waveforms during IGBT turn-on

Anti parallel diodes, D6 and D7, offer further protection to the load and IGBT respectively in the case of parasitic line inductances. The diodes D1, D2 and D3 eliminate any line disturbances from adversely affecting the circuit. The capacitors C 1-5 act as line voltage filters, reducing the voltage disturbances caused by the switching of load voltages that could cause erroneous operation of the circuit elements.

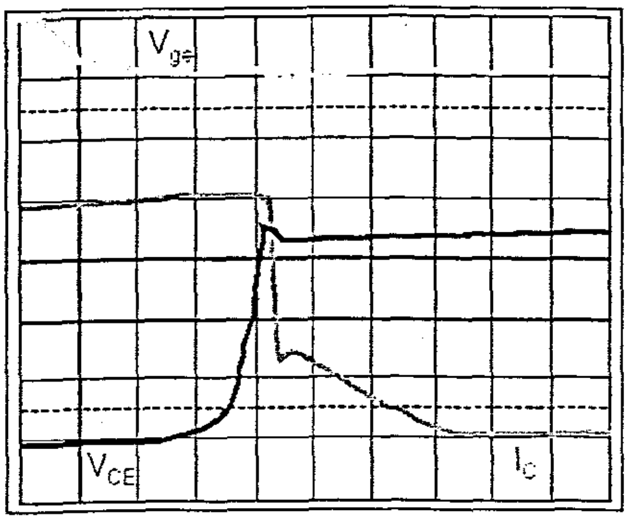

Figure 4.17 Typical waveforms during IGBT turn-off

4.1.3.2 Evaluation of the low cost IGBT power controller

In a low power load application, i.e. two incandescent light bulbs in series, the circuit performs well. The power to the load is controlled successfully such that the dc voltage in the load is decreased and increased, which is visibly noticed. However when the controller is used to drive a heavier load, e.g. 800W it failed. Evaluation of the reasons stem from a combination of the following reasons:

- That although the nominal current rating of the IGBT is well with acceptable limits for the load under test, the surge current rating falls far below the inrush current generated with the IR heater.
- The IGBT anti-parallel diode, D7, failed to protect the IGBT from line inductances.
- More effective line voltage filtering to reduce or eliminate the generation of the voltage spikes was needed.

Coupled with the reasons listed above, some additional information is warranted. That the IGBT is a new product on the market makes the unit prices fairly costly in comparison to a triac. This makes the design phase of a controller of this nature an expensive undertaking, due to component testing, failures and replacement. The IGBT is a DC voltage switch that does not directly control an ac load it operates in the dc side of a rectifier. This circuit configuration also succumbs to failure due to the common grounds of the ac and dc voltage sides.

In the final evaluation of this IGBT controller it is deemed unsuitable for the type of load under control and again a better method of power control was sought. (A listing of the software program in C code used for the IGBT circuit is provided in Appendix 5).

4.1.4 Solid-state switch with PWM cycle control

The two methods of power control presented above proved in practise to fall short of expectations envisaged for the type of load being controlled. Another method considered involved the use of an opto-isolated solid-state switch (SSS). The SSS has two integrated back-to-back SCR's as its control elements. It operates as a zero-voltage switch, which means it turns on and turns off at a zero crossing. The type of SSS used in this paper shown in figure 4.18 is the 240D10 manufactured by Opto 22.

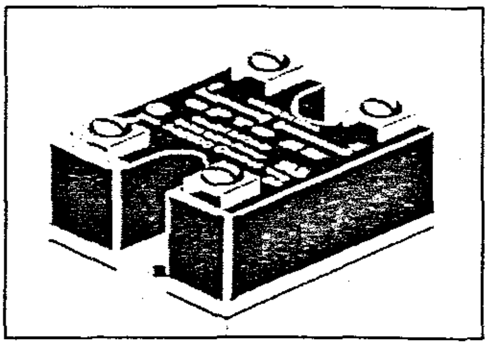

Figure 4.18 240D10 solid-state switch

Some the features of this SSS model include the following:

- 4000V optical isolation of input to output
- Nominal current rating of 10A
- Peak surge current rating of 110A
- Peak repetitive voltage maximum of 600V
- Zero voltage turn on
- Turn on time: ½ cycle maximum
- Turn off time: ½ cycle maximum
- Integrated snubber circuit

A SSS is a popular alternative to its mechanical counterpart, the mechanical relay or contactor. These components suffer from drawbacks that include more frequent component replacement, poor control ability due to its slow cycle times, dirty contacts degrade its performance and the heater life may be shortened due to thermal shock (Evalds, 2002). The electronic configuration of a SSS as depicted in figure 4.19 comprises a LED on the input, which serves to electrically isolate the high voltage side

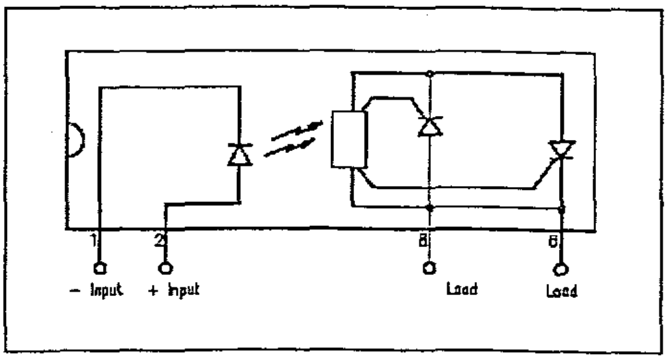

Figure 4.19Internal structure of a solid-state switch

from the low voltage microcontroller circuit. This feature of isolation is always of great importance when high and low voltages are present in the same circuit, as the case in voltage switching circuits. Over voltage protection of electronic components necessitates isolation because a low voltage, typically 5V is usually used to drive much higher voltages, such as 240Vrms. The two back-to-back SCR's control both cycles of the ac line voltage when triggered by a pulse-width modulated waveform.

The simplified block diagram of the SSS power controller is given in figure 4.20. The operation of the circuit is straightforward and can be described as follows:

- Using the keypad an IR heater temperature is chosen.
- The micro controller software program determines the appropriate pulse width of a PWM waveform.
- The generated train of pulses is used to drive the input of the SSS.
-

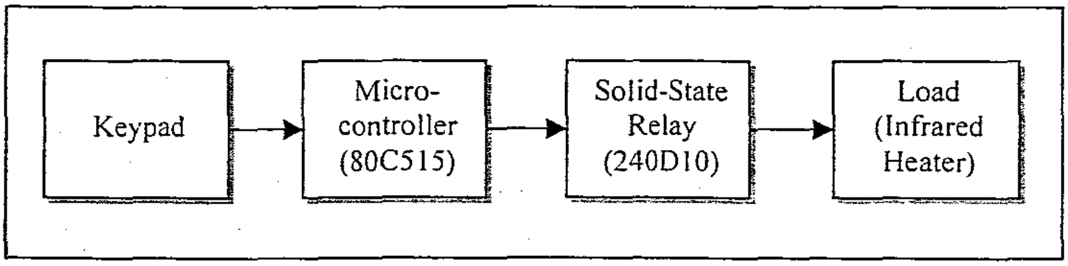

Figure 4.20 Solid-state power controller configuration

- With reference to the line voltage zero crossing, the power delivered to the IR heater is varied accordingly.
- The resultant temperature of the IR heater is measured with an infrared sensor (IR thermometer), the operation of which is discussed in section 4.3.

Figure 4.21 depicts the zero voltage switching capability of the SSS. The SSS always switches in whole or half cycles of the line voltage, thereby avoiding the occurrence of EMI and RFI generation. Table 4.2 presents a power control selection chart giving a range of loads or heaters and their suitable control methods (Evalds, 2002).

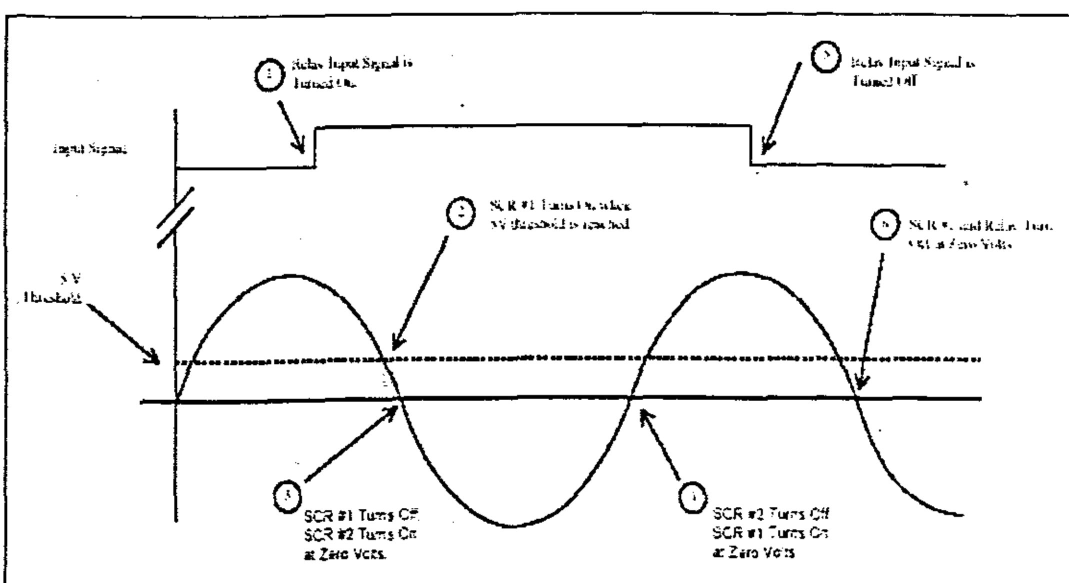

Figure 4.21 The zero voltage switching of the solid-state switch

Table 4.2 Power control selection chart

Heater/load type	Heater/load characteristics	Control type	Typical applications
Constant resistant elements	Slow response	On/off, zero-voltage switched	Large tank heating
Medium-wave infrared ceramic	Faster response	Zero-voltage switched	Thermoforming, textiles, industrial furnaces and fast water heat
Medium-wave infrared quartz	Fastest precise response	Phase-angle fired	Paper and pulp drying
Silicon-carbide heaters	Load changes in resistance with age	Phase-angle fired	High temperature ovens
Short-wave infrared elements	High in-rush currents	Phase-angle fired with soft start	High speed paper and ink dryers

4.1.4.1 Evaluation of the SSS power controller

This configuration performed well and out of the three methods investigated for power control, emerged as a clear favourite. This is due to many factors, some of which include the following:

- The rugged design of the SSS unit lends itself to the control large loads and is easily capable of handling the type of load in question.
- The circuit configuration is simple and straightforward when compared to the other methods studied.

- In reference to table 4.2 (Evalds, 2002), zero-voltage switching is the preferred method of control for the type of load under study, namely a medium-wave infrared ceramic heater.

Additional factors that make this type of control the preferred method is the low cost of the unit compared to the other components studied and also the almost non-existent disturbances in the line voltages that dominated the other types of control studied. Figure 4.22 provides a pictorial representation of how the solid-state switch controls the amount of cycles of the ac mains voltage. Using a pulse-width modulated waveform (PWM) the percentage power delivered to a load is varied. (The diagram serves only as a guide and does not demonstrate actual measurements). (The software program in C code for the SSS power control is incorporated into the software listings of Appendices 2 and 3)

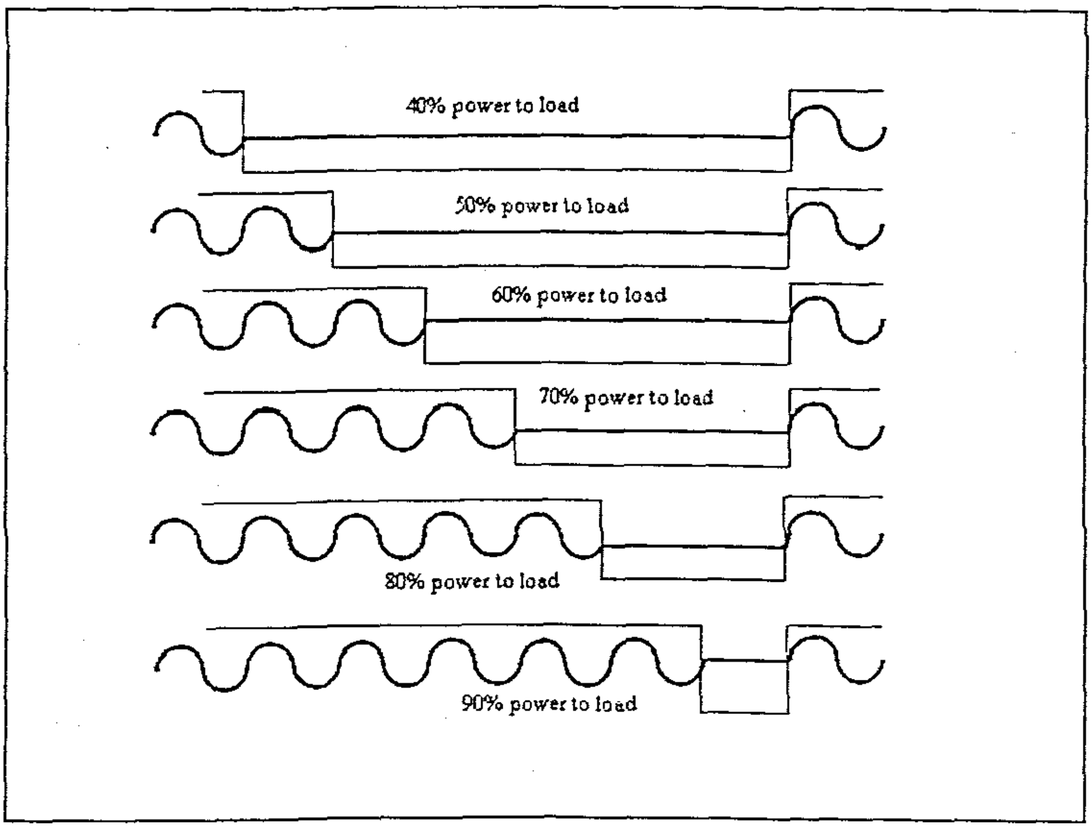

Figure 4.22 The cycle control method using the solid-state switch

4.2 Infrared Radiation Heater

Electric infrared radiation heaters are typically manufactured to pass electric current through a heating element made of an alloy of nickel and chromium called nichrome. The heating element is usually sheathed in either a quartz glass case or encased in a ceramic material. The type of IR heater studied for this paper is the latter, the ceramic encased type. It should be noted that many other types of heating elements are available on the market, e.g. tungsten.

The type of IR heater used in an industrial installation is usually dependant on the application involved. The four most common types of heaters and their suited applications are summarised below (Salamander, 1999):

- Quartz tubes are suited for instant on, instant off applications, where heat sensitive materials are exposed for prolonged periods to a heat source.
- Quartz lamps are also instant on and off type and have a high watt density, best for high-speed processors.
- Metal-sheath elements used for convection heating needs (e.g. ovens) and are rugged, cost effective and efficient.
- Ceramic elements are characterised by their gentle heat and are suited for applications needing an oven and where heating zones are required.

Infrared heaters are available in broadly three categories; long wave, medium wave and short wave. The type of infrared heater used in this study was the super high temperature ceramic radiator (SHTS) manufactured by Elstein and has a maximum operating temperature of 900°C. In addition it has the following specifications:

- Rated power 800W at 230V
- Radiation efficiency more than 75%
- Heat-up constant approximately 1.2 minutes (63% maximum value)
- Area power densities up to $80kW/m^2$

4.3 Temperature Sensor

Temperature measurement is accomplished through various methods and fall into mainly four types. These include the following:

- Thermocouples: these are the most widely used types of sensors in the industrial manufacturing environments. They function by producing a voltage from the temperature gradient that develops at the junction of two dissimilar metals.
- Resistance temperature detectors (RTD's): operate on the principle that the resistance to the flow of electricity changes with temperature. RTD's are more stable and accurate than thermocouples, but cannot be used to measure extremely high temperatures.
- Thermistors: also change resistance with changing temperatures, but are more sensitive than thermocouples or RTD's. They are however highly non-linear and limited to measuring temperatures of a few hundred degrees Celsius.
- Infrared (non-contact) devices are the preferred method of measurement when the other types are not feasible. They are used in conditions when the above contact type methods prove troublesome such as monitoring moving objects, in environments with safety hazards present, where contamination of the target is likely and when the distance to the target is considerably far.

Infrared sensors also called radiation detectors produce an output signal that correspond to the amount of infrared radiation that strikes the detector. IR detectors are classified as either thermal or photon-type detectors. Thermal infrared detectors convert incoming radiation into heat thereby raising the temperature of the detector. This change in temperature is then converted into an electrical signal and processed. Broadly defined there are three types of thermal detectors that include:

- Bolometer, the resistance varies with received radiation.
- Pyroelectric, surface charge varies in response to received radiation.
- Thermopile, consists of multiple thermocouples in series whose voltage output varies with received radiation

Photon-type detectors respond to photons being emitted by an object. The infrared radiation causes changes in the electrical properties of the photon detector. These changes can then be monitored as an output signal. There are two main types of photon infrared detectors (Yoder, 2000):

- Photoconductive: exhibit increased conductivity with received radiation.
- Photovoltaic: convert received radiation into electrical current.

Infrared detectors are further subdivided into various products available for commercial, industrial and processing use. The existing types fall into four categories:

- *Infrared thermocouples*: there outputs emulate a thermocouple output and used in situations where temperatures swings are limited.
- *Infrared thermometers*: detect infrared energy emitted by objects above absolute zero. A basic design uses a lens to focus infrared radiation onto an infrared detector. Ambient temperature variations need to be compensated for in order to ensure accuracy of measurements.
- *Infrared line scanners*: produce a thermal map of the surface of a product moving along a line, mainly used in steel rolling and glass fiber production.
- *Infrared thermal imagers*: produce a two-dimensional image of a complete scene being heated and useful for detecting hot spots and triggering alarms.

The type of infrared sensor employed in this paper is a Thermalert CI sensor available from Raytek (Raytek C13B). Its specifications include:

- Output linear voltage: 10mV/°C
- Optical resolution of 4:1 at 90% energy
- Spectral response range from 7-18μm
- Detecting element via thermopile
- Repeatability of ±1% of reading
- Temperature resolution of < 0.5°C
- Emissivity fixed at 0.95

- Response time of 350 ms
- Temperature range: 0°C to 500°C

4.3.1 Installation considerations

When installing the infrared sensor in a particular application there are some important aspects that need careful planning. The adherence to some simple practices will ensure that the measurements obtained are accurate and reliable (Ackland, 1998).

First establish the target size i.e. the area to be measured, should fill the instruments field of view. Suppliers usually recommend that the target size exceed the field of view by 50%. Because infrared sensors detect radiation from all sources i.e. from energy transmitted, reflected and emitted by and object. The sensor has to accurately isolate the emitted radiation for this is the indication of its temperature. If the field of view is larger than the target size, the background will affect the temperature reading, as shown in figure 4.23 below.

Another consideration is the determination of the optical resolution and is defined by

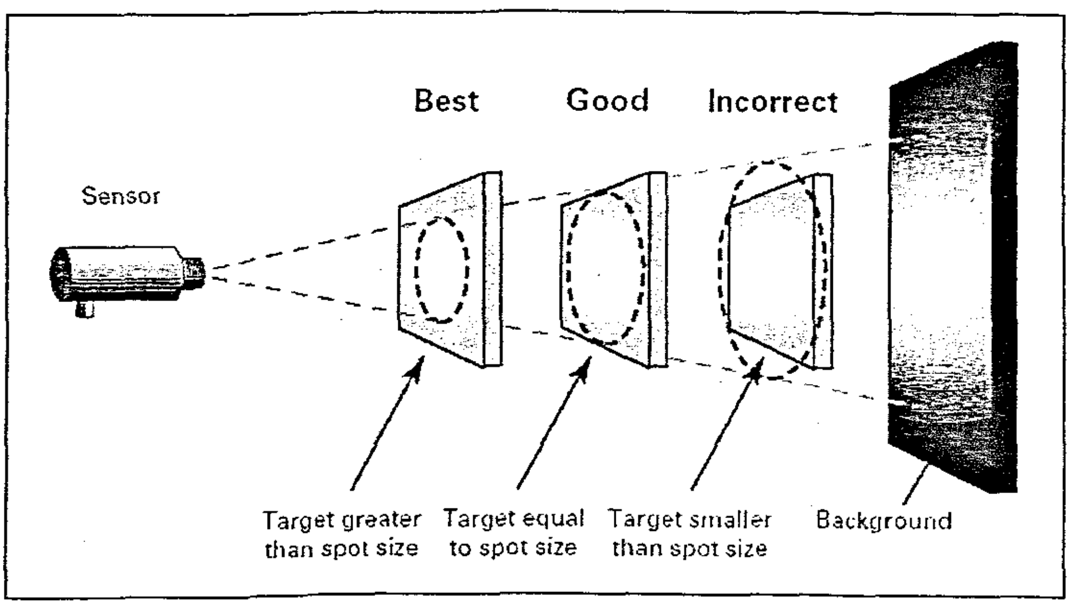

Figure 4.23 Estimation of the proper target size to an application

the D:S ratio. Comparing the distance of the object to the sensor (D) to the size or diameter of the spot (S) being measured. Optical charts as the one shown in figure 4.24 help determine the target spot size on a fixed-focus instrument. Infrared sensors available have D:S ratios that range from low resolution e.g. 2:1, to high resolution e.g. 300:1. The choice of D:S ratio depends on the size of the object to be measured and the distance the sensor is from the target.

The emissivity of the target material determines the spectral response of the sensor needed. Some materials are transparent at certain wavelengths and need to be measured at wavelengths were it is opaque. In order to measure metals at high temperature a suitable wavelength is 8-1μm. Plastic films such as polyethylene and polypropylene respond favourably at a wavelength of 3.43 μm. In general, low temperature conditions have a spectral response that lies in the 8-14μm-wavelength range. Typically fixed-emissivity instruments are sufficient for low temperature applications.

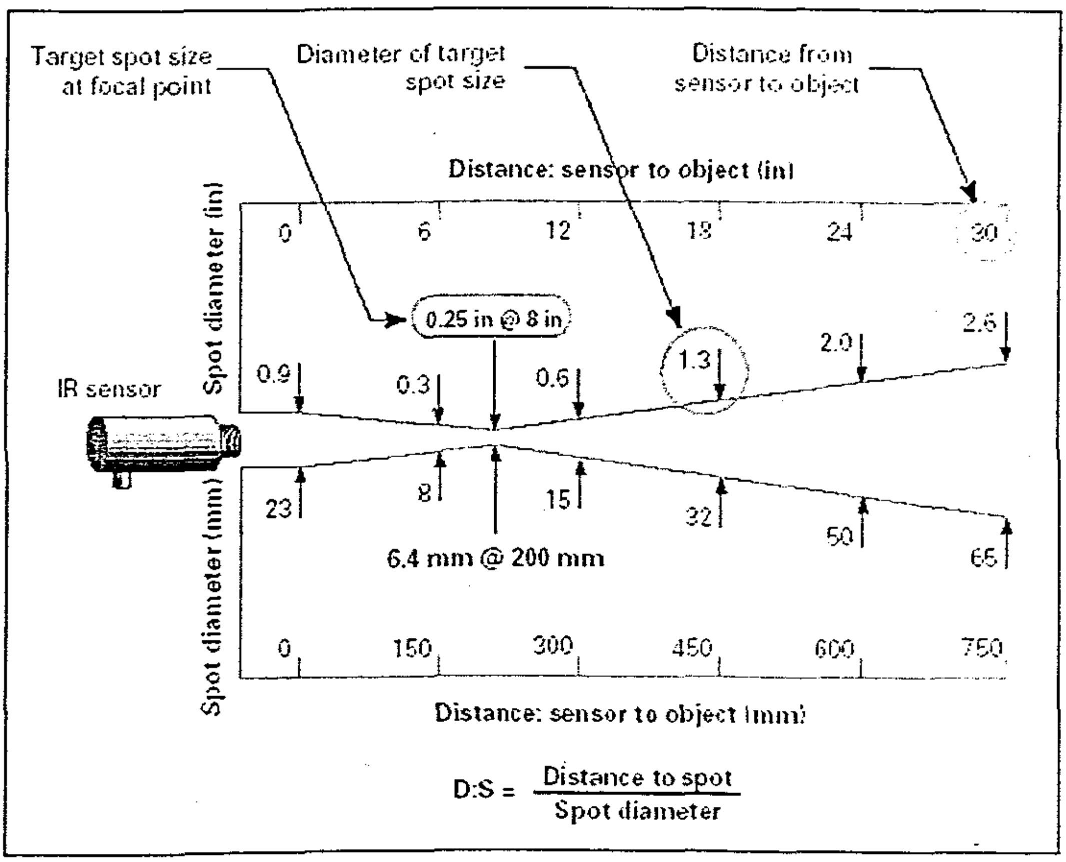

Figure 4.24 Determination of the D:S ratio for an infrared temperature sensor

4.4 Data Acquisition

The data acquisition for temperature measurement instituted in this paper is accomplished in two ways. In the first instance it is needed to complete the experiment in which the transfer function of an IR heater is found. Because the software used to complete the experiment was LabVIEW, a compatible hardware unit the DAQPad-1200 was chosen to facilitate the measurement procedure. In the development of the controller however the software used was the high level language, C, this precipitated the use of the on-board analog-to-digital converter. Both these methods when implemented proved very successful.

4.4.1 National Instruments DAQPad-1200

The temperature sensor is interfaced to the data acquisition hardware, the National Instruments DAQPad-1200. This hardware is a low-cost high performance DAQ unit that communicates with a computer through the parallel port on IBM PC/AT/XT and compatibles. The features of this unit are the following:

- Eight analog input channels, configured as eight single ended or four differential inputs.
- 12-bit successive-approximation ADC
- Two 12-bit DAC's with voltage outputs
- 24 lines of TTL-compatible digital I/O
- Three 16-bit counter/timers for timing I/O
- Conversion time (including acquisition time) of 8.5μm

The DAQPad-1200 is also completely software configurable and self-calibrated. The unit works with two different parallel port types, the Centronics port for printers and the Enhanced Parallel Port (EPP).

The unit is programmed and operates with LabVIEW software and can briefly be described as follows:

- The DAQPad-1200 on-board A/D samples the input sensor temperature. The integrated conversion performed by the sensor, 10mV/°C, represents a temperature as a voltage between 0V and 5V.
- These samples are time stamped and graphed and stored in a text file for processing at a later stage.

The software program is configured as a data logger to facilitate the transportation of information to a spreadsheet file. Then using the graphics tool in MsExcel the information is plotted on a graph, as shown in figures 3.5 to 3.8.

4.4.2 80C515 Analog-to-Digital converter

The on-board analog-to-digital converter (ADC) of the 80C515 has the following features:

- Eight multiplexed input channels
- Programmable internal reference voltages
- 8-bit resolution within reference voltage range
- 13 machine cycles conversion time (includes sampling time)
- Internal start-of-conversion trigger
- Interrupt request generation after each conversion

The 80C515 method of conversion is via successive approximation using a capacitor array. The mode in which the ADC is used can be described as follows:

- Single conversion mode
- 2.5V internal reference voltage

The temperature sensor's linear voltage output facilitates interfacing to the on-board ADC of the microcontroller.

5. ANALYSIS OF RESULTS

A PID based model has been designed, developed, tested and implemented. Closed loop controllers such as the PID controller developed are useful in applications requiring an embedded process. A microprocessor is well suited to successfully incorporate the computations needed of a digital controller. The results discussed in this section pertain only to the PID controller developed and does not deal with the experiment to derive the transfer function of the IR heater, as outlined in section 3.3.1.

5.1 Control system and controller integration

The model of the PID controller instituted in this instance does not incorporate any automatic tuning regimen. An auto-tuning functionality would be able to recalculate the parameters for the process gain, K_p, the integral time, T_i and the derivative time, T_d as the system dynamics change. This dictates a much more vigorous and computationally intensive algorithm to implement.

The approach taken in this paper is to design and implement a model of a PID controller successfully such that the controller adequately and reliably tracks a temperature profile.

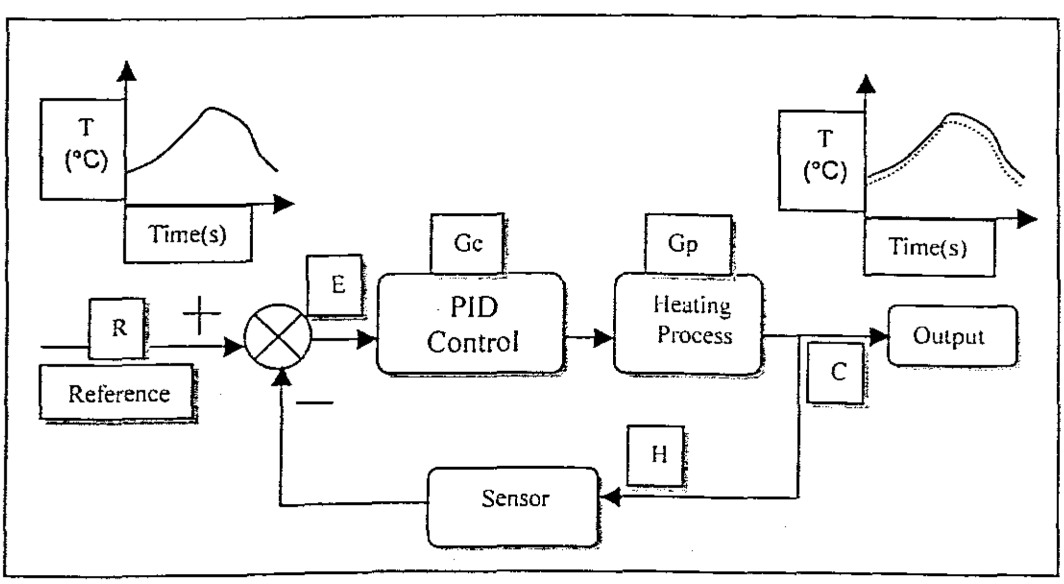

Figure 5.1 The Control System for the IR controller

Temperature profiles are necessary for the proper processing of many different types of materials and an example of this is given in figure 1.2. Subjecting the controller to the control system as illustrated in figure 5.1 and observing how closely the output (C) follows the input (R) was used as the measure of the success of the controller implemented.

The mathematical description of the PID controller as given in equation 3.11, needs to adequately achieve synergy with the mathematical model of the complete control system as stated in equation 5.1.

$$\frac{C(s)}{R(s)} = \frac{Gc(s)Gp(s)}{1 + Gc(s)Gp(s)H(s)} \qquad (5.1)$$

As a result the PID controller developed needs to effectively meet the transient and steady state conditions of the closed loop system. If significant deviations from the set point occur it could possibly be cause for concern if the product being processed is temperature sensitive, meaning it has a temperature profile that allows for very little deviation or offset. This study does not compare the heating profiles for any particular material against the response of the controller developed. However another approach was taken, which satisfactorily addresses this issue.

5.2 Comparative testing of the PID controller

In order to gauge the effectiveness of the PID controller developed, a simpler proportional type of controller was designed to serve as a basis for comparison. The *on/off regulator* does not require the same intense computations as that of the PID instituted. The on/off algorithm as illustrated in figure 5.2 simply ensures that the set point temperature is maintained within reasonable limits. The algorithm does not adjust the pulse-width of the firing pulse when increasing the temperature, as in the case of the PID algorithm.

A brief explanation of the on/off algorithm is as follows:

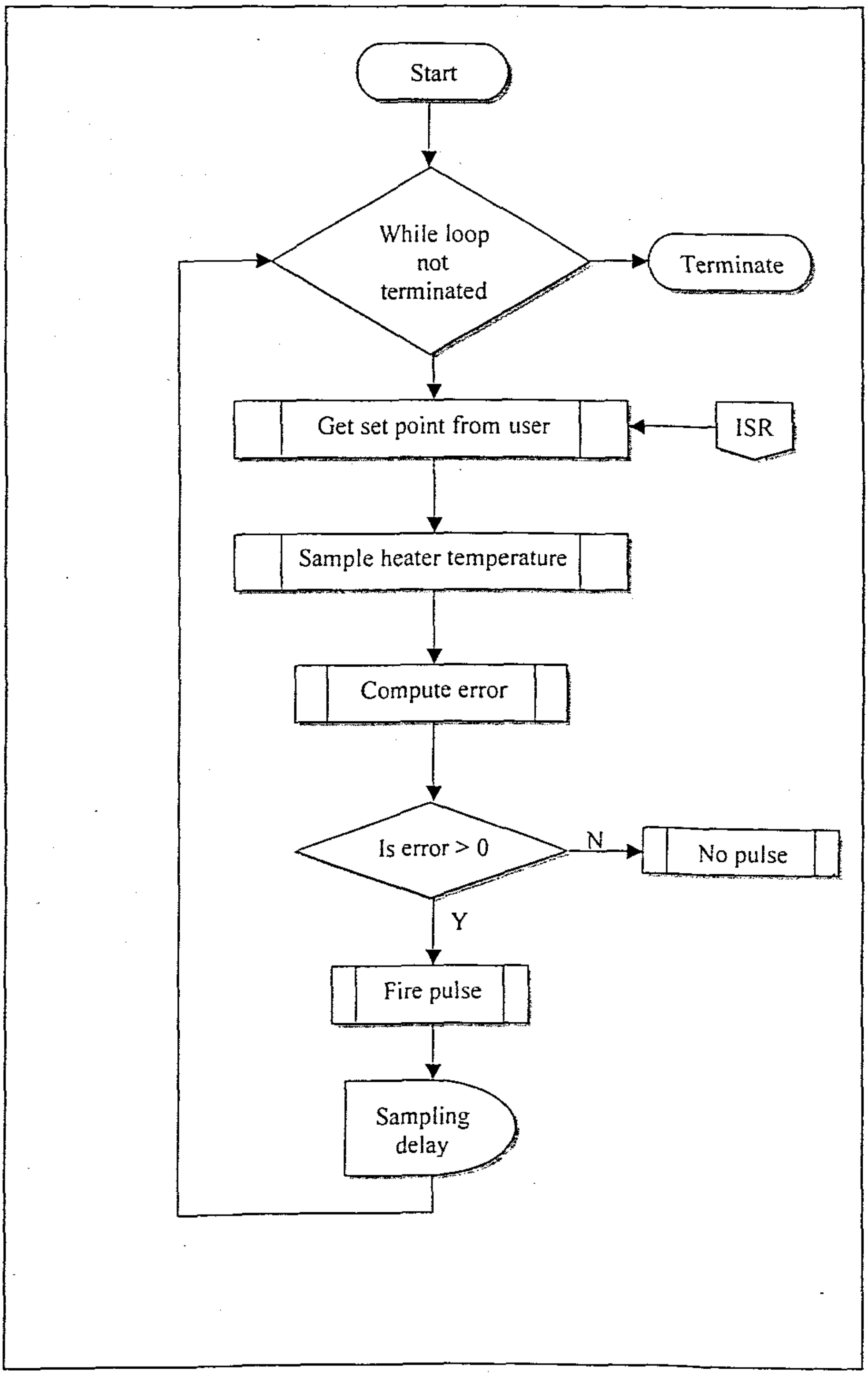

Figure 5.2 Flowchart of the proportional algorithm

- After the initialisation of the variables and functions used, the program executes with the set point as zero, until the user enters a temperature set point above zero.
- The heater temperature is sampled and an error is generated.
- If the error is positive (> 0), a firing pulse is initiated, however if the error is less than or equal zero (<= 0), no firing pulse is initiated.
- The program waits for the sampling period to complete before taking another measurement of the heater temperature and repeats the loop.

Laboratory tests have been performed using both the PID and on/off controllers. Each controller was set to follow a predetermined temperature profile and the results plotted on MsExcel charts. Figure 5.3 illustrates the laboratory set up for the IR heater and the Raytek temperature sensor and how they were arranged in order to complete the tests outlined below. The infrared heater was aligned and fixed to an aluminium

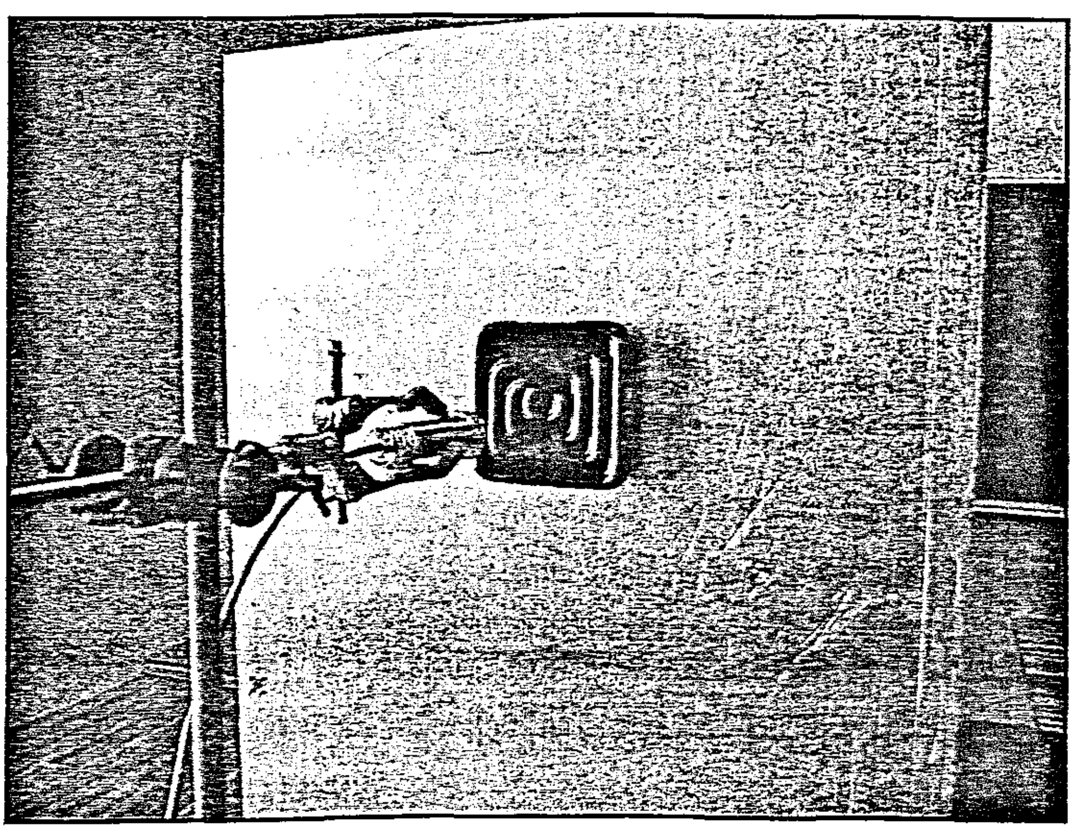

Figure 5.3 Laboratory arrangement showing the IR heater and temperature sensor

plate. The reason for the aluminium used, was that it possesses a low emissivity and a high degree of reflectivity. Since the temperature sensor is a function of the emissivity, only the emissivity from the IR heater then has a bearing on the temperature reading.

5.2.1 Comparative tests at a sampling period of 1 second

Figures 5.4 to 5.6 show the temperature profiles plotted by the two controllers. Table 5.1 indicates an arbitrary desired profile (profile 1) programmed into the microcontroller, the response curves for the on/off and PID models are shown in figure 5.4.

Table 5.1 Temperature set points for profile 1

Phase	Temperature set point (°C)
1	40
2	80
3	150
4	200
6	150

Table 5.2 indicates the desired profile (profile 2) for the on/off and PID models and their response curves are illustrated in figure 5.5.

Table 5.2 Temperature set points for profile 2

Phase	Temperature set point (°C)
1	80
2	100
3	220
4	160

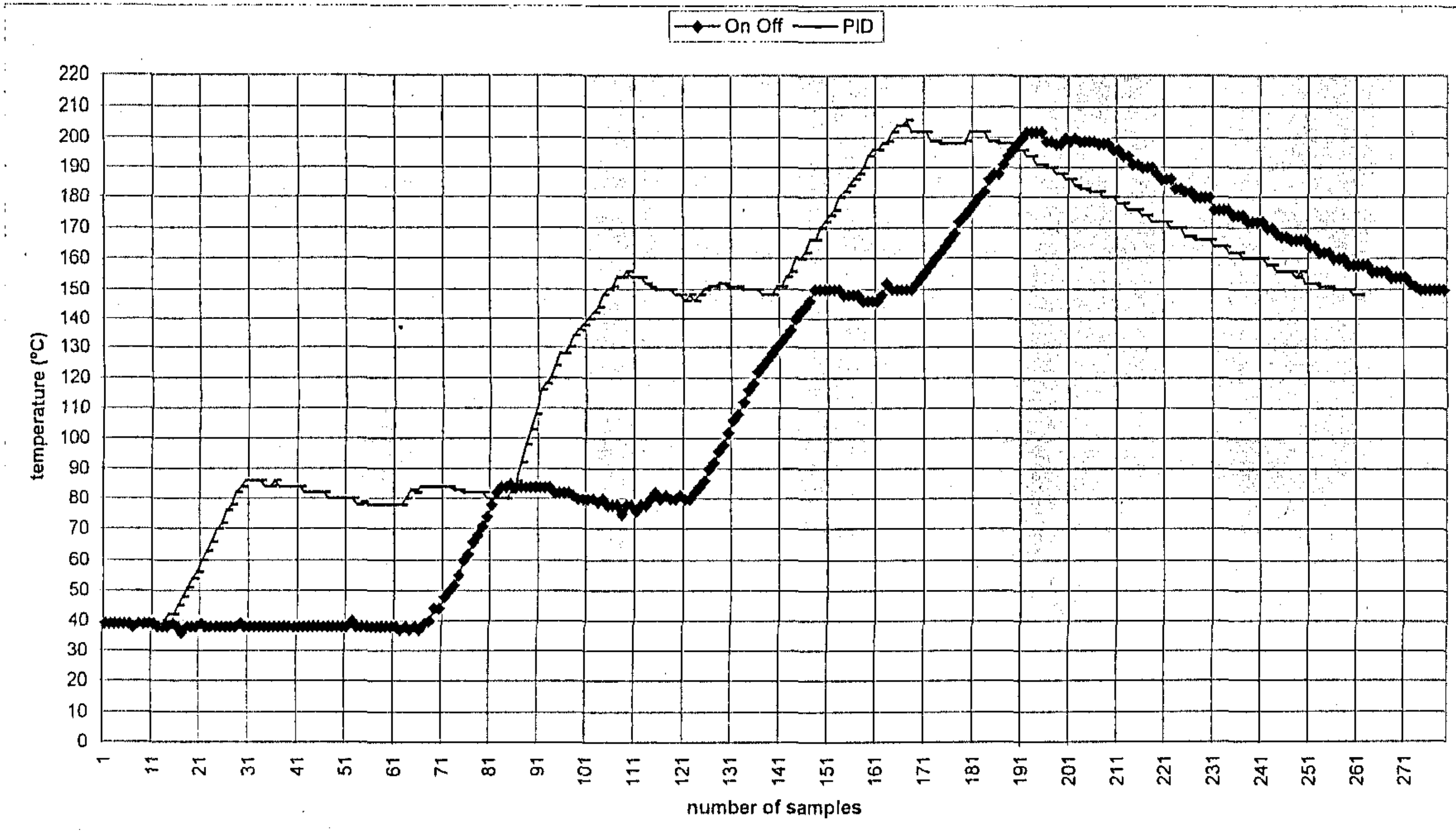

Figure 5.4 On/Off and PID controller comparison for profile 1

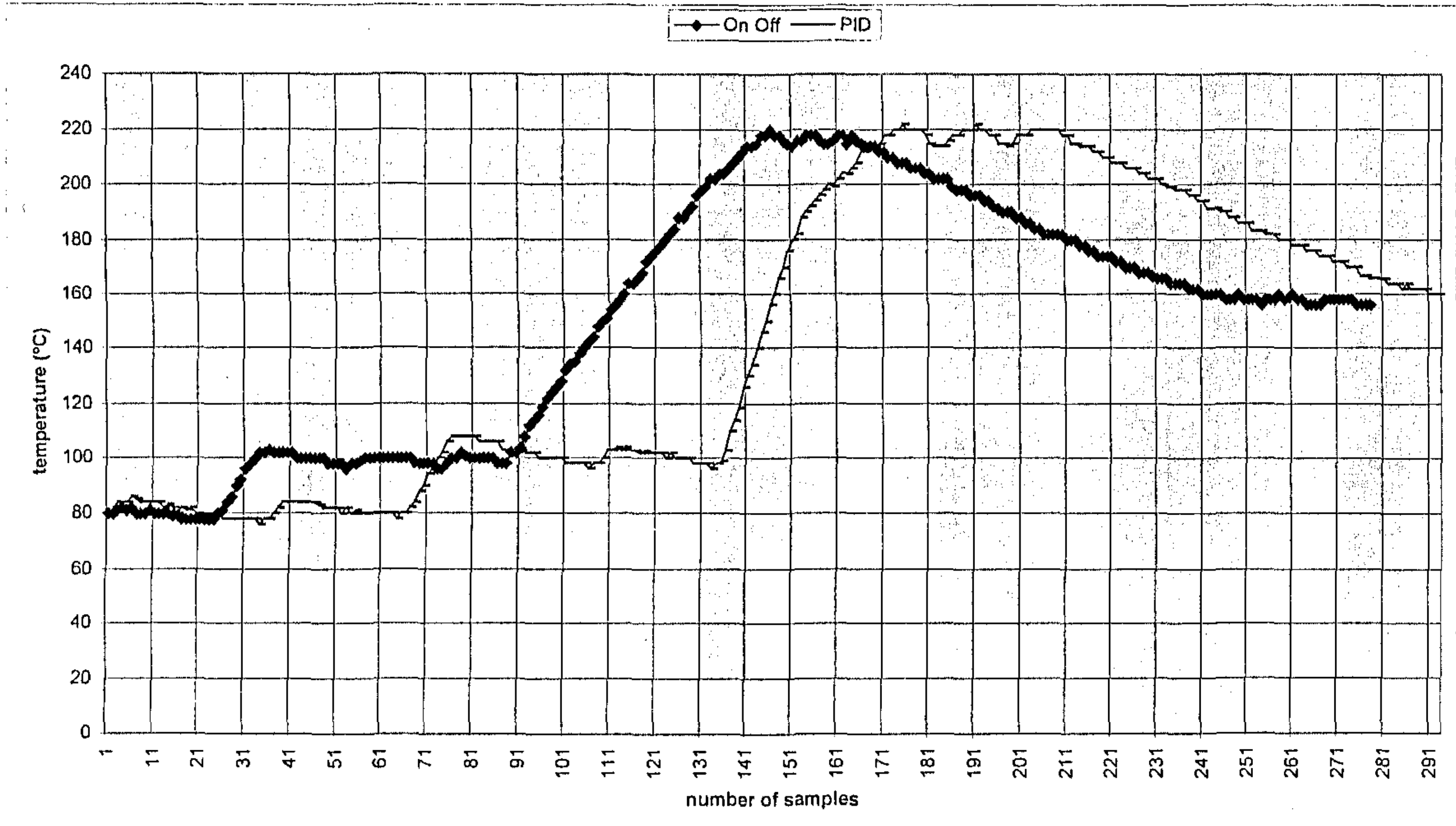

Figure 5.5 On/Off and PID controller comparison for profile 2

Table 5.3 Comparison of PID and on/off controllers at a sampling period of 1 sec

	PID Controller	ON/Off Controller
% Overshoot (100°C)	8%	3%
Temperature offset (220°C)	8°C	4°C
Rise time (sec) (100°C to 220°C)	38 sec	57 sec

Inspection of the curves in figures 5.4 and 5.5 achieved with a sampling interval of 1 second, reveal how the two types of controllers compare. A more concise comparison is done in table 5.3 with the values obtained through a study of figure 5.5. The factors considered in this evaluation of the curves are; percentage overshoot, temperature offset and rise time.

The deduction that is evident from the two controllers with a sampling period of 1 second is that unless rise times are critical and a certain temperature offset is acceptable, the PID controller is adequate. Otherwise it is a more viable option to use the on/off controller. Because of the heating dynamics of this type of infrared heater, the warm-up curve is strongly affected by the long heating time constant.

5.2.2 Comparative tests at a sampling period of 100ms

The PID model produces a significantly better response when the sampling interval is increased to 100 milliseconds. Figures 5.6 (profile 3) and 5.7 (profile 4) trace the curves for the PID and on/off models for the new sampling period. Only a restricted portion is shown here because the buffer used to store the list of temperatures, saturates after 512 samples are received. Nevertheless the portion clearly demonstrates the improved performance of the PID controller over its on/off counterpart. The curve of figure 5.6 traces a set point from 100°C to 160°C. The assessment of figure 5.6 as revealed in

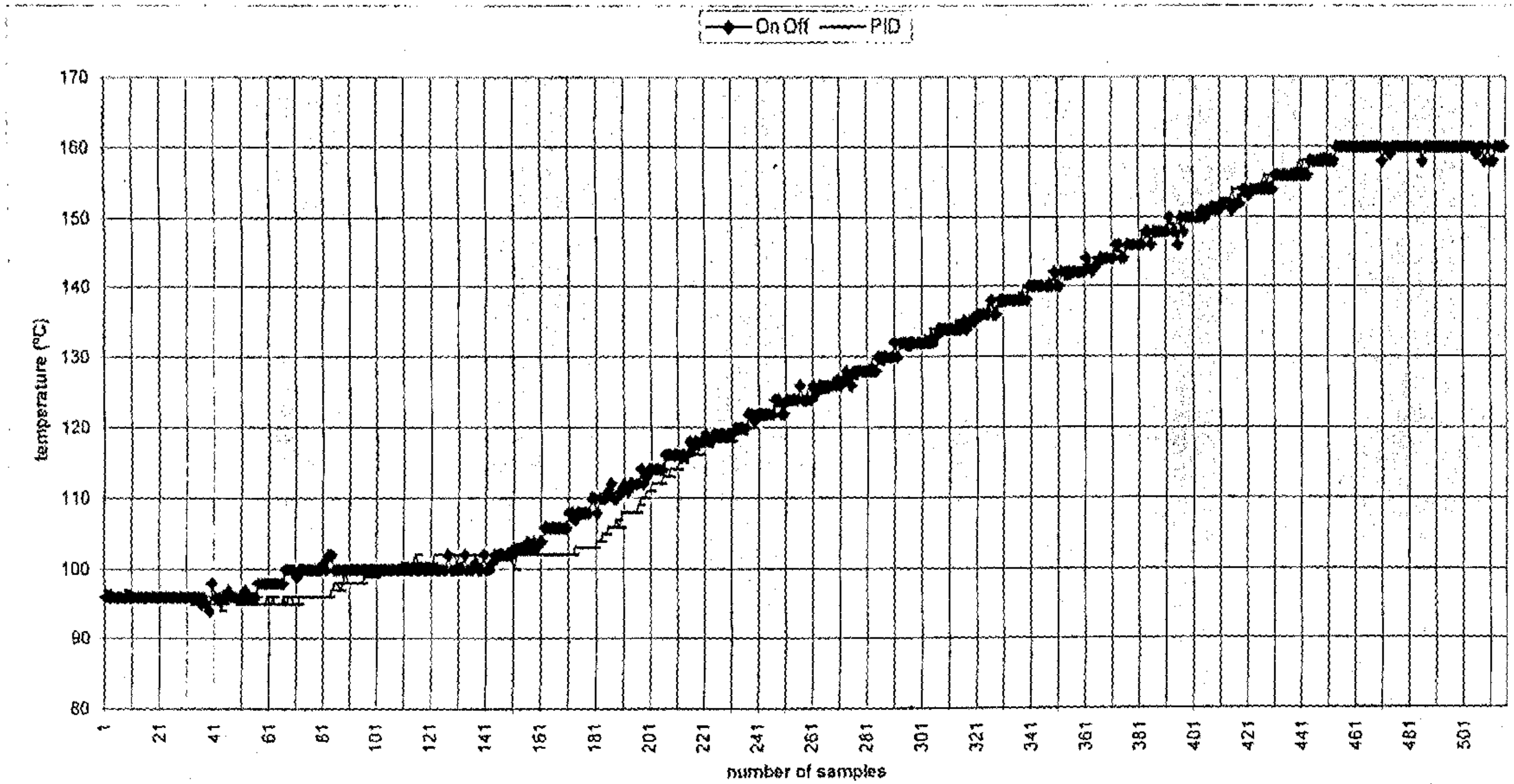

Figure 5.6 On/Off and PID controller comparison for profile 3

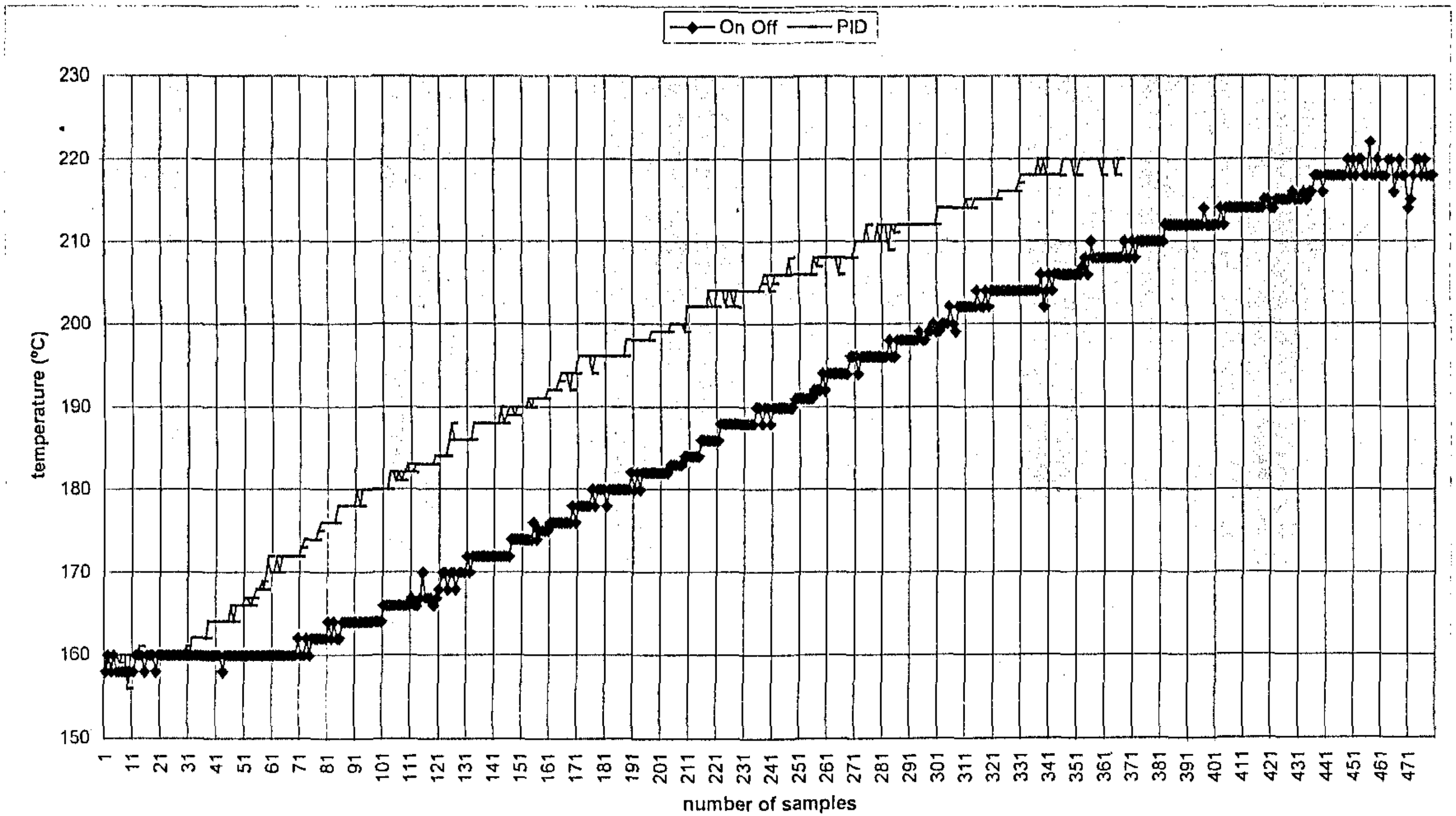

Figure 5.7 On/Off and PID controller comparison for profile 4

Table 5.4 Comparison of PID and on/off controllers at a sampling period of 100ms for figure 5.6

	Interval	PID Controller	On/Off Controller
% Overshoot	100°C	1%	0%
	160°C	0%	0%
Temperature Offset	100°C	2°C	3°C
	160°C	0°C	2°C
Rise time (sec)	100°C to 160°C	284 sec	312 sec

table 5.4, leads to the conclusion that with an increased sampling period the PID controller implemented for this paper exhibits an improved performance when compared to a simple on/off controller.

For the measurements taken in the tests performed, two components in the feedback loop dictate the accuracy of the readings. These components are the infrared temperature sensor and the analog-to-digital converter (ADC). A review of some of the important specifications for the sensor were covered in chapter four, section 4.3. In sections 5.3 and 5.4 some of the finer details of the temperature measurements are considered.

5.3 Infrared temperature sensor

The manufacturer, Raytek, provided the parameters of the sensor that are quoted below, which describe their Thermalert CI series of sensors (C13B).

- Accuracy: (a) 100°C to 500°C ± 3°C, (b) 30°C to 99°C ±6°C
- The temperature resolution better than 0.5°C.

- The sensor was placed at a distance of 100mm from the IR heater, which forms a spot size (diameter) of 15mm at the focal point, as indicated by the optical chart in figure 4.23. This spot diameter proved adequate since the IR heater dimensions are 41 x 41 mm.
- The sensing head was designed to operate in ambient temperatures from 0°C to 70°C. Because the air temperatures at the time of the measurements were in the region of 25°C to 35°C, the manufacturer's limits were never exceeded.
- The instrument conforms to the following standards of conformity for the European community:
    - EN50081-1: 1992, Electromagnetic emissions
    - EN50082-1: 1992, Electromagnetic susceptibility

5.4 Analog-to-digital converter (ADC)

The Siemens 80C515 microcontroller on-board ADC was briefly discussed in chapter four, section 4.4.2. Some of the more pertinent factors influencing the accuracy of the ADC measurement are as follows:

- With a 10-bit resolution the ADC can distinguish an incoming voltage into 1024 different levels (2^{10}).
- Since the range of the input signal extends from 0V to 5V, the least significant bit (LSB) corresponds to 5.0mV. With a linear output voltage of 10mV/°C from the sensor, a 0.5°C resolution of the input signal is possible.
- The sensor is interfaced to the ADC through a single-ended input configuration. Although this method is simple to implement, it suffers from a high sensitivity to noise.
- The 80C515 possesses an internal calibration mechanism and executes two basic functions, an offset and a linearity calibration. A calibration feature is useful since the ADC design parameters are adjusted for if a noteworthy drift occurs. After each reset operation a calibration procedure is automatically initiated.

5.5 Overview of Analysis

Some of the more important factors that could influence the temperature readings were presented. The measurements should therefore be accepted strictly as a trend when interpreting them. The conclusions however that emerge from the comparative testing of the two models are clear. The PID controller shows an improved performance at higher temperatures. The PID model achieves a better rise time, a critical parameter for many industrial processes, than the on/off regulator. The temperature offset is also greatly diminished as well as the percentage overshoot, which are all important parameters to consider when implementing any controller.

6. CONCLUSION AND RECOMMENDATIONS

This dissertation is based on theoretical and practical work regarding the design of an infrared radiation heating profile controller. Both modeling and experimental techniques have been employed. The focus has been on developing a programmable and cost-effective controller. This study considered only electric infrared heaters.

A model for a temperature profile controller for an infrared radiation heater has been proposed. The model is based on a proportional-integral-derivative (PID) control structure. The PID control design is the oldest and most widely used form of control in industry. Temperature control is particularly suited to this type of design. Ziegler-Nichols methods have been employed because of their simplicity and effectiveness. The Ziegler-Nichols method is another tried and trusted technique used for many years by control engineers. The controller developed though only a simplified first order model with lag, proved very effective for the purposes of temperature profiling.

The results obtained from comparative tests performed revealed the high efficiency of the PID model relative to an on/off controller. The tests using a sampling period of 100ms, although they only covered a restricted temperature range, exposed the improved performance of the PID design over its on/off counterpart. Although extensive tests have not been conducted on the controller for the purposes of this study, the PID model showed promising results. Elaborate testing and verification of the results are left as a suggestion for any further work and study.

6.1 Problems solved in the dissertation

The problem that this dissertation was required solve was the theoretical design and hardware implementation of an infrared radiation heating profile controller. This problem was further divided into many sub-problems, which include the following:

- Conduct an experiment to determine the mathematical model (transfer function) of an infrared radiation heater.

- Design and implement the hardware set-up for the experiment described above.
- Develop the software program that would allow the accurate display of the heating and cooling curves of the IR heater under test.
- Investigate the various types of control models available (P, PI and PID) that would be suitable for type of temperature control required for this study.
- Investigate a hardware platform that proves suitable for the power control requirements of an IR heater.
- Develop a simpler type of control model, a proportional controller against which the developed PID control algorithm could be subjected to comparative testing.

6.1.1 Experimentally determine the mathematical model of an IR heater.

In order to obtain an accurate mathematical expression of the IR heater used in this research, a step response test of the IR heater was completed. This method of testing was done in accordance with the Ziegler-Nichols method, a popular and simple way of achieving the required results. These results were plotted in a graphical format and the curves were analysed. Simulation of the obtained transfer function, using Matlab software, showed good agreement with the practical results. Although the transfer function represented a first-order model with transport lag, the simulated results reflected an acceptable accuracy.

6.1.2 Investigate a hardware platform for the power control of an IR heater.

Various methods of power control of the IR heater were investigated and tested. Some of these methods included:

- Phase angle control using a triac
- Fast switching with an IGBT
- Cycle control with a solid-state switch

The method that proved most successful was the cycle control with a solid-state switch. The hardware model incorporated this power control design in the final controller circuit. The other types of power control proved problematic for a host of reasons and some of these include:

- They introduced power line disturbances into the controller circuitry.
- Electromagnetic interference (EMI) as well as radio frequency interference (RFI) was introduced.
- The type of control method selected proved unsuitable for the type of load being controlled.
- The power control components (triac and IGBT) failed or were damaged when used to control the rated load.

The problems listed above all contribute to making the load and the control circuit unstable and therefore are unsuitable as a method of control.

6.1.3 Investigate the various types of temperature control models available.

The type of temperature control algorithm implemented for this research was the PID type control. This type of control method is common for the purposes required in the temperature control problem of this study. In order to gauge accurately the effectiveness of the controller developed, a simpler type of controller, a proportional controller, was developed. The PID controller was subjected to comparative testing. The results confirm the superiority of the PID control model as opposed to the P type control structure.

6.2 Applications of the results

The results obtained in this research provide the following applications:

- A method of temperature control of an IR heater;
- And serves as a basis for more intensive IR study.

6.3 Recommendations for further study

The recommendations on the conclusion of this study acknowledges that IR processing, whether it be heating or drying, is still a modest researched area. Much work remains to be done concerning the investigation of the effects of infrared radiation on various materials. With the use of the controller developed in this paper the study of IR and its effects on many materials are now possible. A summary of the potential applications and improvements of the controller are presented below:

- A further comparative study using an auto-tuning PID controller, that automatically recalculates the parameters of the process as the load demand changes, is a consideration.
- The enlargement of the buffer used to store the list of temperatures for plotting needs to be increased so as to provide a clearer picture of the complete temperature profile.
- Subject the controller to tests on some industrial processes such as the reflow soldering technique as described in section 1.4.1 and observe the response. A measure of results is a good indicator of the efficiency of the controller.
- Increase the heating capacity of the infrared heaters i.e. increase the power densities of the heaters, by mounting an arrangement of heaters on a panel. This is a more useful and practical way to study the effect on industrial processes.
- Also conduct experiments to determine the spectral radiation densities of different heaters and various heater arrangements.

The research conducted for this dissertation serves as a basis for more intensive study of the many aspects of infrared processing. With an amplified heating capacity that an arrangement of many infrared heaters offers, a more worthwhile exploration of IR heating is possible. A modification of the power electronics components in this study would make this controller a more functionally competent unit for industrial purposes.

6.4 Publications in connection with dissertation

1. Adonis, M and Khan, MTE.: 2001. "Infrared Heating Profile Controller" Proceedings of the 3rd International Conference on Control Theory and Applications, Pretoria, South Africa, pp.445-449

2. Adonis, M and Khan, MTE.: 2003. Hardware development of an infrared heating profile controller. Journal of Engineering, Design and Technology.

7. REFERENCES

Ackland, K.June.1998.Selecting the right infrared temperature sensor. Temperature. InTech.

Afzal, T.M; Abe, T. 1999: Some fundamental attributes of far infrared radiation drying of potato. Drying Technology, Vol.17, No.1-2, pp. 137-155.

Altera, 1999.Technical Note: Reflow Soldering Guidelines for Surface-Mount Devices. Application note 81,January 1999,ver.3.

Anonymous.1993.Powder Coat.: better system = improved results. Modern Metals, Vol.49, pp.76-80.

Anonymous.1994.Perfect finishes with infrared. Metallurgia,Vol.61,pp.7-8.

Anonymous.1996a.Infrared heating systems offer dry/cure advantages.AdhesivesAge, Vol.39, pp.30-31.

Anonymous.1996b.Electricity, seen through a glass brightly.Process Engineering, Vol.77, pp.21.

Anonymous.1997.Environmental marketplace – Catalytic Infrared heating. Environmental Manager, Vol.8, pp.15.

Anonymous.1998.Explosive Cooking.Discover, Vol.19, pp.32.

Anonymous.Sep.1999.The Salamander News.Vol. 7, No. 9

Blanc, D.1999.Convective and radiant (IR) curing of bulk and waterborne epoxy coatings as thin layers.Polymer Engineering and Science,Vol.39, pp.2487-2497.

Blanc, D; Vessot, S; Laurent, P; Gérard, J.F.; Andrieu, J. 1997: Study and modeling of coated car painting film by infrared or convective drying. Drying Technology, Vol. 15, No. 9, pp. 2303-2323.

Blanc, D; Laurent, P; Andrieu, J; Gérard, J.F. 1997: Convective and Radiant (IR) Curing of Bulk and Waterborne Epoxy Coatings as thin layers. Part I: Methodology. Polymer Engineering and Science, Vol. 37, No. 12, pp. 1959-1969.

Botero, U.1997.Infrared radiation effects on some functional characteristics of wheat flour. Masters thesis (M.Sc.). University of Manitoba (Canada). Masters Abstracts International, Vol.36, pp438.

Broadbent, A.D.1998.Comparisonof thermal fixation of reactive dyes on cotton using infrared radiation or hot air.American Chemical Society, Vol.37, pp.1781-1785.

Broadbent, A.D; Coté, B; Fecteau, T; Khatibi-Sarabi, P; Thérien, N. 1994: Pre-drying textile fabrics with infrared radiation. Textile Research Journal, Vol. 64, No. 3, pp. 123-129.

Çengel, Y.A. 1997. Introduction to thermodynamics and heat transfer. U.S.A; Mc-Graw-Hill.

Chen, Y.S.1995.Infrared heating and welding of thermoplastics and composites. Thesis(PH.D.)Ohio State University.Dissertation Abstracts International, Vol. 56, pp5148.

ControlIR.Technical brochure: ControlIR-930/935-D-01-B available at: http://www.researchinc.com/tsd/Products/ControlIR/controlir.htm

Cox,NR;McGee,DE.1989.Use of high density IR for the rapid heating of metals. Industrial Heating, pp46-48.

Dhib, R.1999.Model-based multivariable control of the drying of a thin sheet of fibres in a continuous infrared dryer.Canadian Journal Of Chemical Engineering, Vol.77, pp.1055-1064.

Dhib, R; Broadbent, A.D; Thérien, N. 1994: Modelling and simulation of the drying of thin sheets in a continuous infrared dryer. The Canadian Journal of Chemical Engineering, Vol. 72, pp. 894-905.

Dhib, R; Thérien, N; Broadbent, A.D. 1998: Derivation of a control orientated low order model of the dynamics of an infrared oven for the continuous drying of a thin sheet of material. The Canadian Journal of Chemical Engineering, Vol. 76, pp. 290-299.

Dow, S.1984.Use of radiant infrared in soldering surface mounted devices to printed circuit boards. Solid State Technology, Vol.27, pp.191-195.

Evalds,P.October.2002.SCR Power Controls Provide Reliable Industrial Electric Heating. Industrial Heating-The International Journal of Thermal Technology, Vol. LXIX, No.10.

Fasina, O.O; Tyler, R.T; Pickard, M.D. 1998: Modelling the infrared radiation heating of agricultural crops. Drying Technology, Vol. 16, No. 9-10, pp. 2065-2082.

Foster,A.1996.Infrared can take the heat.The Engineer, pp22.

Gefran.1999.Technical Brochure: Solid State power Units, power under control.Oct.

Hashimoto, A; Kameoka, T. 1998: Effect of infrared radiation on drying characteristics of wet porous materials. Drying'98 – Proceedings of the 11th International Drying Symposium, pp.1891-1898.

Heikkilä, P. 1993: A study on the drying process of pigment coated paper webs. PhD Thesis. Report 92-125-A. Department of Chemical Engineering. Åbo Akademi.

Heraeus.1992.Technical Brochure: The Golden Figure Eight, 8 convincing arguments in favour of a unique principle of infrared heat technology. May.

Hottel, H.C. 1954. Radiant-Heat Transmission, in W.H McAdams ed., Heat Transmission, 3rd ed. U.S.A; Mc-Graw-Hill.

Hottel, H.C; Sarofim, A.F.1996.Radiant heat transfer. Mark's standard handbook for mechanical engineers, 10th ed.U.S.A; McGraw-Hill.

Howard, P.1996.End-use Electrotechnologies.Energy Engineering,vol.93,pp.51-65.

Incropera, F.P; DeWitt, D.P.1996. Introduction to heat transfer, 3rd ed. U.S.A. John Wiley and sons.

IR2000.1998.Technical Brochure:Elstein infrared-system for economical radiation heat.Oct.Elstein.

Katsuhiko, O. 1990. Modern control engineering, 2nd ed. U.S.A; Prentice-Hall.

Knights, M.1997a.Thermoformers give glowing reviews to halogen heat lamps.Plastics Technology, Vol.43, pp.16.

Knights, M.1997b.Tumbling clamshell oven puts new spin on rotomolding. Plastics Technology, Vol. 43, pp. 35.

Lampinen, M.J; Ojala, K.T; Koski, E. 1991. Modelling and measurements of infrared dryers for coated paper. Drying Technology, Vol. 9, No. 4, pp. 973-1017.

Lavitt,M.1996.Infrared deicing technique called ready for operational use. Aviation Week And Space Technology, Vol.145, pp.104-105.

Leigh, JR. 1988. Temperature measurement and control. United Kingdom; Peter Peregrinus.

Le Person, S; Puiggali, J.R; Baron, M; Roques, M. 1998: Near infrared drying of pharmaceutical thin films: experimental analysis of internal mass transport. Chemical Engineering and Processing, Vol. 37, pp. 257-263.

Mohan, N; Underland, T.M; Robbins, W.P.1995. Power electronics: converters, applications and design, 2nd ed.U.S.A.John Wiley and sons.

Myers,J.1984.Halogen lamps used as heaters for thermoforming. Modern Plastics, Vol.70, pp.21.

Navarri, P; Andrieu, J; Gevaudan, A. 1992: Studies on infrared and convective drying of non-hygroscopic solids. Drying'92 – Proceedings of the 8th International Drying Symposium, pp.685-693.

Navarri, A;Andrieu, J. 1993: High intensity infrared drying study. Part I. Case of capillary-porous material. Chemical Engineering and Processing, Vol. 32, pp.311-318.

Ojala, K.T; Lampinen, M.J. 1995. Modelling measurements and efficiencies of infrared dryers for paper drying. Handbook of Industrial Drying, 2nd ed, pp. 931-976.

Parouffe, J.M; Dostie, M; Mujamdar, A.S; Poulin, A. 1992: Convective transport in infrared drying. Drying'92 – Proceedings of the 8th International Drying Symposium, pp.695-703.

Pettersson, M; Stenström, S. 1998. Absorption of infrared radiation and the radiation transfer in paper. Part 2: Application to infrared dryers. Journal of Pulp and Paper Science, Vol. 24, No. 11, pp. 356-363

Pettersson, M. 1999. Heat transfer and energy efficiency in infrared paper dryers. Doctral Dissertation. Lund University (Sweden), pp. 39-40.

Rösler, M; Klinke, E; Kunz, G. 1995: Drying of Organic Coatings by Infrared Radiation of Different Wavelengths. Radtech Europe, 7th conference on radiation curing, Maastricht, pp. 462-468.

Sandu, C. 1986: Infrared radiative drying in food engineering: a process analysis. Biotechnology Progress, Vol. 2, No. 3, pp. 109-119.

Schumacher,H.1996.Infra-red soldering from the viewpoint of base material manufacturer. Circuit World, Vol.22, pp.4-8.

Silventoien, I; Palosaari, S. 1982: Drying of water-borne coatings. Acta Polytechnica Scandinavica, pp. 1-22.

Van Denend,T.1998.Infrared Predrying Yields Significant benefits. American Dyestuff Reporter, Vol.8, pp.45-46.

Yamazaki, Y; Hashimoto, A; Honda, T; Shimizu, M. 1992: Optical characteristics of gelatinous materials in infrared radiation drying. Drying'92 – Proceedings of the 8th International Drying Symposium. pp. 712-721.

Yoder,J.May.2000.Taking the mystery out of infrared sensors. Control for the Process Industries.

APPENDIX 1

EMITTANCE VALUES OF PARTICULAR MATERIALS

Surface	Temperature (Celcius)	Emittance
	Metals	
Aluminium, polished	170	0.039
Gold, polished	130	0.018
Iron, pure polished	93	0.06
Iron, hot rolled	20	0.77
Lead, pure polished	37.8	0.05
Nickel, bright	100	0.041
Platinum, polished	93	0.05
Platinum, black	93	0.93
	Paints	
Varnish, dark glossy	37.8	0.89
Enamel	20	0.85-0.95
Red lead paint	100	0.93
	Miscellaneous	
Brick	20	0.93
Ice, smooth	0	0.966
Ice, rough crystals	0	0.985
Water	37.8	0.96

APPENDIX 2

C CODE LISTING OF THE PID CONTROLLER

```
/***********************************************************************/
/*    THIS PROGRAM READS THE TEMPERATURE ON AN INTERFACED  */
/*    ADC AND SENDS AN ACTUATING SIGNAL WHICH IS DEPENDANT  */
/*    ON THE SIZE OF THE ERROR BETWEEN THE                  */
/*    REFERENCE AND MEASURED OUTPUT                         */
/*                                                          */
/*    THIS IS AN IMPLEMENTATION OF A PID LOOP FOR TEMPERATURE */
/*                  CONTROL                                 */
/*                                                          */
/*              By:  Marco Adonis                           */
/*                                                          */
/***********************************************************************/

/* Header files */

#include <stdio.h>        /* standard I/O .h-file*/
#include <stdlib.h>       /* standard library .h-file*/
#include <reg515.h>    /*special function register for 80C515*/
#include <math.h>
#define y 50000                        /* freq = 10Hz (T = 100ms)*/

/* Function Prototypes */

void serial_init(void);      /* Initialize the serial port */
int ADC (void);             /* Analogue to digital routine */
void delay(void);                    /* Delay function */
void display(void);        /* Monitor current temperature */
void pulse(void);                    /* PWM waveform generator */
void PWM_control(void);
void keypad(void);

/* Variable declaration */
long u_delta = 0;
long r_in = 0;
unsigned int x = 0;


/***********************************************************************/
/*                  MAIN FUNCTION                                      */
/***********************************************************************/

void main(void){

long error_0 = 0;
long error_1 = 0;
long error_2 = 0;
long y_out = 0;
long u = 0;
long u_old = 0;
```

```
long u1 = 0;
long u2 = 0;
long u3 = 0;
long u_old_1 = 0;
long u_old_2 = 0;

EX1 = 1;                /*interrupt for keypad*/
IT1 = 1;
EAL = 1;

serial_init();   /*initialise serial port*/

/***************************************************/
/*                    PID loop initialsation       */
/***************************************************/

y_out = ADC();               /* sample output*/
y_out = (y_out);
error_0 = r_in - y_out;              /*compute error*/

error_2 = error_0;

y_out = ADC();
y_out = (y_out);
error_0 = r_in - y_out;

error_1 = error_0;

/* To compute the previous actuator output
  u_old = (28*error_0) - (49*error_1)*/

u_old_1 = (28*error_0);
u_old_2 = (49*error_1);
u_old = u_old_1 + u_old_2;

/***************************************************/
/*                MAIN PID CONTROL loop            */
/***************************************************/

/*The PID loop computes the actuator output after each sampling interval
u = (u_old + (28*error_0) - (49*error_1) + (21*error_2))*/

while(!RI){

        y_out = ADC();
        y_out = (y_out);
        error_0 = (r_in - y_out);

        u1 = (28*error_0);
        u2 = (49*error_1);
```

```
        u3 = (21*error_2);

        u = u1 + u2 + u3 + u_old;

/* The computation of the incremental actuator output */
        u_delta = (u - u_old);

        PWM_control();              /*determine pulse-width*/

        u_old = u;
        error_2 = error_1;
        error_1 = error_0;

        pulse();                    /*call fire pulse*/
        delay();                    /*sampling delay*/
        display();

        error_0 = 0;
        u_delta = 0;
        x = 0;
        }
}

/* Function Declarations */

/**************************************************/
/*              SERIAL PORT INITIALISATION          */
/**************************************************/

void serial_init(void){

SCON = 0x5A;                        /* Initialise UART to mode 1 */
BD = 1;                             /* Generate baudrate internally */
PCON |= 0x80;                       /* Set to 9600 baud @12MHz */
}

/****************************************************/
/*              ANALOG TO DIGITAL CONVERTER           */
/****************************************************/

int ADC (void){

unsigned short value = 0;       /* Temperature value returned */

        ADCON = 0xF2;           /* Select channel 2,single conversion mode */
   DAPR = 0x80;                 /* Direct conversion, 2.5V int ref Voltage */
        while (BSY);  /* Wait while converting */
        {;}
        value = ADDAT;          /* Store value */
```

```
        return (value); /* Return temperature measurement */
        }

/**************************************************/
/*              IMPLEMENTING INTERVAL DELAY              */
/**************************************************/

void delay(void){

unsigned short i;                    /* Set up loop counters */

    i = 0;
    while(i<10000)                   /* Middle loop */
        {
        i++;
        }
  }

/****************************************************/
/*          MONITOR THE CURRENT TEMPERATURE              */
/****************************************************/

void display(void){

unsigned short q,value = 0;          /* Declare variables */

    printf("\n");
    value = ADC();                   /* Get temperature from ADC */
    printf("%3d",value);             /* Print values */
        for(q=0;q<=26;q++){
        printf("\b");                }
}

/**************************************************/
/*      Pulse-width modulated waveform determination      */
/**************************************************/

void PWM_control(void){

if (u_delta <= 0)
    {
    T2I0 = 0;             /*stop PWM pulses*/
    ET2 = 0;
    TF2 = 1;
    }
    else if ( u_delta >0 && u_delta <= 5000){
    x = 10000;                       /*pwm = 10ms*/
    }
    else if ( u_delta >5000 && u_delta <= 15000){
    x = 20000;                       /*pwm = 20ms*/
```

```
        }
        else if ( u_delta >15000)
        x = 30000;                      /*pwm = 30ms*/
        }
}

/* temperature profile presets*/

void keypad(void){

P5 && 0x0f;

        if (P5 == 1)
        {
        r_in = 80;              /*temperature 80°C*/
        }
        else if (P5 == 2){
        r_in = 170;             /*temperature 170°C*/
}
        else if (P5 == 3){
        r_in = 160;             /*temperature 160°C*/
        }
        else if (P5 == 4){
        r_in = 200;             /*temperature 200°C*/
        }
        else if (P5 == 5){
        r_in = 220;             /*temperature 220°C*/
        }
        else if (P5 == 6){
        r_in = 0;               /*temperature 0°C*/
        }
}

void External1 (void) interrupt 2 using 0
{
keypad();
}

void pulse(void)
{

        CCL3 = (65536UL - x);
        CCH3 = (65536UL - x) >> 8;/* Compare value (duty cycle) */
        CRCL = (65536UL - y);
        CRCH = (65536UL - y) >> 8;          /* Reload value (50ms period) */
        T2CON = 0x91;           /* Select reload mode 0 and ... */
                                /* Bit to start/stop timer */
        CCEN = 0x80;            /* Enable compare */
        TF2 = 0;                /* Clear interrupt request flag */
        ET2 = 1;                /* Enable timer 2 overflow interrupt */
```

```
}

void Timer2 (void) interrupt 5 using 0
{
TF2 = 0;                        /* Clear overflow flag */
}

/******************************* END ***********************/
```

APPENDIX 3

C CODE LISTING FOR ON/OFF CONTROLLER

```
/**************************************************************/
/*THIS PROGRAM READS THE TEMPERATURE ON AN INTERFACED   */
/* ADC AND SENDS AN ACTUATING SIGNAL WHICH IS DEPENDANT  */
/* ON THE SIZE OF THE ERROR BETWEEN THE REFERENCE AND     */
/*                    MEASURED OUTPUT                     */
/*                                                        */
/*      THIS IS AN IMPLEMENTATION OF A PROPORTIONAL       */
/*        CONTROL LOOP FOR TEMPERATURE CONTROL            */
/*                                                        */
/*                  By:  Marco Adonis                     */
/*                                                        */
/*                  HARDWARE Version                      */
/**************************************************************/

/* Header files */

#include <stdio.h>          /* standard I/O .h-file*/
#include <stdlib.h>         /* standard library .h-file*/
#include <reg515.h>          /* special function register for 80C515*/
#define y 50000                    /*freq = 10Hz (T = 100Ms)*/

/* Function Prototypes */

void serial_init(void);       /* Initialize the serial port */
int ADC (void);              /* Analogue to digital routine */
void delay(void);                  /* Delay function */
void display(void);          /* Monitor current temperature */
void pulse(void);                  /* PWM waveform generator */
void PWM_control(void);
void keypad(void);

/* Variable declaration */

long error = 0;
long r_in = 0;
unsigned int x = 0;

/********************************************************/
/*              MAIN FUNCTION                           */
/********************************************************/

void main(void){

long y_out = 0;

EX1 = 1;            //interrupt for zero crossing
IT1 = 1;
EAL = 1;

serial_init();
```

```
/**************************************************/
/*                    ON/OFF CONTROL LOOP        */
/**************************************************/

while(!RI){

        y_out = ADC();    /*sample output*/
        y_out = (y_out);
        error = (r_in - y_out); /*compute error*/

        PWM_control();

        pulse();
        delay();
        display();

        x = 0;
        error = 0;
        }
}

/* Function Declarations */

/*********************************************************/
/*              SERIAL PORT INITIALISATION               */
/*********************************************************/

void serial_init(void){

        SCON = 0x5A;            /* Initialise UART to mode 1 */
        BD = 1;                 /* Generate baudrate internally */
        PCON |= 0x80;           /* Set to 9600 baud @12MHz */
        }

/*********************************************************/
/*              ANALOG TO DIGITAL CONVERTER              */
/*********************************************************/

int ADC (void){

unsigned short value = 0;     /* Temperature value returned */

ADCON = 0xF2;      /* Select channel 2,single conversion mode */
DAPR = 0x80;       /* Direct conversion, 2.5V int ref Voltage */
while (BSY);  /* Wait while converting */
{;}
value = ADDAT;            /* Store value */

return (value); /* Return temperature measurement */
```

```
                }

/*********************************************************/
/*              IMPLEMENTING INTERVAL DELAY               */
/*********************************************************/

void delay(void){

        unsigned short i;               /* Set up loop counters */

        i = 0;
                while(i<10000)          /* Middle loop */
                {
                i++;
                }
}

/**********************************************************/
/*          MONITOR THE CURRENT TEMPERATURE                */
/**********************************************************/

void display(void){

unsigned short q,value = 0;    /* Declare variables */

printf("\n");
        value = ADC();                 /* Get temperature from ADC */
        printf("%3d",value);  /* Print values */
        for(q=0;q<=26;q++){
        printf("\b");
        }
}

/*********************************************************/
/*              Pulse-width modulated waveform determination    */
/*********************************************************/

void PWM_control(void){

if (error <= 0){
        T2I0 = 0;               /*put heater 'off'*/
        ET2 = 0;
        TF2 = 1;
        }
        else if (error > 0){
                x = 10000;   /* put heater 'on'*/
                }
}

void pulse(void)
```

```
{
        CCL3 = (65536UL - x);
        CCH3 = (65536UL - x) >> 8;/* Compare value (duty cycle) */
        CRCL = (65536UL - y);
        CRCH = (65536UL - y) >> 8;          /* Reload value (50ms period) */
        T2CON = 0x91;       /* Select reload mode 0 and ...*/
/* Bit to start/stop timer */
        CCEN = 0x80;                        /* Enable compare */
        TF2 = 0;                    /* Clear interrupt request flag */
        ET2 = 1;                    /* Enable timer 2 overflow interrupt */
}

/* temperature profile presets*/

void keypad(void){

P5 && 0x0f;

        if (P5 == 1)
        {
        r_in = 120;                 /*temperature 120°C*/
        }
        else if (P5 == 2){
        r_in = 170;                 /*temperature 170°C*/
        }
        else if (P5 == 3){
        r_in = 160;                 /*temperature 160°C*/
        }
        else if (P5 == 4){
        r_in = 200;                 /*temperature 200°C*/
        }
        else if (P5 == 5){
        r_in = 220;                 /*temperature 220°C*/
        }
        else if (P5 == 6){
        r_in = 0;                   /*temperature 0°C*/
        }
}

void External1 (void) interrupt 2 using 0
{
keypad();
}

void Timer2 (void) interrupt 5 using 0
{
TF2 = 0;                            /* Clear overflow flag */
}

/******************************* END *****************************/
```

APPENDIX 4

C CODE LISTING OF TRIAC POWER CONTROL PROGRAM

```
/*******************************************************************/
/*      Program to fire a pulse on zero-crossing of AC line voltage   to vary the   */
/*   load power of an IR emitter & thru ADC read the load temp & store results    */
/*      in a log file                                                              */
/*      POWER CONTROL USING A TRIAC                                                */
/*******************************************************************/

#include <stdio.h>
#include <stdlib.h>
#include <reg515.h>
#include <math.h>

/* Message Statements */
code char menu[] =
"\n********** MENU ************"
"\nPress 'f' to select firing angle"
"\nPress 's' to start the program";
code char txt1[] = "\nSelect the firing angle between 0 and 10 milliseconds >>  ";
code char txt2[] = "\nMeasurements in progress(Hit Q to exit)\n ";

/* Function prototypes */
void serial_init(void);                         /* interrupt serial port */
void set_firing_angle(void);
void check_angle(void);
void pulse_delay(void);
void fire_delay(void);
void delay(void);
void program_start(void);
void program_loop(void);

/* Variables declaration */

unsigned short set_fire = 0;
//unsigned short interval = 0;

/* MAIN FUNCTION */
void main(void){
char c;
EX0 = 1;
IT0 = 1;
EAL = 0;                    // clear all interrupts

serial_init();

        while(1){
        printf(menu);
        c = getchar();
        switch(c)
```

```
        {
        case 'f':
                set_firing_angle();
                break;
        case 's':
                program_start();//program_loop();
                break;
        default:
                printf(menu);
                break;
                }}}

/* serial port initialisation */

void serial_init(void){

SCON = 0X5A;
BD = 1;
PCON |= 0X80;
}

/* setting firing angle */
void set_firing_angle(void){

printf(txt1);
scanf(" %d", &set_fire);
printf("/n Firing angle delay set to %2d ms", set_fire);
//interval = 9 - set_fire;
}

void program_start(void){
P4 = 1;                                 // pulse in positive half
pulse_delay();
P4 = 0;
}
void pulse_delay(void){

CRCL = 0x18;                            // 1ms pulse delay
CRCH = 0Xfc;
T2CON = 0x11;
TF2 = 0;//1;
ET2 = 1;
}
```

```
if(set_fire != 0){
fire_delay();
P4 = 1;                                  // pulse in positive half
pulse_delay();
P4 = 0;
delay();
fire_delay();
P4 = 1;                                  // pulse in negative half
pulse_delay();
P4 = 0;
}
else{
P4 = 1;                                  // pulse in positive half
pulse_delay();
P4 = 0;
delay();
P4 = 1;                                  // pulse in negative half
pulse_delay();
P4 = 0;
}}

void pulse_delay(void){

CRCL = 0x18;                             // 1ms pulse delay
CRCH = 0Xfc;
T2CON = 0x11;
TF2 = 1;
ET2 = 1;
}

void fire_delay(void){

CRCL = (65536UL – (set_fire*1000));            // variable firing pulse delay
CRCH = (65536UL – (set_fire*1000)) >> 8;
T2CON = 0x11;
TF2 = 1;
ET2 = 1;
}

void delay(void){

CRCL = (9000 – (set_fire*1000));                    // variable interval delay
CRCH = (9000 – (set_fire*1000)) >> 8                T2CON = 0x11;
TF2 = 1;
ET2 = 1;
}
```

```
/*****************************************************************/
/*      Function Definitions for Interrupt Service Routines follow       */

void External0 (void) interrupt 0 using 0
{
program_start();
}

void Timer2 (void) interrupt 5 using 0
{
TF2 = 0;
}
```

APPENDIX 5

C CODE LISTING OF IGBT POWER CONTROL PROGRAM

```
/**************************************************************/
/* THIS PROGRAM OUTPUTS A CONTINUOUS STRING OF PULSES AT A */
/*FREQUENCY of 100Hz                                       */
/* (ie. 10ms Period)                                       */
/* INT0 STARTS THE PULSE PROGRAM                           */
*/ A TEST PROGRAM FOR IGBT POWER CONTROL                   */
/**************************************************************/

#include <stdio.h>
#include <stdlib.h>
#include <reg515.h>
//#define x 7497
#define y 8330

void pulse(void);
void keypad(void);
int x = 0;

void main(void)
{
EX0 = 1;            //interrupt for zero crossing
IT0 = 1;
EX1 = 1;            //interrupt for keypad
IT1 = 1;
EAL = 1;

while(1){};
}

void keypad(void)
{

P5 && 0x0f;
        if (P5 == 13)
        {
        T2I0 = 0;
        ET2 = 0;
        TF2 = 1;
        }           // keypad press decoding
        else if (P5 == 3){
        x = 833;
        }
        else if (P5 == 1){
        x= 1666;
        }
        else if (P5 == 2){
        x= 2499;
        }
        else if (P5 == 4){
        x = 3332;
```

```
	}
	else if (P5 == 5){
	x = 4165;
	}
	else if (P5 == 6){
	x = 4998;
	}
	else if (P5 == 8){
	x = 5831;
	}
	else if (P5 == 9){
	x = 6664;
	}
	else if (P5 == 10){
	x = 7497;
	}
	pulse();
}

void pulse(void)
{
	CCL3 = (65536UL - x);
	CCH3 = (65536UL - x) >> 8;//0XFF;/* Compare value (50% duty cycle) */
	CRCL = (65536UL - y);
	CRCH = (65536UL - y) >> 8;//0Xfe;		/* Reload value (500Us period)
*/
	T2CON = 0x91;//11;//19;/* Select reload mode 0 *//* Bit to start/stop timer */
	CCEN = 0x80;//A8;				/* Enable compare */
	TF2 = 0;					/* Clear interrupt request flag */
	ET2 = 1;				/* Enable timer 2 overflow interrupt */
}

void external0(void) interrupt 0 using 0
{
pulse();
}

void External1 (void) interrupt 2 using 0
{
keypad();
}

void Timer2 (void) interrupt 5 using 0
{

TF2 = 0;				/* Clear overflow flag */
T2I0 = 0;
pulse();
}
```